Post-Newtonian factorized multipolar waveforms for spinning, nonprecessing black-hole binaries

Yi Pan,[1] Alessandra Buonanno,[1] Ryuichi Fujita,[2] Etienne Racine,[1] and Hideyuki Tagoshi[3]

[1]*Maryland Center for Fundamental Physics & Joint Space-Science Institute, Department of Physics, University of Maryland, College Park, Maryland 20742, USA*

[2]*Raman Research Institute, Bangalore 560 080, India*

[3]*Department of Earth and Space Science, Graduate School of Science, Osaka University, Toyonaka 560 0043, Japan*

(Received 13 July 2010; published 1 March 2011)

We generalize the *factorized* resummation of multipolar waveforms introduced by Damour, Iyer, and Nagar to spinning black holes. For a nonspinning test particle spiraling a Kerr black hole in the equatorial plane, we find that factorized multipolar amplitudes which replace the residual relativistic amplitude $f_{\ell m}$ with its ℓth root, $\rho_{\ell m} = f_{\ell m}^{1/\ell}$, agree quite well with the numerical amplitudes up to the Kerr-spin value $q \leq 0.95$ for orbital velocities $v \leq 0.4$. The numerical amplitudes are computed solving the Teukolsky equation with a spectral code. The agreement for prograde orbits and large spin values of the Kerr black-hole can be further improved at high velocities by properly factoring out the lower-order post-Newtonian contributions in $\rho_{\ell m}$. The resummation procedure results in a better and systematic agreement between numerical and analytical amplitudes (and energy fluxes) than standard Taylor-expanded post-Newtonian approximants. This is particularly true for higher-order modes, such as (2,1), (3,3), (3,2), and (4,4), for which less spin post-Newtonian terms are known. We also extend the factorized resummation of multipolar amplitudes to generic mass-ratio, nonprecessing, spinning black holes. Lastly, in our study we employ new, recently computed, higher-order post-Newtonian terms in several subdominant modes and compute explicit expressions for the half and one-and-half post-Newtonian contributions to the odd-parity (current) and even-parity (odd) multipoles, respectively. Those results can be used to build more accurate templates for ground-based and space-based gravitational-wave detectors.

DOI: 10.1103/PhysRevD.83.064003 PACS numbers: 04.25.Nx, 04.30.Db

I. INTRODUCTION

An international network of kilometer-scale laser-interferometric gravitational-wave detectors, consisting of the Laser-Interferometer Gravitational-wave Observatory (LIGO) [1] and Virgo [2] are currently operating at the best sensitivity ever in the frequency range 10–10^3 Hz. We expect that in the next decade the Laser-Interferometer Space Antenna (LISA) [3] will be also operating but in the frequency range $10^{-4} - 10^{-1}$ Hz.

Binary black holes are among the most promising sources for those detectors. During the last 30 years, the search for gravitational waves from coalescing black-hole binaries with LIGO, Virgo, and LISA has prompted the development of highly-accurate, analytical template families to be employed in matched-filtering analysis. Those template families are based on the post-Newtonian (PN) approximation of the two-body dynamics and gravitational radiation [4,5]. In PN theory, the multipolar waveforms are derived as a Taylor expansion in v/c (v being the binary characteristic velocity and c the speed of light). More recently, Damour, Iyer, and Nagar [6,7] have proposed a resummation of the multipolar waveforms in which the Taylor-expanded multipolar waveforms computed in PN theory are rewritten in a factorized, resummed form as

$$h_{\ell m} = h_{\ell m}^{(N,\epsilon_p)} \hat{S}_{\rm eff}^{(\epsilon_p)} T_{\ell m} e^{i\delta_{\ell m}} f_{\ell m}. \quad (1)$$

The several factors in the above $h_{\ell m}$ have the following meaning. The factor $h_{\ell m}^{(N,\epsilon_p)}$ is the leading Newtonian term; $\hat{S}_{\rm eff}^{(\epsilon_p)}$ is the relativistic conserved energy or angular momentum of the effective moving source; $T_{\ell m}$ resums an infinite number of leading logarithms entering the tail effects; $e^{i\delta_{\ell m}}$ is a supplementary phase which contains phase effects which are not contained in the complex $T_{\ell m}$; and, finally, $f_{\ell m}$ contains residual terms which can be carefully resummed to improve its behavior as function of ℓ. The better agreement of the factorized multipolar waveforms to the exact numerical results suggests that the factors entering the $h_{\ell m}$'s can capture effects, such as the presence of a pole in the effective source for quasicircular orbits and the inclusion of all leading logarithms in tail terms, that are missed when expanded in a PN series and truncated at a certain PN order.

In Refs. [6,8], the factorized waveforms for a test particle orbiting around a Schwarzschild black hole were computed, including also the case of comparable-mass nonspinning black holes. It was found that factorized waveforms agree better with numerical (exact) results than Taylor-expanded waveforms. In particular, in the test-particle limit, Ref. [6] compared the analytical factorized (l, m) modes and gravitational-wave energy flux to the numerical results obtained by Berti [9], solving the Teukolsky equation. The factorized waveforms have been also employed in the

TABLE I. PN orders currently available in the multipolar waveforms $C_{\ell m}$ (in the adiabatic approximation $C_{\ell m} = -m^2\Omega^2 h_{\ell m}$). In the first two rows, we list the nonspin and spin PN orders beyond the leading-order Newtonian term $C_{22}^{(N,0)}$. In the next two rows, we list the nonspin and spin PN orders beyond the leading-order term for each mode $C_{\ell m}^{(N,\epsilon_p)}$. In the last two rows, we list the PN orders beyond the leading-order term for each mode $C_{\ell m}^{(N,\epsilon_p)}$ that are needed to compute the nonspin 5.5PN-energy flux and the spin 4PN-energy flux. For each $C_{\ell m}$, the two columns refer to the parity of the multipolar waveform $\epsilon_p = 0$ and $= 1$.

	C_{2m}		C_{3m}		C_{4m}		C_{5m}		C_{6m}		C_{7m}		C_{8m}	
	0	1	0	1	0	1	0	1	0	1	0	1	0	1
PN orders beyond $C_{22}^{(N,0)}$ (nonspin)	5.5	6	5	5.5	4.5	5	4	4.5	3.5	4	3	3	3	3.5
PN orders beyond $C_{22}^{(N,0)}$ (spin)	4	4	4	4	4	4	4	4	4	4	4	4	4	4
PN orders beyond $C_{\ell m}^{(N,\epsilon_p)}$ (nonspin)	5.5	5.5	4.5	4.5	3.5	3.5	2.5	2.5	1.5	1.5	0.5	0.5	0	0
PN orders beyond $C_{\ell m}^{(N,\epsilon_p)}$ (spin)	4	3.5	3.5	3	3	2.5	2.5	2	2	1.5	1.5	1	1	0.5
PN orders beyond $C_{\ell m}^{(N,\epsilon_p)}$ needed for nonspin 5.5PN-flux	5.5	4.5	4.5	3.5	3.5	2.5	2.5	1.5	1.5	0.5	0.5	0	0	0
PN orders beyond $C_{\ell m}^{(N,\epsilon_p)}$ needed for spin 4PN-flux	4	3	3	2	2	1	1	0	0	0	0	0	0	0

effective-one-body formalism and compared to waveforms computed in numerical-relativity simulations [8,10,11]. Also in this case, the agreement of the factorized waveforms to the numerical waveforms is better than the one of the Taylor-expanded waveforms, especially during the last stages of inspiral and plunge, and close to merger.

In this paper, we extend the factorized multipolar waveforms to the case of a test particle orbiting around a Kerr black hole on the equatorial plane. In the case of a test particle orbiting around a Schwarzschild black hole, the Taylor-expanded multipolar waveforms were derived through the PN order needed to compute the 5.5PN energy flux [12], although their explicit formulas were not available in the literature. In the case of a test particle orbiting around a Kerr black hole on the equatorial plane, spin terms in the Taylor-expanded multipolar waveforms were derived through the PN order needed to compute the 4PN energy flux [13], but their explicit formulas were not published. Motivated by this work, Tagoshi and Fujita [14] have recently computed the spinning and nonspinning Taylor-expanded multipolar waveforms up to 4PN and 5.5PN order (see Table I for a summary), respectively. Also, recently, Fujita and Iyer [15] have independently computed the nonspinning Taylor-expanded multipolar waveforms up to 5.5PN order.

Since, as said above, explicit expressions of the Taylor-expanded multipolar waveforms are not available in the literature, even at lower PN orders [12,13], we write those expressions explicitly in this paper (see Appendix A), decomposing them in -2 spin-weighted spheroidal harmonics. Then, we apply the transformation from -2 spin-weighted spheroidal harmonics to -2 spin-weighted spherical harmonics and build the factorized multipolar waveforms decomposed in -2 spin-weighted spherical harmonics. The latter decomposition is the one commonly used in the fields of numerical relativity and gravitational-wave data analysis. Finally, we compare the factorized waveforms to numerical (exact) waveforms for a test particle orbiting around a Kerr black hole, on the equatorial plane, solving the Teukolsky equation [16–18]. Finally, we derive the factorized multipolar waveforms for spinning, nonprecessing black holes of comparable masses. Those factorized waveforms were recently used in the spinning effective-one-body model of Ref. [19] and compared to numerical-relativity simulations of spinning, nonprecessing equal-mass black holes from the Caltech-Cornell-CITA collaboration.

This paper is organized as followed. In Sec. II, we work out the factorized waveforms decomposed in -2 spin-weighted spherical harmonics for a test particle orbiting a Kerr black hole, on the equatorial plane. In Sec. III, we compare the gravitational-wave energy flux and the (l, m) modes of analytical factorized waveforms to numerical waveforms. The numerical results are obtained solving the Teukolsky equation [16–18]. In Sec. IV, we derive the factorized waveforms for generic mass-ratio spinning, nonprecessing black holes. Section V summarizes our main conclusions. In Appendix A, we write the Taylor-expanded multipolar waveforms in the test-particle limit through the PN order currently known. In Appendices B, C, D, and E, we give the complete expressions of the $f_{\ell m}$'s, $C_{\ell m}$'s, $\rho_{\ell m}$'s, and $\delta_{\ell m}$'s for $4 < l \leq 8$. Finally, in Appendix F, we compute the l and m dependence of the spin terms in the mass and current-multipole moments at 0.5PN order and 1.5PN order, respectively.

II. FACTORIZED MULTIPOLAR WAVEFORMS FOR A TEST PARTICLE ORBITING AROUND A KERR BLACK HOLE

We consider a nonspinning test particle orbiting around a Kerr black hole and extend the factorized waveforms of Ref. [6] to the case where the motion is quasicircular and confined to the equatorial plane, that is the spinning, nonprecessing case. The factorized multipolar waveforms are built as the production of a leading-order term $h_{\ell m}^{(N,\epsilon_p)}$ and a higher-order correction term $\hat{h}_{\ell m}$ consisting four factors [6]

$$h_{\ell m} = h^{(N,\epsilon_p)}_{\ell m}\hat{h}_{\ell m} = h^{(N,\epsilon_p)}_{\ell m}\hat{S}^{(\epsilon_p)}_{\rm eff}T_{\ell m}e^{i\delta_{\ell m}}f_{\ell m}, \quad (2)$$

where ϵ_p denotes the parity of the multipolar waveform. In the quasicircular case, ϵ_p is the parity of $\ell + m$: $\epsilon_p = \pi(\ell + m)$. Henceforth, we use natural units $G = c = 1$. The leading term $h^{(N,\epsilon_p)}_{\ell m}$ in Eq. (2) is the Newtonian order waveform

$$h^{(N,\epsilon_p)}_{\ell m} = \frac{M\nu}{R}n^{(\epsilon_p)}_{\ell m}c_{\ell+\epsilon_p}(\nu)v^{(\ell+\epsilon_p)}Y^{\ell-\epsilon_p,-m}\left(\frac{\pi}{2},\phi\right), \quad (3)$$

where v is the orbital velocity, $Y^{\ell m}(\theta,\phi)$ are the scalar spherical harmonics, $n^{(\epsilon_p)}_{\ell m}$ are

$$n^{(0)}_{\ell m} = (im)^\ell\frac{8\pi}{(2\ell+1)!!}\sqrt{\frac{(\ell+1)(\ell+2)}{\ell(\ell-1)}}, \quad (4a)$$

$$n^{(1)}_{\ell m} = -(im)^\ell\frac{16\pi i}{(2\ell+1)!!}\sqrt{\frac{(2\ell+1)(\ell+2)(\ell^2-m^2)}{(2\ell-1)(\ell+1)\ell(\ell-1)}}, \quad (4b)$$

and $c_{\ell+\epsilon_p}(\nu)$ are functions of the symmetric mass-ratio $\nu \equiv m_1m_2/M^2$, with $M = m_1 + m_2$:

$$c_{\ell+\epsilon}(\nu) = \left(\frac{1}{2} - \frac{1}{2}\sqrt{1-4\nu}\right)^{\ell+\epsilon-1} + (-)^{\ell+\epsilon}\left(\frac{1}{2} + \frac{1}{2}\sqrt{1-4\nu}\right)^{\ell+\epsilon-1}. \quad (5)$$

Although in this section, we consider the test-particle limit $m_1 \equiv M \gg m_2 \equiv \mu$, that is $\nu \to 0$, the above relations will be used for generic ν in Sec. IV and Appendix F.

We shall define the source factor $\hat{S}^{(\epsilon_p)}_{\rm eff}$ and the tail factors $T_{\ell m}$ in Sec. II B. In Secs. II B and II C we compute the imaginary and real PN spin effects in the $e^{i\delta_{\ell m}}$'s and $f_{\ell m}$'s, respectively. We shall obtain those quantities by requiring that when we Taylor expand the factorized waveforms (2) the results coincide through 4PN order, for the spin terms, and 5.5PN order, for the nonspinning terms, with the Taylor-expanded waveforms given in Sec. II A and Appendix A.

A. Taylor-expanded multipolar waveforms

The Newman-Penrose scalar $\Psi_4 = -(\ddot{h}_+ - i\ddot{h}_\times)$ can be decomposed in either -2 spin-weighted spherical harmonics ${}_{-2}Y_{\ell m}(\theta,\phi) \equiv {}_{-2}P_{\ell m}(\theta)e^{im\phi}$, or -2 spin-weighted spheroidal harmonics ${}_{-2}S^{a\omega_0}_{\ell m}(\theta)e^{im\phi}$ as

$$\begin{aligned} r\Psi_4 &= \sum_\ell\sum_{m=-\ell}^{\ell}C_{\ell m}{}_{-2}Y_{\ell m}(\theta,\phi)e^{i\omega_0(r^*-t)}, \\ &= \sum_\ell\sum_{m=-\ell}^{\ell}C_{\ell m}\frac{{}_{-2}P_{\ell m}(\theta)}{\sqrt{2\pi}}e^{i\omega_0(r^*-t)+im\phi}, \\ &= \sum_\ell\sum_{m=-\ell}^{\ell}Z_{\ell m\omega_0}\frac{{}_{-2}S^{a\omega_0}_{\ell m}(\theta)}{\sqrt{2\pi}}e^{i\omega_0(r^*-t)+im\phi}, \end{aligned} \quad (6)$$

where a is the spin of the Kerr black hole, having the dimension of length (while we also define $q \equiv a/M$) and $\omega_0 = m\Omega$ is a multiple of the orbital frequency Ω. Since -2 spin-weighted spheroidal harmonics are eigenfunctions of the Teukolsky equation, it is natural to expand its solution in the spheroidal basis. In the fields of numerical relativity and gravitational-wave data analysis, however, the -2 spin-weighted spherical harmonics are commonly used because they do not depend on the spin and the frequency as the -2 spin-weighted spheroidal harmonics do.

The -2 spin-weighted spherical and spheroidal harmonic bases are related by

$${}_{-2}S^{a\omega_0}_{\ell m}(\theta) = {}_{-2}P_{\ell m}(\theta) + a\omega_0\sum_{\ell'}c^{\ell'}_{\ell m}{}_{-2}P_{\ell' m}(\theta) + (a\omega_0)^2\sum_{\ell'}d^{\ell'}_{\ell m}{}_{-2}P_{\ell' m}(\theta) + \mathcal{O}(a\omega_0)^3. \quad (7)$$

The coefficients $c^{\ell'}_{\ell m}$ and $d^{\ell'}_{\ell m}$ are given in Ref. [13] as

$$c^{\ell'}_{\ell m} = \begin{cases} \frac{2}{(\ell+1)^2}\sqrt{\frac{(\ell+3)(\ell-1)(\ell+m+1)(\ell-m+1)}{(2\ell+1)(2\ell+3)}}, & \ell' = \ell+1 \\ -\frac{2}{\ell^2}\sqrt{\frac{(\ell+2)(\ell-2)(\ell+m)(\ell-m)}{(2\ell+1)(2\ell-1)}}, & \ell' = \ell-1 \\ 0, & \text{otherwise} \end{cases}, \quad (8)$$

and if $\ell' = \ell$ we have

$$d^{\ell'}_{\ell m} = -\frac{1}{2}[(c^{\ell+1}_{\ell m})^2 + (c^{\ell-1}_{\ell m})^2], \quad (9)$$

while if $\ell' \neq \ell$ we have

$$\begin{aligned} d^{\ell'}_{\ell m} = \frac{1}{\lambda_0(\ell)-\lambda_0(\ell')}\Bigg\{ & -[2m+\lambda_1(\ell,m)][\delta_{\ell'\ell+1}c^{\ell+1}_{\ell m} + \delta_{\ell'\ell-1}c^{\ell-1}_{\ell m} - \delta_{\ell'\ell}\lambda_2(\ell,m)] \\ & - 4c^{\ell+1}_{\ell m}\sqrt{\frac{2\ell+3}{2\ell'+1}}\langle\ell+1,m,1,0|\ell',m\rangle\langle\ell+1,2,1,0|\ell',2\rangle - 4c^{\ell-1}_{\ell m}\sqrt{\frac{2\ell-1}{2\ell'+1}}\langle\ell-1,m,1,0|\ell',m\rangle\langle\ell-1,2,1,0|\ell',2\rangle \\ & + \frac{2}{3}\left[\delta_{\ell'\ell} - \sqrt{\frac{2\ell+1}{2\ell'+1}}\langle\ell,m,2,0|\ell',m\rangle\langle\ell,2,2,0|\ell',2\rangle\right]\Bigg\}, \end{aligned} \quad (10)$$

where $\langle j_1, m_1, j_2, m_2 | J, M\rangle$ is a Clebsch-Gordan coefficient and

$$\lambda_0(\ell) = (\ell - 1)(\ell + 2), \tag{11}$$

$$\lambda_1(\ell, m) = -2m(\ell^2 + \ell + 4)/(\ell^2 + \ell), \tag{12}$$

$$\lambda_2(\ell, m) = -2(\ell + 1)(c_{\ell m}^{\ell+1})^2 + 2\ell(c_{\ell m}^{\ell-1})^2 + \frac{2}{3} - \frac{2}{3}\frac{(\ell + 4)(\ell - 3)(\ell^2 + \ell - 3m^2)}{\ell(\ell + 1)(2\ell + 3)(2\ell - 1)}. \tag{13}$$

In the nonspinning case, ${}_{-2}S_{\ell m}^{a\omega_0}(\theta)$ reduces to ${}_{-2}P_{\ell m}(\theta)$, which has the closed expression

$${}_{-2}P_{\ell m}(\theta) = (-1)^m \sqrt{\frac{(l+m)!(l-m)!(2l+1)}{2(l+2)!(l-2)!}} \times \sin^{2l}\left(\frac{\theta}{2}\right) \sum_{r=0}^{l+2} \binom{l+2}{r} \binom{l-2}{r-2-m} (-1)^{l-r+2} \times \cot^{2r-2-m}\left(\frac{\theta}{2}\right). \tag{14}$$

The -2 spin-weighted spherical harmonic basis is orthonormal in the sense that

$$\int_0^\pi {}_{-2}P_{\ell m}(\theta)\, {}_{-2}P_{\ell' m'}(\theta) \sin\theta d\theta = \delta_{\ell\ell'}\delta_{mm'}. \tag{15}$$

To explicitly write the modes $C_{\ell m}$ and $Z_{\ell m\omega_0}$ expanded in v, we find it convenient to introduce the following notation:

$$C_{\ell m} = C_{\ell m}^{(N,\epsilon_p)} \hat{C}_{\ell m}, \tag{16}$$

$$Z_{\ell m\omega_0} = Z_{\ell m\omega_0}^{(N,\epsilon_p)} \hat{Z}_{\ell m\omega_0}, \tag{17}$$

where $C_{\ell m}^{(N,\epsilon_p)}$ and $Z_{\ell m\omega_0}^{(N,\epsilon_p)}$ represent the Newtonian contributions and, as said above, ϵ_p denotes the parity of the multipolar waveform. In the adiabatic limit, $C_{\ell m} = -m^2\Omega^2 h_{\ell m}$. Therefore, whereas the Newtonian contribution to $C_{\ell m}$ and $h_{\ell m}$ differ by a factor of $-m^2\Omega^2$, the PN corrections are the same, i.e., $\hat{C}_{\ell m} = \hat{h}_{\ell m}$. The Newtonian contributions in the $C_{\ell m}$'s or $Z_{\ell m\omega_0}$'s are [see Eq. (3)],

$$C_{\ell m}^{(N,\epsilon_p)} = Z_{\ell m\omega_0}^{(N,\epsilon_p)} = -m^2 \nu n_{\ell m}^{(\epsilon_p)} c_{\ell+\epsilon_p}(\nu) v^{(\ell+\epsilon_p+6)} Y^{\ell-\epsilon_p,-m}(\pi/2, \phi), \tag{18}$$

where we define $v = (M\Omega)^{1/3}$. In Refs. [12,13], the Taylor-expanded multipolar waveforms were calculated at the PN order needed to compute the nonspinning 5.5PN-energy flux and spin 4PN-energy flux, respectively. For the purpose of the present paper, Tagoshi and Fujita [14] extended the computation of the multipolar waveforms at higher PN order. Although those new PN corrections are not sufficient for computing the energy flux at the next order (6PN and 4.5PN order in the nonspinning and spinning cases, respectively), they do improve our knowledge of the multipolar waveforms, as we shall discuss below. In Table I, we list the PN orders available to us in each multipolar waveform $C_{\ell m}$, while the explicit Taylor-expanded waveforms $\hat{Z}_{\ell m\omega_0}$'s are given in Appendix B.

We compute the $\hat{C}_{\ell m}$'s from the $\hat{Z}_{\ell m\omega_0}$'s by applying Eq. (7) and the orthogonality condition of the -2 spin-weighted spherical harmonics

$$\begin{aligned} C_{\ell m} &= \int_{S^2} d\Omega r \Psi_4 {}_{-2}Y_{\ell m}^* e^{-i\omega_0(r^*-t)} \\ &= \int_{S^2} d\Omega \sum_{\ell'} \sum_{m'=-\ell'}^{\ell'} Z_{\ell' m'\omega_0} \frac{-2S_{\ell' m'}^{a\omega_0} {}_{-2}P_{\ell m}^*}{2\pi} e^{i(m'-m)\phi}, \\ &= \int_0^\pi \sin\theta d\theta \sum_{\ell'} Z_{\ell' m\omega_0} \Big[{}_{-2}P_{\ell' m} + a\omega_0 \sum_{\ell''} c_{\ell' m}^{\ell''} {}_{-2}P_{\ell'' m} \\ &\quad + (a\omega_0)^2 \sum_{\ell''} d_{\ell' m}^{\ell''} {}_{-2}P_{\ell'' m} \Big] {}_{-2}P_{\ell m}^*, \\ &= Z_{\ell m\omega 0} + a\omega_0 \sum_{\ell'} c_{\ell' m}^{\ell} Z_{\ell' m\omega 0} + (a\omega_0)^2 \sum_{\ell'} d_{\ell' m}^{\ell} Z_{\ell' m\omega 0} \\ &\quad + \mathcal{O}(a\omega_0)^3. \end{aligned} \tag{19}$$

We notice that the mixing of spheroidal waveforms happens among modes with the same m and different ℓ.

The $C_{\ell m}$ modes are computed in perturbation theory [12,13,20,21] using a coordinate system different from the one used in PN calculations [22,23]. When expressing both modes in terms of the orbital frequency they should coincide. However, the presence of tail terms in both calculations demands a careful treatment. In PN calculations, the tail terms contain a freely specifiable constant r_0 that corresponds to the difference in the origins of the retarded time in radiative coordinates and in harmonic coordinates in which the equations of motion are given (see e.g., Eq. (3.16) in Ref. [23]). This constant can be absorbed into the phase of the PN modes (see e.g., Eq. (8.8) in Ref. [23]) once it is traded with x_0 (or v_0) [22] as

$$\log x_0 \equiv 2\log v_0 \equiv \frac{11}{18} - \frac{2}{3}\gamma_E - \frac{4}{3}\log 2 - \frac{2}{3}\log(r_0/M), \tag{20}$$

where $\gamma_E = 0.577215\ldots$ is the Euler's constant, and throughout the paper, we use "log" to denote the natural logarithm. In perturbation-theory calculations, Schwarzschild or Boyer-Lindquist coordinates are used. The waveforms at infinity are naturally expressed with

the tortoise coordinate, and the relation between the Schwarzshild or Boyer-Lindquist coordinate and the tortoise coordinate has an arbitrary constant which in Refs. [12,13,20,21] is fixed to $-2M\log(2M)$ [24].

We find that to recover the PN results we need to express some of the γ_E's in the perturbation-theory modes [14] in terms of x_0 and r_0 using Eq. (20) and set $r_0 = 2M/\sqrt{e}$. More specifically, we replace some of the γ_E's using the following equation [22]

$$\log v_0 \equiv \frac{11}{36} - \frac{1}{3}\gamma_E - \frac{2}{3}\log 2 - \frac{1}{3}\log(2e^{-1/2}). \tag{21}$$

We notice that the constant r_0 will appear later in our definition of the tail term $T_{\ell m}$ of the factorized resummed waveforms. In fact, since the $T_{\ell m}$ term resums all tail integrals that contain r_0 at known orders, it is the only term in the resummed waveforms that depends on r_0. Finally, to ease the notation, we follow Ref. [6] and introduce $\mathrm{eulerlog}_m(v^2) = \gamma_E + \log 2 + \log m + 1/2\log v^2$ into our $C_{\ell m}$ expressions.

Below we list the $\hat{C}_{\ell m}$'s through $l = 4$ and give the expressions for $4 < \ell < 8$ in Appendix B. The differences between the $\hat{C}_{\ell m}$'s and $\hat{Z}_{\ell m \omega_0}$'s concern only spin terms. We obtain

$$\hat{C}_{22} = \hat{Z}_{22\omega_0} - \frac{20q}{189}v^5 + \frac{40q^2}{567}v^6 + \frac{386q}{1701}v^7 + \left[-\frac{40\pi q}{189} + \frac{7720q^2}{83349} + \frac{20}{63}iq - \frac{80}{63}iq\log\left(\frac{v}{v_0}\right)\right]v^8, \tag{22a}$$

$$\hat{C}_{21} = \hat{Z}_{21\omega_0} - \frac{q}{63}v^3 + \frac{8q}{189}v^5 - \left[\frac{\pi q}{63} - \frac{271q^2}{4536} - \left(\frac{1}{45} + \frac{2}{63}\log 2\right)iq + \frac{2}{21}iq\log\left(\frac{v}{v_0}\right)\right]v^6 - \left(\frac{607q}{12474} + \frac{q^3}{378}\right)v^7, \tag{22b}$$

$$\hat{C}_{33} = \hat{Z}_{33\omega_0} - \frac{3q}{20}v^5 + \frac{3q^2}{32}v^6 + \frac{117q}{220}v^7, \tag{22c}$$

$$\hat{C}_{32} = \hat{Z}_{32\omega_0} + \frac{4q}{3}v - \frac{31q}{9}v^3 + \left[\frac{8\pi q}{3} - \frac{46q^2}{27} + 16iq\log\left(\frac{v}{v_0}\right)\right]v^4 + \left(-\frac{7694q}{4455} + \frac{4q^3}{3}\right)v^5 + \left[-\frac{2683q^2}{810} - \frac{62\pi q}{9} + \frac{iq}{5} - \frac{124}{3}iq\log\left(\frac{v}{v_0}\right)\right]v^6, \tag{22d}$$

$$\hat{C}_{31} = \hat{Z}_{31\omega_0} + \frac{32q}{9}v^3 - \frac{16q^2}{3}v^4 - \frac{79q}{36}v^5 + \left[\frac{32\pi q}{9} - \frac{4349q^2}{2592} - \frac{16}{9}(1 + 4\log 2)iq + \frac{64}{3}iq\log\left(\frac{v}{v_0}\right)\right]v^6 + \left[\frac{286q^3}{27} - \frac{16\pi q^2}{3} + \frac{8iq^2}{3} + \frac{32}{3}iq^2\log 2 - \frac{3935q}{3564} - 32iq^2\log\left(\frac{v}{v_0}\right)\right]v^7, \tag{22e}$$

$$\hat{C}_{44} = \hat{Z}_{44\omega_0} - \frac{224q}{1375}v^5 + \frac{672q^2}{6875}v^6, \tag{22f}$$

$$\hat{C}_{43} = \hat{Z}_{43\omega_0} + \frac{5q}{4}v - \frac{1396q}{275}v^3 + \left[-\frac{17q^2}{8} + \frac{15\pi q}{4} - \frac{21iq}{4} + \frac{15}{2}iq\log\left(\frac{3}{2}\right) + \frac{45}{2}iq\log\left(\frac{v}{v_0}\right)\right]v^4 + \left(\frac{15q^3}{8} + \frac{51567q}{28600}\right)v^5, \tag{22g}$$

$$\hat{C}_{42} = \hat{Z}_{42\omega_0} + 3qv^3 - \frac{6q^2}{7}v^4 - \frac{17953q}{2750}v^5 + \left[-\frac{3562709q^2}{673750} + 6\pi q - 9iq + 36iq\log\left(\frac{v}{v_0}\right)\right]v^6, \tag{22h}$$

$$\hat{C}_{41} = \hat{Z}_{41\omega_0} + \frac{5q}{4}v - \frac{919q}{275}v^3 + \left[-\frac{191q^2}{56} + \frac{5\pi q}{4} - \frac{7iq}{4} - \frac{5}{2}iq\log 2 + \frac{15}{2}iq\log\left(\frac{v}{v_0}\right)\right]v^4 + \left(\frac{110711q}{28600} - \frac{95q^3}{56}\right)v^5, \tag{22i}$$

where the $\hat{Z}_{\ell m}$'s can be found in Appendix A. We notice that whereas the $\hat{Z}_{\ell m}$'s contain 0.5PN spin terms (relative to $Z^N_{\ell m}$'s), the $\hat{C}_{\ell m}$'s do not, except for $\hat{C}_{21}$. The spin terms in the multipolar waveforms (22a)–(22i) agree with the currently known spin terms computed in Ref. [25] and with the 0.5PN and 1.5PN spin terms in the odd and even-parity modes computed in Appendix F.

B. Source and tail terms

In the limit of a nonspinning test particle of mass μ orbiting around a Kerr black hole of mass M in a quasicircular equatorial orbit, the energy and orbital angular momentum, in Boyer-Lindquist coordinates, read [26]

$$\frac{E(r)}{\mu} = \frac{1 - 2M/r + aM^{1/2}/r^{3/2}}{\sqrt{1 - 3M/r + 2aM^{1/2}/r^{3/2}}}, \tag{23}$$

$$\frac{L(r)}{\mu M} = \sqrt{\frac{r}{M}}\frac{1 - 2aM^{1/2}/r^{3/2} + a^2/r^2}{\sqrt{1 - 3M/r + 2aM^{1/2}/r^{3/2}}}, \tag{24}$$

where $r = (1 - av^3)^{2/3}/v^2$. The source term in the factorized waveform (2) is

$$\hat{S}_{\rm eff}^{(\epsilon)} = \begin{cases} \frac{E(r)}{\mu}, & \epsilon = 0, \\ \frac{L(r)}{(\mu M/v)}, & \epsilon = 1, \end{cases} \tag{25}$$

where $\mu M/v$ is the Newtonian angular momentum. We use the resummed tail factor $T_{\ell m}$ given in Eq. (19) of Ref. [6]

$$T_{\ell m} = \frac{\Gamma(\ell + 1 - 2i\hat{k})}{\Gamma(\ell + 1)} e^{\pi\hat{k}} e^{2i\hat{k}\log(2kr_0)}, \tag{26}$$

where $k = m\Omega$, $\hat{k} = H_{\rm real}k$, and the real Hamiltonian in the test-particle limit reduces to $H_{\rm real} = M$. Once again, we emphasize that the constant r_0 must take a fixed numerical value, $2M/\sqrt{e}$ [27], to reproduce the correct test-particle limit waveforms. We notice that there is no spin contribution to $T_{\ell m}$ since the latter resums the corrections to the waveform when traveling through a long-range Coulomb-type potential generated by the mass M [28,29]. Spin effects generate a short-range potential, thus they do not contribute to $T_{\ell m}$.

We compute the phase correction factors $e^{i\delta_{\ell m}}$ in Eq. (2) by Taylor expanding the factorized waveforms $h_{\ell m}$ given in Eq. (2), comparing the result with the $C_{\ell m}$ waveforms derived in Sec. II A (in the circular-orbit, adiabatic approximation $C_{\ell m} = -(m\Omega)^2 h_{\ell m}$), and collecting all imaginary terms into $\delta_{\ell m}$. We obtain

$$\delta_{22} = \frac{7}{3}v^3 + \left(\frac{428\pi}{105} - \frac{4q}{3}\right)v^6 + \frac{20q}{63}v^8 + \left(\frac{1712\pi^2}{315} - \frac{2203}{81}\right)v^9, \tag{27a}$$

$$\delta_{21} = \frac{2}{3}v^3 + \left(\frac{107\pi}{105} - \frac{17q}{35}\right)v^6 + \frac{3q^2}{140}v^7 + \left(\frac{214\pi^2}{315} - \frac{272}{81}\right)v^9, \tag{27b}$$

$$\delta_{33} = \frac{13}{10}v^3 + \left(\frac{39\pi}{7} - \frac{81q}{20}\right)v^6 + \left(\frac{78\pi^2}{7} - \frac{227827}{3000}\right)v^9, \tag{27c}$$

$$\delta_{32} = \frac{2}{3}v^3 + 4qv^4 + \left(\frac{52\pi}{21} - \frac{136q}{45}\right)v^6 + \left(\frac{208\pi^2}{63} - \frac{9112}{405}\right)v^9, \tag{27d}$$

$$\delta_{31} = \frac{13}{30}v^3 + \left(\frac{61q}{20} + \frac{13\pi}{21}\right)v^6 - \frac{24q^2}{5}v^7 + \left(\frac{26\pi^2}{63} - \frac{227827}{81000}\right)v^9, \tag{27e}$$

$$\delta_{44} = \frac{14}{15}v^3 + \left(\frac{25136\pi}{3465} - \frac{464q}{75}\right)v^6, \tag{27f}$$

$$\delta_{43} = \frac{3}{5}v^3 + \frac{11q}{4}v^4 + \frac{1571\pi}{385}v^6, \tag{27g}$$

$$\delta_{42} = \frac{7}{15}v^3 + \left(\frac{212q}{75} + \frac{6284\pi}{3465}\right)v^6, \tag{27h}$$

$$\delta_{41} = \frac{1}{5}v^3 + \frac{11q}{12}v^4 + \frac{1571\pi}{3465}v^6. \tag{27i}$$

Notice that the nonspinning terms in the $\delta_{\ell m}$ already appeared in Ref. [6], except for the terms at 3PN order (v^6) [Ref. [6] did compute δ_{22} at 3PN order]. We find that those 3PN-order terms in the $\delta_{\ell m}$ are necessary to obtain full agreement between the factorized waveforms and the nonspinning $\hat{C}_{\ell m}$ waveforms through 3PN order. We note that the nonspinning terms at 3PN order in the $\delta_{\ell m}$'s are the same as the 3PN phase terms in $Z_{\ell m\omega_0}$ in Ref. [21]. This happens because in the test-particle limit the PN expansion of $T_{\ell m}$ does not contain imaginary terms at 3PN. Thus, for $q = 0$, the phase corrections $\delta_{\ell m}$ at 3PN order do not contain any additional terms other than the 3PN phase terms in $Z_{\ell m\omega_0}$. We further note that some of the above δ's can be obtained directly in the standard PN and test-particle limit calculations. For example, the terms proportional to πv^6 and $\pi^2 v^9$ (for $q = 0$) are the same as the phase factors in the asymptotic amplitude in the test-particle limit calculations (e.g., Eqs. (30)–(32) in Ref. [21] and Eq. (4.17) in Ref. [30]).

C. Taylor-expanded residual terms and their resummation

In the circular-orbit, adiabatic approximation $C_{\ell m} = -(m\Omega)^2 h_{\ell m}$. By Taylor expanding the factorized waveforms $h_{\ell m}$ given in Eq. (2), comparing the result with the $C_{\ell m}$ waveforms derived in Sec. II A, and factoring out the imaginary terms in the $\delta_{\ell m}$ of Eqs. (27a)–(27i), we derive the $f_{\ell m}$'s in Eq. (2). We notice that in the case of even-parity modes, the determination of the $f_{\ell m}$ is unique. In the case of odd-parity modes, it depends on the choice of the source which, as explained above, can be either the energy or the angular momentum. We denote with $f^L_{\ell m}$ and $f^H_{\ell m}$ the odd-parity modes computed with the energy and angular-momentum sources, respectively. [Since in both cases the source is a real quantity, the phases $\delta_{\ell m}$'s remain the same.] We obtain through $\ell = 4$ (see Appendix C for modes with $4 < \ell \leq 8$)

$$f_{22} = 1 - \frac{43}{21}v^2 - \frac{4q}{3}v^3 + \left(q^2 - \frac{536}{189}\right)v^4 - \frac{118q}{63}v^5 + \left(\frac{8q^2}{63} - \frac{856\,\mathrm{eulerlog}_2(v^2)}{105} + \frac{21428357}{727650}\right)v^6 + \frac{1562q}{189}v^7 + \left(\frac{232q^2}{189} + \frac{36808\,\mathrm{eulerlog}_2(v^2)}{2205} - \frac{5391582359}{198648450}\right)v^8 + \left(\frac{458816\,\mathrm{eulerlog}_2(v^2)}{19845} - \frac{93684531406}{893918025}\right)v^{10}, \tag{28a}$$

$$f^L_{21} = 1 - \frac{3q}{2}v - \frac{59}{28}v^2 + \frac{61q}{12}v^3 + \left(-3q^2 - \frac{5}{9}\right)v^4 + \frac{3}{16}q(4q^2 - 27)v^5 + \left(\frac{4163q^2}{252} - \frac{214\,\mathrm{eulerlog}_1(v^2)}{105} + \frac{88404893}{11642400}\right)v^6 + \left(-\frac{2593q^3}{168} + \frac{107}{35}q\,\mathrm{eulerlog}_1(v^2) - \frac{11847887q}{1058400}\right)v^7 + \left(\frac{6313\,\mathrm{eulerlog}_1(v^2)}{1470} - \frac{33998136553}{4237833600}\right)v^8 + \left(\frac{214\,\mathrm{eulerlog}_1(v^2)}{189} - \frac{214752050459}{21794572800}\right)v^{10}, \tag{28b}$$

$$f_{33} = 1 - \frac{7}{2}v^2 - 2qv^3 + \left(\frac{3q^2}{2} - \frac{443}{440}\right)v^4 + \frac{2q}{3}v^5 + \left(-\frac{7q^2}{4} - \frac{78\mathrm{eulerlog}_3(v^2)}{7} + \frac{147471561}{2802800}\right)v^6 + \left(\frac{6187q}{330} - q^3\right)v^7 + \left(39\,\mathrm{eulerlog}_3(v^2) - \frac{53641811}{457600}\right)v^8, \tag{28c}$$

$$f^L_{32} = 1 - \frac{164}{45}v^2 + \frac{2q}{3}v^3 + \left(q^2 + \frac{854}{495}\right)v^4 - \frac{1148q}{135}v^5 + \left(\frac{4q^2}{3} - \frac{104\,\mathrm{eulerlog}_2(v^2)}{21} + \frac{110842222}{4729725}\right)v^6 + \left(\frac{17056\,\mathrm{eulerlog}_2(v^2)}{945} - \frac{97490306}{1702701}\right)v^8, \tag{28d}$$

$$f_{31} = 1 - \frac{13}{6}v^2 - 2qv^3 + \left(\frac{1273}{792} - \frac{5q^2}{2}\right)v^4 + \frac{38q}{9}v^5 + \left(\frac{43q^2}{12} - \frac{26\,\mathrm{eulerlog}_1(v^2)}{21} + \frac{400427563}{75675600}\right)v^6 + \left(\frac{11q^3}{3} - \frac{2657q}{594}\right)v^7 + \left(\frac{169\,\mathrm{eulerlog}_1(v^2)}{63} - \frac{12064573043}{1816214400}\right)v^8, \tag{28e}$$

$$f_{44} = 1 - \frac{269}{55}v^2 - \frac{8q}{3}v^3 + \left(2q^2 + \frac{63002}{25025}\right)v^4 + \frac{262q}{55}v^5 - \left(\frac{2203q^2}{495} + \frac{50272\,\mathrm{eulerlog}_4(v^2)}{3465} - \frac{11985502766}{156080925}\right)v^6, \tag{28f}$$

$$f^L_{43} = 1 - \frac{111}{22}v^2 + \left(\frac{3q^2}{2} + \frac{225543}{40040}\right)v^4 - \frac{12113q}{1540}v^5 + \left(\frac{11337315611}{277477200} - \frac{3142\,\mathrm{eulerlog}_3(v^2)}{385}\right)v^6, \tag{28g}$$

$$f_{42} = 1 - \frac{191}{55}v^2 - \frac{8q}{3}v^3 + \left(2q^2 + \frac{76918}{25025}\right)v^4 + \frac{368q}{55}v^5 - \left(\frac{97q^2}{495} + \frac{12568\,\mathrm{eulerlog}_2(v^2)}{3465} - \frac{5180369659}{312161850}\right)v^6, \tag{28h}$$

$$f^L_{41} = 1 - \frac{301}{66}v^2 + \left(\frac{3q^2}{2} + \frac{760181}{120120}\right)v^4 - \left(\frac{10q^3}{3} + \frac{20033q}{13860}\right)v^5 + \left(\frac{4735160051}{2497294800} - \frac{3142\,\mathrm{eulerlog}_1(v^2)}{3465}\right)v^6, \tag{28i}$$

where, as introduced above, we have defined $\mathrm{eulerlog}_m(v^2) = \gamma_E + \log 2 + \log m + 1/2 \log v^2$ with $m = 1, 2, 3, \ldots$. Note that all the nonspinning terms in Eqs. (28a)–(28i) appear at even powers of v and the spin terms at odd powers of v. Moreover, except for the (2,1) odd-parity mode, all the other odd-parity modes do not have a spin contribution at 0.5PN order. This is consistent with the results of Appendix F.

As emphasized in Ref. [6], the decomposition of the Taylor-expanded multipolar waveform into several factors [see Eq. (2)] is in itself a resummation procedure. In fact, the factorization of $T_{\ell m}$ has absorbed powers of $m\pi$, which introduce large coefficients in the Taylor-expanded waveform. Moreover, in the quasicircular case assumed here, the factorization of the energy or angular-momentum sources has extracted the pole located at the light-ring position $v = \sqrt{M/r_{\rm lr}}$ with $r_{\rm lr} = 2M[1 + \cos[2/3 \arccos(\mp a/M)]]$ (where $\mp$ refers to prograde and retrograde orbits, respectively), which causes the coefficient of v^{2n} in any PN-expanded quantity to grow as $r^n_{\rm lr}$ as $n \to \infty$. As we shall see in Sec. III, despite those improvements, the $f_{\ell m}$'s above are not close enough to the exact results for large velocities.

As we shall discuss in detail in Sec. III, the $f_{\ell m}$'s in the form of Taylor-expanded power series $f_{\ell m} = \sum_{k=0}^{N_{\ell m}} f^{(k)}_{\ell m} v^k$ can be further improved by applying the Padé summation and/or the ρ resummation [6]. In the Padé summation, we replace $f_{\ell m}$ with its Padé approximant, i.e. with the rational function $(\sum_{k=0}^{M} a_k v^k)/(\sum_{k=0}^{N} b_k v^k)$, with $a_0 = b_0 = 1$ and $M + N = N_{\ell m}$. The ρ resummation consists in finding the polynomial function $\rho_{\ell m} = \sum_{k=0}^{N_{\ell m}} \rho^{(k)}_{\ell m} v^k$ such that the Taylor-expanded power series of its ℓth power $(\rho_{\ell m})^\ell$ agrees with $f_{\ell m}$ through order $N_{\ell m}$.

The motivation for the ρ resummation is to reduce the magnitude of the 1PN-order nonspinning coefficient $f^{(2)}_{\ell m}$ of $f_{\ell m}$, which grows linearly with ℓ (see Sec. IID of Ref. [6]). In the nonspinning case, since $\rho^{(1)}_{\ell m} = f^{(1)}_{\ell m} = 0$, we have $\rho^{(2)}_{\ell m} = f^{(2)}_{\ell m}/\ell$ and the linear dependence of ℓ is removed from $\rho^{(2)}_{\ell m}$. We find that such dependence on ℓ does also affects the 1.5PN spin terms in the even-parity modes computed as function of ℓ and m in Appendix F. In fact, we find that $h^{\rm even}_{\ell m} = -2\ell q v^3/3$, and so $f^{\rm even}_{\ell m} = -2\ell q v^3/3$. Thus, we apply the ρ resummation also to the spin terms and find (see Appendix D for modes with $4 < \ell < 8$)

$$\rho_{22} = 1 - \frac{43}{42}v^2 - \frac{2q}{3}v^3 + \left(\frac{q^2}{2} - \frac{20555}{10584}\right)v^4 - \frac{34q}{21}v^5 + \left(\frac{89q^2}{252} - \frac{428\,\mathrm{eulerlog}_2(v^2)}{105} + \frac{1556919113}{122245200}\right)v^6 + \left(\frac{q^3}{3} + \frac{18733q}{15876}\right)v^7$$
$$+ \left(-\frac{q^4}{8} + \frac{18353q^2}{21168} + \frac{9202\mathrm{eulerlog}_2(v^2)}{2205} - \frac{387216563023}{160190110080}\right)v^8 + \left(\frac{439877\,\mathrm{eulerlog}_2(v^2)}{55566} - \frac{16094530514677}{533967033600}\right)v^{10}, \tag{29a}$$

$$\rho^L_{21} = 1 - \frac{3q}{4}v + \left(-\frac{9q^2}{32} - \frac{59}{56}\right)v^2 + \left(\frac{1177q}{672} - \frac{27q^3}{128}\right)v^3 - \left(\frac{47009}{56448} + \frac{865q^2}{1792} + \frac{405q^4}{2048}\right)v^4$$
$$- \left(\frac{98635q}{75264} - \frac{2031q^3}{7168} + \frac{1701q^5}{8192}\right)v^5 + \left(-\frac{15309q^6}{65536} + \frac{3897q^4}{16384} + \frac{9032393q^2}{1806336} - \frac{107\,\mathrm{eulerlog}_1(v^2)}{105} + \frac{7613184941}{2607897600}\right)v^6$$
$$+ \left(-\frac{72171q^7}{262144} + \frac{18603q^5}{65536} - \frac{55169q^3}{16384} + \frac{107}{140}q\,\mathrm{eulerlog}_1(v^2) - \frac{3859374457q}{1159065600}\right)v^7$$
$$+ \left(\frac{6313\,\mathrm{eulerlog}_1(v^2)}{5880} - \frac{1168617463883}{911303737344}\right)v^8 + \left(\frac{5029963\,\mathrm{eulerlog}_1(v^2)}{5927040} - \frac{63735873771463}{16569158860800}\right)v^{10}, \tag{29b}$$

$$\rho_{33} = 1 - \frac{7}{6}v^2 - \frac{2q}{3}v^3 + \left(\frac{q^2}{2} - \frac{6719}{3960}\right)v^4 - \frac{4q}{3}v^5 + \left(\frac{5q^2}{36} - \frac{26\,\mathrm{eulerlog}_3(v^2)}{7} + \frac{3203101567}{227026800}\right)v^6 + \left(\frac{q^3}{3} + \frac{5297q}{2970}\right)v^7$$
$$+ \left(\frac{13\,\mathrm{eulerlog}_3(v^2)}{3} - \frac{57566572157}{8562153600}\right)v^8, \tag{29c}$$

$$\rho^L_{32} = 1 - \frac{164}{135}v^2 + \frac{2q}{9}v^3 + \left(\frac{q^2}{3} - \frac{180566}{200475}\right)v^4 - \frac{2788q}{1215}v^5 + \left(\frac{488q^2}{405} - \frac{104\,\mathrm{eulerlog}_2(v^2)}{63} + \frac{5849948554}{940355325}\right)v^6 + \left(\frac{17056\,\mathrm{eulerlog}_2(v^2)}{8505} - \frac{10607269449358}{3072140846775}\right)v^8, \tag{29d}$$

$$\rho_{31} = 1 - \frac{13}{18}v^2 - \frac{2q}{3}v^3 + \left(\frac{101}{7128} - \frac{5q^2}{6}\right)v^4 + \frac{4q}{9}v^5 + \left(-\frac{49q^2}{108} - \frac{26\,\mathrm{eulerlog}_1(v^2)}{63} + \frac{11706720301}{6129723600}\right)v^6 + \left(\frac{q^3}{9} - \frac{2579q}{5346}\right)v^7 + \left(\frac{169\,\mathrm{eulerlog}_1(v^2)}{567} + \frac{2606097992581}{4854741091200}\right)v^8, \tag{29e}$$

$$\rho_{44} = 1 - \frac{269}{220}v^2 - \frac{2q}{3}v^3 + \left(\frac{q^2}{2} - \frac{14210377}{8808800}\right)v^4 - \frac{69q}{55}v^5 + \left(\frac{217q^2}{3960} - \frac{12568\,\mathrm{eulerlog}_4(v^2)}{3465} + \frac{16600939332793}{1098809712000}\right)v^6, \tag{29f}$$

$$\rho^L_{43} = 1 - \frac{111}{88}v^2 + \left(\frac{3q^2}{8} - \frac{6894273}{7047040}\right)v^4 - \frac{12113q}{6160}v^5 + \left(\frac{1664224207351}{195343948800} - \frac{1571\,\mathrm{eulerlog}_3(v^2)}{770}\right)v^6, \tag{29g}$$

$$\rho_{42} = 1 - \frac{191}{220}v^2 - \frac{2q}{3}v^3 + \left(\frac{q^2}{2} - \frac{3190529}{8808800}\right)v^4 - \frac{7q}{110}v^5 + \left(\frac{2323q^2}{3960} - \frac{3142\,\mathrm{eulerlog}_2(v^2)}{3465} + \frac{848238724511}{219761942400}\right)v^6, \tag{29h}$$

$$\rho^L_{41} = 1 - \frac{301}{264}v^2 + \left(\frac{3q^2}{8} - \frac{7775491}{21141120}\right)v^4 + \left(-\frac{5q^3}{6} - \frac{20033q}{55440}\right)v^5 + \left(\frac{1227423222031}{1758095539200} - \frac{1571\,\mathrm{eulerlog}_1(v^2)}{6930}\right)v^6. \tag{29i}$$

Lastly, we may use $E(r)$ instead of $|\boldsymbol{L}|$ as the source term in Eq. (2) for the odd-parity modes. The corresponding $f^H_{\ell m}$ and $\rho^H_{\ell m}$ expressions are given in Appendices C and D, respectively.

In the next section, we shall investigate the numerical (exact) $\rho_{\ell m}$'s and compare them with the analytical ones. We shall find that the agreement between the numerical and analytical $\rho_{\ell m}$ is quite good, except for some modes. Guided by the comparison with numerical results, we shall apply the Padé summation to the $\rho_{\ell m}$'s and also work out an improved resummation which consists in factoring out the lower-order PN terms in the Taylor-expanded $\rho_{\ell m}$'s. We find that this factorization brings the zeros of the analytical $\rho_{\ell m}$ closer to the numerical (exact) ones.

III. COMPARISON BETWEEN ANALYTICAL AND NUMERICAL RESULTS FOR THE TEST-PARTICLE LIMIT CASE

We have two goals to achieve in this section. The first is to accurately model the amplitude of the (l, m) modes for several values of the spin parameter q and velocity v. The second is to obtain the best agreement between the numerical (exact) and analytical energy fluxes *without* introducing adjustable parameters in the analytical model.

The numerical values of the energy flux used in this paper are obtained with a high precision numerical code which solves the Teukolsky equation [16–18]. The homogeneous solution of the radial Teukolsky equation is obtained numerically by using a formalism developed by Mano, Suzuki, and Takasugi [31]. In this method, the homogeneous solutions are expressed in terms of series of two kinds of special functions, hypergeometric functions and confluent hypergeometric functions. In Refs. [16,17], it was shown that the series converges very fast and one can compute numerically the homogeneous solutions very accurately. The homogeneous solution obtained with this method was applied to the numerical calculation of gravitational waves emitted by a particle in a quasicircular and equatorial orbit around a Kerr black hole [16,17]. In this paper, for the comparison with analytical formulas, we compute the $Z_{\ell m\omega_0}$ (and thus the $C_{\ell m}$) as well as $(dE/dt)_{\ell m}$ for various q and Ω. The computation is done with the double precision accuracy, and the estimated accuracy of $Z_{\ell m\omega_0}$ (and thus the $C_{\ell m}$) as well as $(dE/dt)_{\ell m}$ is about 14 significant figures. As in Ref. [16], the accuracy is estimated by comparing the energy flux with that of Ref. [32], in which the accuracy was estimated as about 20 significant figures.

A. Hierarchy between the (l, m)'s modes

In Fig. 1, we study the hierarchy among the numerically-computed modes and plot $|h_{\ell m}|/|h_{22}|$ versus v for the representative spin cases: $q = 0.95$, 0, and -0.95. The parameter v varies between 0.1 and $v_{\mathrm{LSO}}(q)$, where we denote with the last stable orbit (LSO) for a test particle in the Kerr geometry.

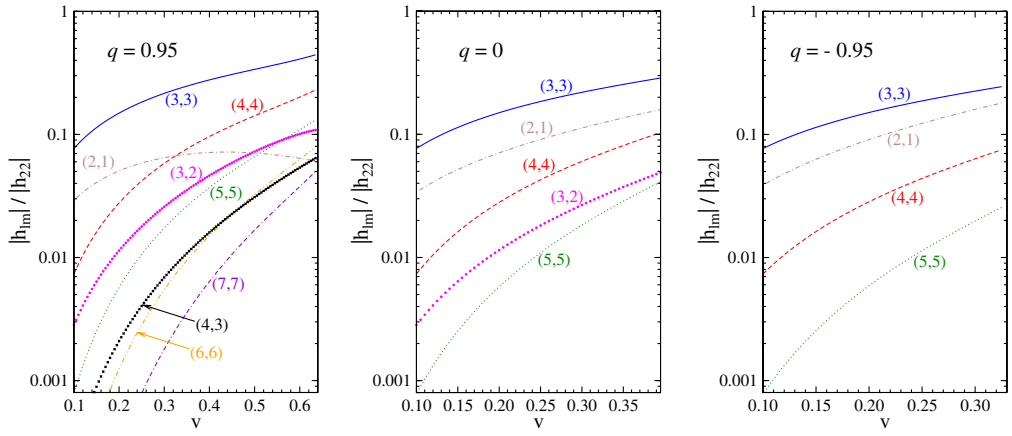

FIG. 1 (color online). Hierarchy of the numerically-computed modes $h_{\ell m}$ relative to that of the dominant h_{22} mode. The spin values in the three panels from left to right are $q = 0.95$, 0, -0.95, respectively. The x axis ranges between 0 and $v_{\rm LSO}(q)$.

The strain waveforms $h_{\ell m}$'s are computed from the $C_{\ell m}$'s under the quasicircular adiabatic assumption, i.e., $h_{\ell m} = -C_{\ell m}/(m\Omega)^2$. As we shall discuss in Sec. III C, the energy flux for quasicircular adiabatic orbits can be computed through the well-known relation

$$F(v) = \frac{1}{16\pi}\sum_{\ell}\sum_{m=-\ell}^{\ell}(m\Omega)^2|h_{\ell m}(v)|^2. \tag{30}$$

Thus, when analyzing the contribution of the $\dot{h}_{\ell m}$'s to the energy flux, we need to remember that $\dot{h}_{\ell m} = iC_{\ell m}/(m\Omega)$. Thus, the dependence of $\dot{h}_{\ell m}$'s on m is different than the one of $h_{\ell m}$'s, and, as a consequence, the hierarchy of the modes in the energy flux is different.

Denoting by $|h_{\ell m}|/|h_{22}|$ the relative strain amplitude and by $|\dot{h}_{\ell m}|^2/|h_{22}|^2$ the relative radiation power, we find the following trends. In the antialigned case $q = -0.95$ and the nonspinning case, the (3,3), (2,1), and (4,4) modes are the largest subdominant modes in terms of strain amplitude. In terms of radiation power, they are also among the largest subdominant modes although their hierarchy changes. The (4,4) mode contributes more power than the (2,1) mode because of its larger m. For the same reason, in the nonspinning case, the (5,5) mode contributes more power than the (2,1) mode and becomes the third strongest subdominant mode. In fact, in the antialigned and nonspinning cases, relative to the (2,2) mode, the (3,3) mode contributes >10% of radiation power at the LSO, only the (3,3) and (4,4) modes contribute >1%, and the (5,5) mode contributes 1% only in the nonspinning case. In the aligned case $q = 0.95$, we plot in Fig. 1 the relative strain amplitudes of 8 modes that are larger than 5% at the LSO. In terms of the relative radiation power, the (3,3), (4,4), (5,5), (6,6), (7,7), and (8,8) modes are the largest subdominant modes. The (3,3), (4,4), and (5,5) modes each contributes >10% relative to the (2,2) mode at the LSO. In particular, the (3,3) mode contributes >30% relative to the (2,2) mode to both the strain amplitude and the radiation power. Accurate modeling of its amplitude is therefore crucial in modeling the full gravitational-wave waveform and the energy flux.

B. Comparison between the analytical and numerical modes

We now examine the amplitude agreement of the numerical and analytical waveforms, focusing mainly on the dominant modes: (2,2), (2,1), (3,3), (3,2), (4,4), and (5,5).

In Figs. 2 and 3, we show several numerical $\rho_{\ell m}$'s versus $x \equiv v^2$ for three representative spin cases: $q = -0.95$, 0, 0.95. Since the latter are real, the numerical $\rho_{\ell m}$'s are obtained using Eq. (2) with $f_{\ell m} = \rho^{\ell}_{\ell m}$, that is dividing the numerical $|h_{\ell m}|^{1/\ell}$ by $(|T_{\ell m}|\hat{S}^{(\epsilon)}_{\rm eff})^{1/\ell}$. The numerical $h_{\ell m}$ are computed from the numerical $C_{\ell m}$ through the relation $h_{\ell m} = -C_{\ell m}/(m\Omega)^2$

Using the 0.5PN (1.5PN) order spin terms in the odd (even)-parity modes computed in Appendix F for generic ℓ and m and the nonspinning 1PN terms derived in Refs. [6,22], we have

$$f^{\rm even}_{\ell m}(x) = 1 - \left(1 - \frac{1}{\ell} + \frac{m^2(\ell+9)}{2\ell(\ell+1)(2\ell+3)}\right)\ell x - \frac{2}{3}\ell q x^{3/2} + \mathcal{O}(x^2), \tag{31}$$

and

$$f^{L}_{\ell m}(x) = 1 - \frac{3}{2}qx^{1/2}\delta_{\ell 2}\delta_{m1} - \left(1 + \frac{1}{\ell} - \frac{2}{\ell^2} + \frac{m^2(l+4)}{2\ell(\ell+2)(2\ell+3)}\right)\ell x + \mathcal{O}(x^{3/2}). \tag{32}$$

Note that the 1.5PN spin terms in the odd-parity modes are not known for generic ℓ and m, but they are available through $\ell = 6$ in this paper.

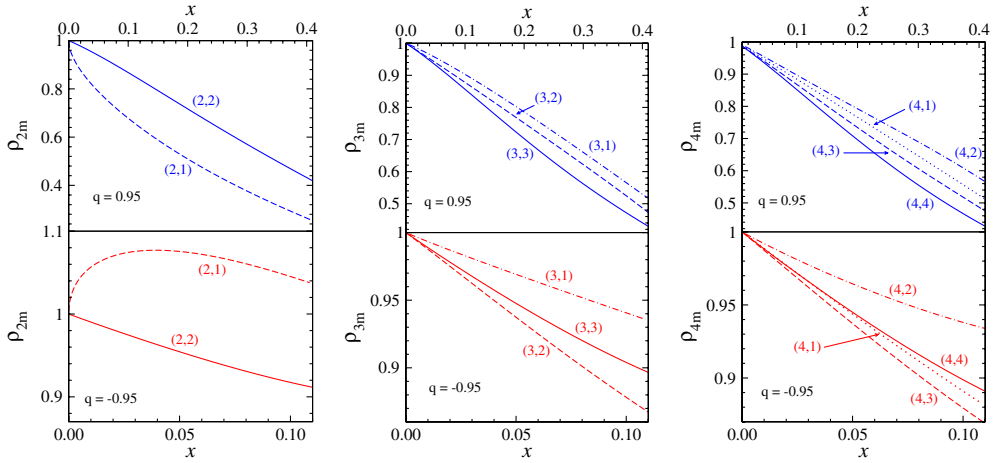

FIG. 2 (color online). We plot the $\rho_{\ell m}$'s extracted from the numerical data as function of $x \equiv v^2$. The upper panels (blue colors) refer to $q = 0.95$, the lower panels (red colors) to $q = -0.95$. The variable x ranges between $0 < x < x_{\rm LSO}(a)$.

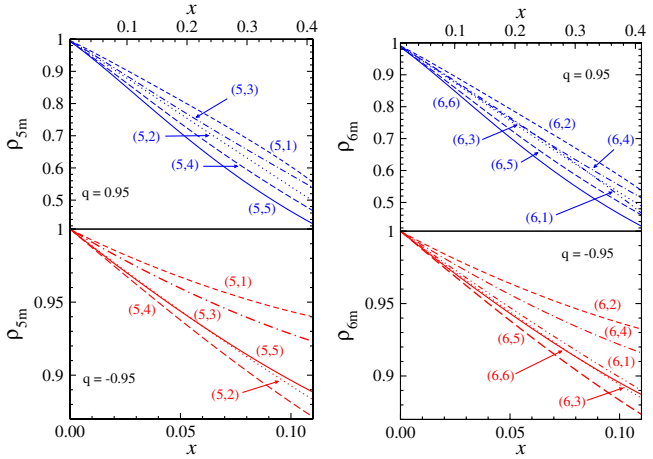

FIG. 3 (color online). We plot the $\rho_{\ell m}$'s extracted from the numerical data as function of $x \equiv v^2$. The upper panels (blue colors) refer to $q = 0.95$, the lower panels (red colors) to $q = -0.95$. The variable x ranges between $0 < x < x_{\rm LSO}(a)$.

Reference [6] pointed out that because the 1PN order term in the $f^{\rm even}_{\ell m}$ and $f^{L}_{\ell m}$ scale as ℓ and is negative, for large ℓ it can cause the $f_{\ell m}$ to go to zero even before reaching the LSO. For example, if we consider the LSO in Schwarzschild, $x_{\rm LSO}(0) = 1/6$ $(v_{\rm LSO}(0) = 1/\sqrt{6} \simeq 0.4082)$, f_{66} at 1PN order has a zero at $v = 0.3634$ [6]. In the even-parity case, the inclusion of the 1.5PN spin term with $q > 0$ can cause the zero to occur even at smaller values of v. In particular, for $q = 0.95$, f_{66} has a zero at $v = 0.3362$ $(v_{\rm LSO}(0.95) = 0.6497)$. By contrast, the cases with $q < 0$ can push the zero to negative or imaginary values, or to values of v above the LSO, thus making it harmless. For example, for $q = -0.95$, f_{66} has a zero at $v = 0.4075$ $(v_{\rm LSO}(-0.95) = 0.3373)$. Similarly, when considering the odd-parity modes for large ℓ, e.g., the f^{L}_{65} mode, we find that in the nonspinning case the 1PN term causes f^{L}_{65} to have a zero at $v = 0.3602$ and the inclusion of 1.5PN spin term causes the zero to move to $v = 0.3502$ for $q = 0.95$ and to $v = 0.3717$ for $q = -0.95$.

In the spin case, the above problem can be even worse than in the nonspinning case for lower values of ℓ. For example, the 1PN term causes a zero in the f_{33} at $v = 0.5345$ which is above $v_{\rm LSO}(0)$, but the inclusion of the 1.5PN spin term moves the zero to $v = 0.4764$ for $q = 0.95$ which is quite below $v_{\rm LSO}(0.95)$.

Motivated by the above discussion and the result in Appendix F that shows that the even-parity 1.5PN spin terms scale as ℓ $(f^{\rm even}_{\ell m} = -2\ell q v^3/3)$, we adopt the ρ resummation also for the spin terms. The $\rho_{\ell m}$'s through 1.5PN order read:

$$\rho^{\rm even}_{\ell m}(x) = 1 - \left(1 - \frac{1}{\ell} + \frac{m^2(\ell+9)}{2\ell(\ell+1)(2\ell+3)}\right)x - \frac{2}{3}qx^{3/2} + \mathcal{O}(x^2), \tag{33}$$

and

$$\rho^L_{\ell m}(x) = 1 - \frac{3}{2}\frac{1}{\ell} q x^{1/2} \delta_{\ell 2}\delta_{m1} - \frac{9}{8}\frac{\ell-1}{\ell^2} q^2 x \delta_{\ell 2}\delta_{m1} - \left(1 + \frac{1}{\ell} - \frac{2}{\ell^2} + \frac{m^2(l+4)}{2\ell(\ell+2)(2\ell+3)}\right) x + \mathcal{O}(x^{3/2}). \tag{34}$$

We notice that the 1PN and 1.5PN terms in ρ_{66} cause a zero at $v = 0.8902$ for $q = 0$ and at $v = 0.7577$ for $q = 0.95$. The zero in ρ_{33} occurs at $v = 0.9258$ for $q = 0$ and at $v = 0.7765$ for $q = 0.95$. All these numbers are larger than $v_{\rm LSO}(q)$. Note however that the ρ resummation may be less effective for $q > 0.95$, since at $q = 1$, the zero in ρ_{66} occurs at $v = 0.7530$ and the zero in ρ_{33} occurs at $v = 0.7713$, both smaller than $v_{\rm LSO}(1) = 0.7937$. Of course all this discussion does not take into account the higher-order PN terms, which can also move the zero to lower or higher values. However, as we shall see below, the behavior of the numerical $\rho_{\ell m}$ is captured by the 0.5PN, 1PN, and 1.5PN terms.

In Figs. 2 and 3, we plot the $\ell = 2, 3, 4, 5, 6$ ($m = \ell, \ell-1, \ldots, 1$) numerical modes versus x. First, as observed in Ref. [6] for the nonspinning case, also for the spin case, the behavior of the $\rho_{\ell m}$ is reasonably *simple*. In particular, except for the (2,1) case which shows a special shape due to the presence of the 0.5PN term ($\sqrt{x}$), all the other modes are well represented by (broken) straight lines with one or two changes in the slope at high frequency. As in the nonspinning case, but less pronounced here, for each value of ℓ, the (negative) slopes of the dominant $m = \ell$ (even-parity) and subdominant $m = \ell - 1$ (odd-parity) modes are close to each other, and these slopes become somewhat closer as ℓ increases. This property is reproduced by the analytical $\rho_{\ell m}$'s

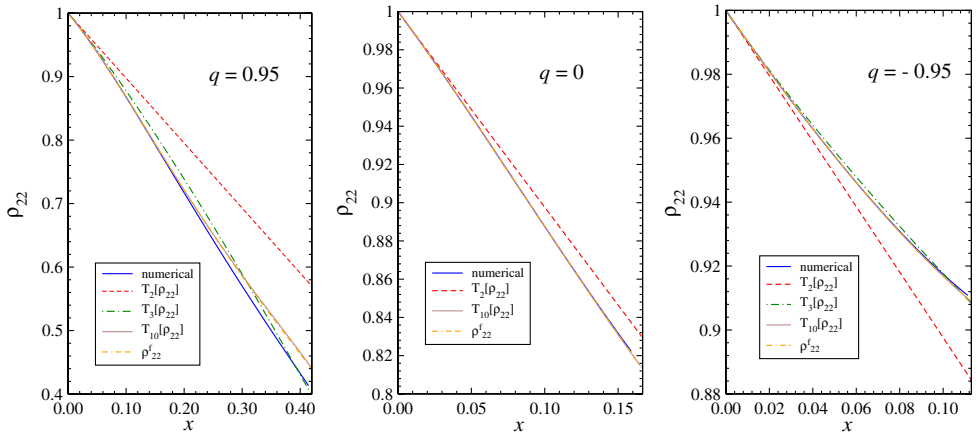

FIG. 4 (color online). Numerical and analytical ρ_{22}'s as functions of $x = v^2$. The three panels are for spin values $q = 0.95$, 0, and -0.95. The notation of the analytical ρ_{22} models follows the definition in Sec. III B. The $T_{10}[\rho_{22}]$ and ρ^f_{22} lines overlap with each other, and in the $q = 0$ case they also overlap with the numerical ρ_{22}.

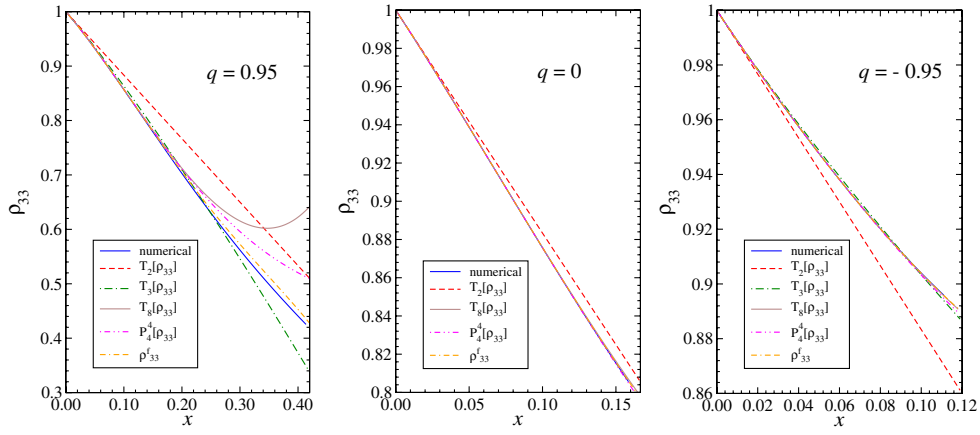

FIG. 5 (color online). Numerical and analytical ρ_{33}'s as functions of $x = v^2$. The three panels are for spin values $q = 0.95$, 0, and -0.95. The notation of the analytical ρ_{33} models follows the definition in Sec. III B. In the antialigned $q = -0.95$ case, the numerical, $T_8[\rho_{33}]$, and ρ^f_{33} lines overlap, while in the nonspinning $q = 0$ case, they also overlap with $P^4_4[\rho_{33}]$.

truncated at 1.5PN order through $\ell = 6$ modes, whose 1.5PN terms are known.

In Figs. 4 and 5, we compare the numerical and analytical ρ_{22} and ρ_{33}, respectively. We use the following notation for the analytical models. We indicate with $\mathrm{T_N}[\rho_{\ell m}]$ the $\rho_{\ell m}$ expanded in Taylor series of v through v^N. We indicate with $\mathrm{P^M_N}[\rho_{\ell m}]$ the Padé-summed $\rho_{\ell m}$ with M and N denoting the order of the polynomial in v in the numerator and denominator, respectively. When applying the Padé summation in presence of logarithms (i.e., $\log(v)$) we treat the latter as constants. We indicate with $\rho^f_{\ell m}$ an improved resummation of the Taylor-expanded $\rho_{\ell m}$'s, which consists in factoring out their 0.5PN, 1PN, and 1.5PN order terms, that is we write

$$\rho^f_{\ell m} = (1 + c^{\ell m}_{1/2} v + c^{\ell m}_1 v^2 + c^{\ell m}_{3/2} v^3)(1 + d^{\ell m}_2 v^4 + \cdots), \tag{35}$$

where the coefficients $c^{\ell m}_{1/2}$, $c^{\ell m}_1$, and $c^{\ell m}_{3/2}$ are the 0.5PN, 1PN, and 1.5PN order terms in the $\rho_{\ell m}$, and the coefficients $d^{\ell m}_i$ with $i \geq 2$ in Eq. (35) are obtained by imposing that the Taylor-expanded $\rho^f_{\ell m}$ coincides with $\rho_{\ell m}$. We shall motivate the introduction of the $\rho^f_{\ell m}$'s in the discussion below, but basically we find that the first factor on the right-hand side of Eq. (35) can capture reasonably well the zeros of the numerical (exact) $\rho_{\ell m}$'s.

For the modes $\ell < 4$, we find the following $\rho^f_{\ell m}$'s:

$$\begin{aligned}\rho^f_{22} = {} & \left(1 - \frac{43}{42}v^2 - \frac{2q}{3}v^3\right)\left[1 + \left(\frac{q^2}{2} - \frac{20555}{10584}\right)v^4 - \frac{34q}{21}v^5 + \left(-\frac{428\,\mathrm{eulerlog}_2(v^2)}{105} + \frac{109q^2}{126} + \frac{656928119}{61122600}\right)v^6\right. \\ & + \left(\frac{2q^3}{3} - \frac{14069q}{7938}\right)v^7 + \left(-\frac{q^4}{8} + \frac{4751q^2}{7056} + \frac{6877264829389}{800950550400}\right)v^8 + \left(-\frac{856\,\mathrm{eulerlog}_2(v^2)q}{315} + \frac{34q^3}{27}\right. \\ & \left.\left. + \frac{245281097q}{45841950}\right)v^9 + \left(\frac{439877\,\mathrm{eulerlog}_2(v^2)}{55566} + \frac{319q^4}{1008} - \frac{1312819q^2}{2667168} - \frac{179558258690231}{8409980779200}\right)v^{10}\right],\end{aligned} \tag{36a}$$

$$\begin{aligned}\rho^{fL}_{21} = {} & \left[1 - \frac{3q}{4}v + \left(-\frac{9q^2}{32} - \frac{59}{56}\right)v^2 + \left(\frac{1177q}{672} - \frac{27q^3}{128}\right)v^3\right]\left[1 + \left(-\frac{405q^4}{2048} - \frac{865q^2}{1792} - \frac{47009}{56448}\right)v^4 + \left(-\frac{729q^5}{2048}\right.\right. \\ & \left. - \frac{141q^3}{1792} - \frac{12137q}{6272}\right)v^5 + \left(-\frac{107\,\mathrm{eulerlog}_1(v^2)}{105} - \frac{18225q^6}{32768} - \frac{9477q^4}{57344} + \frac{2534545q^2}{903168} + \frac{2662510933}{1303948800}\right)v^6 \\ & + \left(-\frac{54675q^7}{65536} + \frac{837q^5}{114688} - \frac{734519q^3}{602112} - \frac{1240566577q}{521579520}\right)v^7 + \left(-\frac{321\,\mathrm{eulerlog}_1(v^2)q^2}{1120} - \frac{898857q^8}{1048576} - \frac{4617q^6}{229376}\right. \\ & \left. - \frac{915459q^4}{1605632} + \frac{139532257q^2}{27165600} + \frac{1799642241599}{2071144857600}\right)v^8 + \left(-\frac{963\,\mathrm{eulerlog}_1(v^2)q^3}{2240} + \frac{125939\,\mathrm{eulerlog}_1(v^2)q}{70560}\right. \\ & \left. - \frac{1043199q^9}{1048576} + \frac{12393q^7}{262144} + \frac{380169q^5}{3211264} - \frac{107920920827q^3}{41726361600} - \frac{494887939808057q}{91130373734400}\right)v^9 \\ & + \left(-\frac{2889\,\mathrm{eulerlog}_1(v^2)q^4}{7168} + \frac{195061\mathrm{eulerlog}_1(v^2)q^2}{188160} + \frac{5029963\,\mathrm{eulerlog}_1(v^2)}{5927040} - \frac{39031389q^{10}}{33554432} + \frac{34610733q^8}{58720256}\right. \\ & \left. - \frac{18644823q^6}{51380224} + \frac{7997241271q^4}{14836039680} + \frac{838234689365819q^2}{145808597975040} - \frac{1133240747153}{386613706752}\right)v^{10}\Bigg],\end{aligned} \tag{36b}$$

$$\begin{aligned}\rho^f_{33} = {} & \left(1 - \frac{7}{6}v^2 - \frac{2q}{3}v^3\right)\left[1 + \left(\frac{q^2}{2} - \frac{6719}{3960}\right)v^4 - \frac{4q}{3}v^5 + \left(-\frac{26\,\mathrm{eulerlog}_3(v^2)}{7} + \frac{13q^2}{18} + \frac{688425313}{56756700}\right)v^6\right. \\ & \left. + \left(\frac{2q^3}{3} - \frac{1073q}{1188}\right)v^7 + \left(\frac{7066253659}{951350400} - \frac{5q^2}{108}\right)v^8\right],\end{aligned} \tag{36c}$$

$$\begin{aligned}\rho^{fL}_{32} = {} & \left(1 - \frac{164}{135}v^2 + \frac{2q}{9}v^3 + \left(\frac{q^2}{3} - \frac{180566}{200475}\right)v^4\right)\left[1 - \frac{2788q}{1215}v^5 + \left(-\frac{104\,\mathrm{eulerlog}_2(v^2)}{63} + \frac{488q^2}{405} + \frac{5849948554}{940355325}\right)v^6\right. \\ & \left. - \frac{457232q}{164025}v^7 + \left(\frac{107912q^2}{54675} + \frac{3002382469466}{731462106375}\right)v^8\right],\end{aligned} \tag{36d}$$

$$\rho^f_{31} = \left(1 - \frac{13}{18}v^2 - \frac{2q}{3}v^3\right)\left[1 + \left(\frac{101}{7128} - \frac{5q^2}{6}\right)v^4 + \frac{4q}{9}v^5 + \left(\frac{2942362219}{1532430900} - \frac{26\,\mathrm{eulerlog}_1(v^2)}{63} - \frac{19q^2}{18}\right)v^6 - \left(\frac{4q^3}{9} + \frac{1625q}{10692}\right)v^7 + \left(\frac{16469528659}{8562153600} - \frac{151q^2}{324}\right)v^8\right], \tag{36e}$$

$$\rho^f_{44} = \left(1 - \frac{269}{220}v^2\right)\left[1 - \frac{2q}{3}v^3 + \left(\frac{q^2}{2} - \frac{14210377}{8808800}\right)v^4 - \frac{683q}{330}v^5 - \left(\frac{12568\,\mathrm{eulerlog}_4(v^2)}{3465} - \frac{1319q^2}{1980} - \frac{7216765000811}{549404856000}\right)v^6\right], \tag{36f}$$

$$\rho^{fL}_{43} = 1 - \frac{111}{88}v^2 + \left(\frac{3q^2}{8} - \frac{6894273}{7047040}\right)v^4 - \frac{12113q}{6160}v^5 + \left(\frac{1664224207351}{195343948800} - \frac{1571\,\mathrm{eulerlog}_3(v^2)}{770}\right)v^6, \tag{36g}$$

$$\rho^{fL}_{42} = \left(1 - \frac{191}{220}v^2 - \frac{2q}{3}v^3\right)\left[1 + \left(\frac{q^2}{2} - \frac{3190529}{8808800}\right)v^4 - \frac{7q}{110}v^5 + \left(-\frac{3142\,\mathrm{eulerlog}_2(v^2)}{3465} + \frac{2021q^2}{1980} + \frac{1947834451721}{549404856000}\right)v^6\right], \tag{36h}$$

$$\rho^{fL}_{41} = \left(1 - \frac{301}{264}v^2 + \left(\frac{3q^2}{8} - \frac{7775491}{21141120}\right)v^4\right)\left[1 + \left(-\frac{5q^3}{6} - \frac{20033q}{55440}\right)v^5 + \left(\frac{1227423222031}{1758095539200} - \frac{1571\,\mathrm{eulerlog}_1(v^2)}{6930}\right)v^6\right]. \tag{36i}$$

We notice that for a few modes, it is convenient to factor out even the 2PN order term. The procedure of factoring out zeros of $\rho_{\ell m}$ can be improved in the future by introducing appropriate adjustable parameters and calibrate them to the numerical result.

In Figs. 4 and 5, we also show results when adopting the Padé summation. We find that the diagonal and nearest-diagonal Padé summation improve the agreement with the numerical results not only for the (3,1) mode but also for the (3,1) and (4,2) modes. An even better agreement for several modes is obtained when using the farthest-diagonal Padé summation. However, this quite interesting result suffers by the presence of spurious poles appearing for several q values, and for this reason we will no longer discuss the Padé-summation in this paper.

Finally, we observe that close to the LSO the even-parity modes ρ^L agree slightly better to the numerical results than ρ^H's. Thus, we adopt in this paper the multipolar waveforms built with the ρ^L. In Figs. 6–8, we compare the Taylor-expanded, ρ^f-resummed, and numerical Newtonian-normalized multipolar amplitudes for the dominant modes. In general, the ρ^f and ρ-resummed amplitudes agree better with the numerical amplitudes than Taylor-expanded amplitudes do, especially for higher-order modes. More specifically, we find that ρ-resummed amplitudes (not shown in Figs. 6–8) differ from the numerical ones by $\lesssim 0.6\%$ up to $v \leq 0.4$ for the (2,2), (2,1), and (3,2) modes and by $\lesssim 1.8\%$ for the (3,3) and (4,4) modes. Their fractional difference grows up to $\sim$1–10 at the LSO when $q = 0.95$.

When applying the ρ^f resummation, we find that the fractional amplitude difference between the numerical and analytical (2,2) amplitude at the LSO is 16% (33%), 0.18% (0.32%), and 0.20% (0.85%) for $q = 0.95$, 0, -0.95, respectively. We indicated in parenthesis the numbers when Taylor-expanded amplitudes are employed. For the (2,1), (3,3), and (4,4) modes, for which fewer spin PN terms are known (see Table I), the improvement due to the ρ^f resummation is more striking. In fact, for the (2,1), (3,3), and (4,4) modes, we obtain a fractional amplitude difference of 2.4% (4.2), 0.2%(0.58%), and 0.0036%(0.15%); 7.5%(2), 0.027%(0.55%), and 0.13%(0.2%); 16%(7.5), 1.7%(28%), and 0.6%(5.8%), for $q = 0.95$, 0, -0.95, respectively.

We summarize the results of Figs. 6–8 as follows. First, we remark that the Taylor-expanded amplitudes agree with the numerical ones quite well for the (2,2) mode where the PN expansion is known through the highest order today (5.5 PN for nonspinning terms and 4PN for spin terms). Thus, for the (2,2) mode, the improvement due to the resummation technique is marginal. We expect that a similar result holds for higher modes when sufficient PN terms are known. Second, the factorized resummed waveforms consistently improve the amplitude agreement with numerical waveforms for several values of q and large spanning of v. In the lower panels of Figs. 6–8, we observe that the fractional amplitude difference between the numerical and ρ^f-resummed waveforms is always smaller than the difference between the numerical and Taylor-expanded waveforms, except around the v values where the numerical and Taylor-expanded amplitudes coincide. For all modes [except the (2,2) mode] and all spin values shown in the figures, we find that ρ^f-resummed amplitudes are typically closer to the

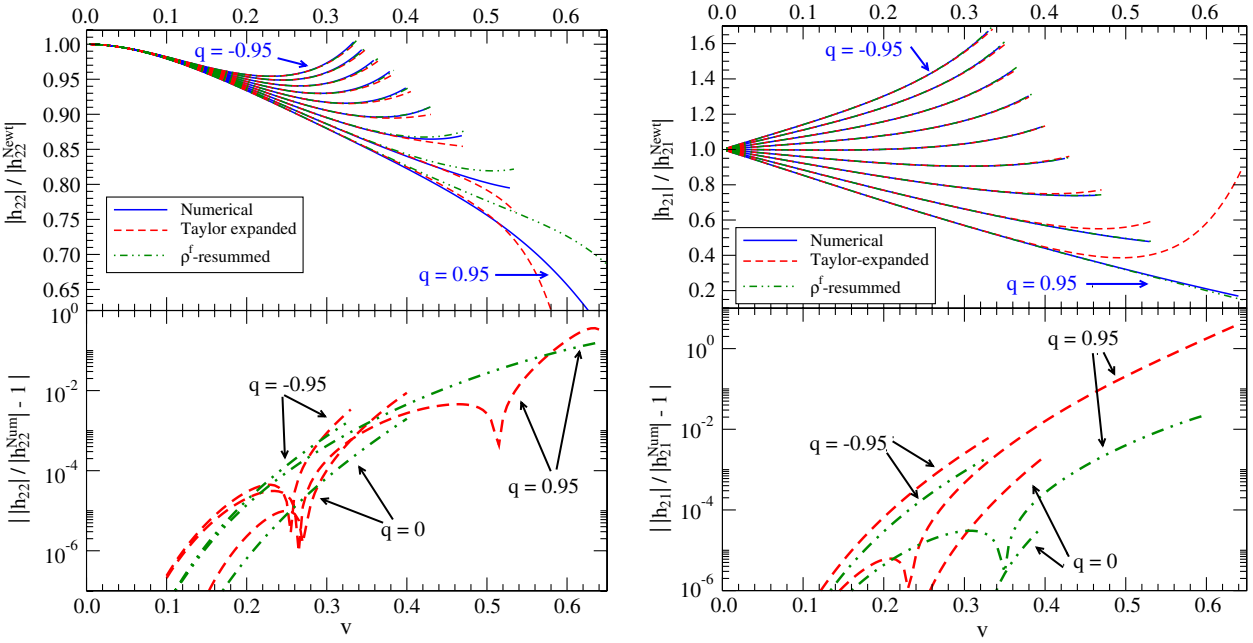

FIG. 6 (color online). Upper panel: Comparison between the numerical and analytical Newtonian-normalized $|h_{22}|$ and $|h_{21}|$ modes for a test particle orbiting around a Kerr black hole in the equatorial plane. For the numerical data and analytical models (Taylor expanded and ρ^f resummed), we have nine curves corresponding to different spin values of the Kerr black hole. From top to bottom, the spins are $q = -0.95$, -0.75, -0.5, -0.25, 0,0.25, 0.5, 0.75, and 0.95. Lower panel: relative fractional difference between analytical and numerical $|h_{\ell m}|$ for the representative spin values $q = -0.95$, 0, 0.95.

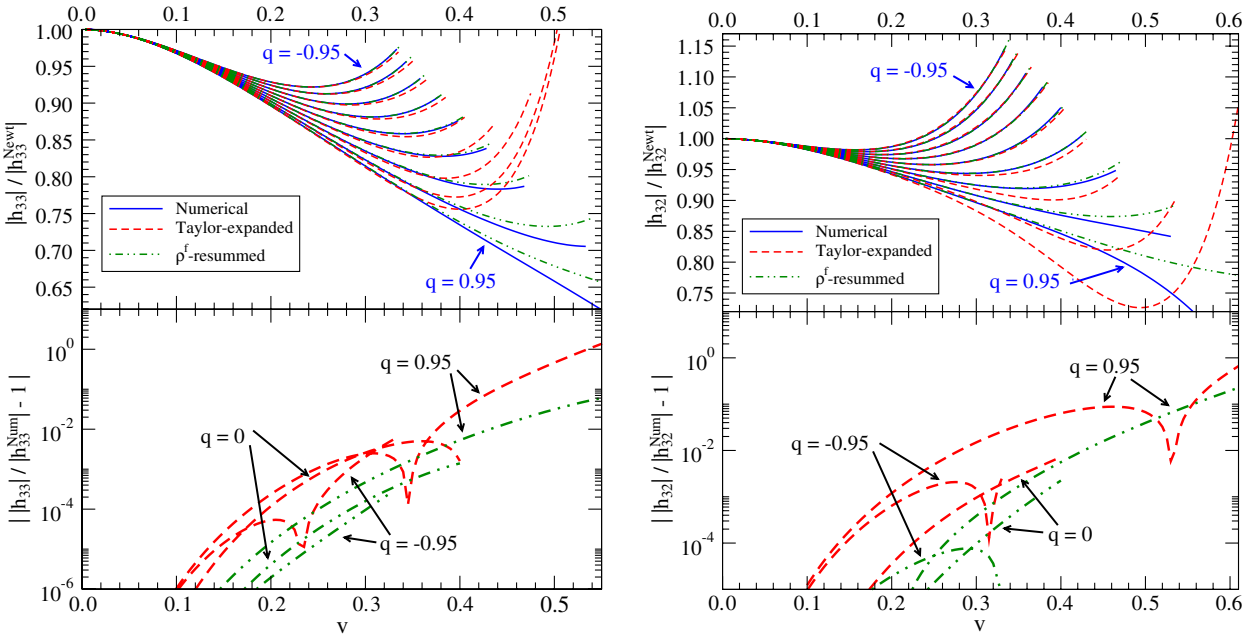

FIG. 7 (color online). Upper panel: Comparison between the numerical and analytical Newtonian-normalized $|h_{33}|$ and $|h_{32}|$ modes for a test particle orbiting around a Kerr black hole in the equatorial plane. For the numerical data and analytical models (Taylor expanded and ρ^f resummed), we have nine curves corresponding to different spin values of the Kerr black hole. From top to bottom, the spins are $q = -0.95$, -0.75, -0.5, -0.25, 0, 0.25, 0.5, 0.75, and 0.95. Lower panel: relative fractional difference between analytical and numerical $|h_{\ell m}|$ for the representative spin values $q = -0.95$, 0, 0.95.

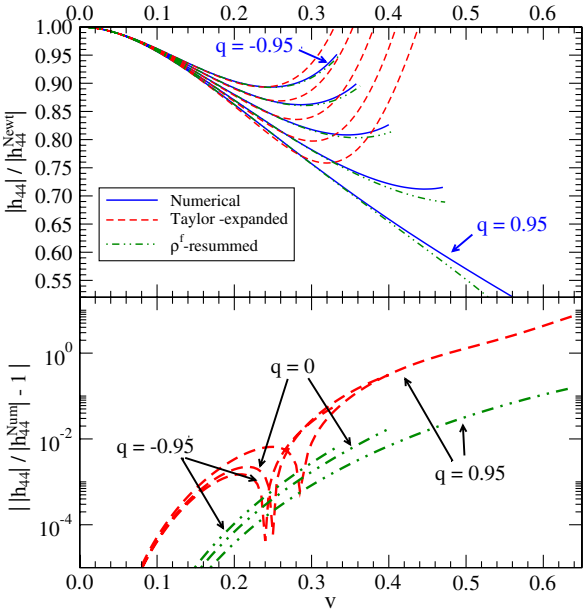

FIG. 8 (color online). Upper panel: Comparison between the numerical and analytical Newtonian-normalized $|h_{44}|$ mode for a test particle orbiting around a Kerr black hole in the equatorial plane. For the numerical data and analytical models (Taylor expanded and ρ^f resummed), we have four curves corresponding to different spin values of the Kerr black hole. From top to bottom, the spins are $q = -0.95$, -0.5, 0, 0.5, and 0.95. Lower panel: relative fractional difference between analytical and numerical $|h_{\ell m}|$ for the representative spin values $q = -0.95$, 0, and 0.95.

numerical amplitudes than Taylor expanded are by an order of magnitude or more.

Finally, for $\ell \geq 5$ modes, the ρ^f resummation is not very successful in modeling the numerical amplitudes but it is better than Taylor-expanded amplitudes. We know nonspinning and spin corrections only through 2.5PN order in the (5,5) mode (see Table I); thus it is not surprising that we cannot model those modes very well. Since the contribution of the $\ell \geq 5$ modes to the radiation power and strain amplitude is not negligible, it would be very useful to calculate higher-order corrections in those modes in the future.

C. Comparison between analytical and numerical energy fluxes

Here we compare numerical and analytical Newtonian-normalized energy fluxes for a test particle orbiting a Kerr black hole in the equatorial plane. The fluxes are computed by summing the power radiated using Eq. (30) and setting $\ell = 8$. For a test particle moving along a quasicircular equatorial orbit, the Newtonian-normalized flux is $F(v)/F_{\rm Newt}(v)$, where $F_{\rm Newt}(v) = 32\nu^2 v^{10}/5$.

We note that the dominant error source of the numerical calculation of the total flux is the truncation at $\ell = 8$ of the mode summation. Let $F_{\ell=8}(v)$ be the contribution from $\ell = 8$ mode for $F(v)$. The fraction, $F_{\ell=8}(v)/F(v)$, is about 10^{-10} around $v = 0.1$ and 10^{-5} to 10^{-2} around the LSO.

In Fig. 9, we compare numerical and analytical Newtonian-normalized energy fluxes for different spin values of the Kerr black hole. In the left panel of Fig. 9, we consider two Taylor-expanded fluxes computed from the Taylor-expanded $h_{\ell m}$'s: one that truncates all terms beyond 5.5PN order and spin terms beyond 4PN order (Taylor expanded truncated), and one that keeps all higher-order terms (Taylor expanded nontruncated). [The former is the Taylor-expanded flux that consistently includes nonspinning effects through 5.5PN order and spin effects through 4PN order [12,13]; the latter includes new higher-order PN terms computed by Tagoshi and Fujita [14].]

In the left panel of Fig. 9, we do not show the Taylor-expanded flux truncated at 4PN order [13] since its agreement with the numerical flux is rather poor. Figures 2 and 3 of Ref. [33] show that in this case the Taylor-expanded flux starts to differ from the numerical one at a relatively low velocity of $v = 0.2$ for all spin values. By contrast, the agreement is substantially improved when we include the 5.5PN order nonspinning terms in the Taylor-expanded-truncated flux. The Taylor-expanded-nontruncated flux agrees better with the numerical flux than the Taylor-expanded-truncated flux for retrograde orbits with $q < 0$, while its agreement is worse for prograde orbits with $q > 0$. For spin values $q > 0.5$, the agreement is especially bad, as the Taylor-nontruncated flux grows too fast when $v > 0.4$. We find that this difference is mainly due to the large new spin term [14] in the (3,3) mode, i.e. $(-q^2 + 9\pi q^2/2 + q89/5)v^7$ in $\hat{Z}_{33\omega_0}$ (real part only). Without any resummation, the Taylor-expanded-truncated flux agrees

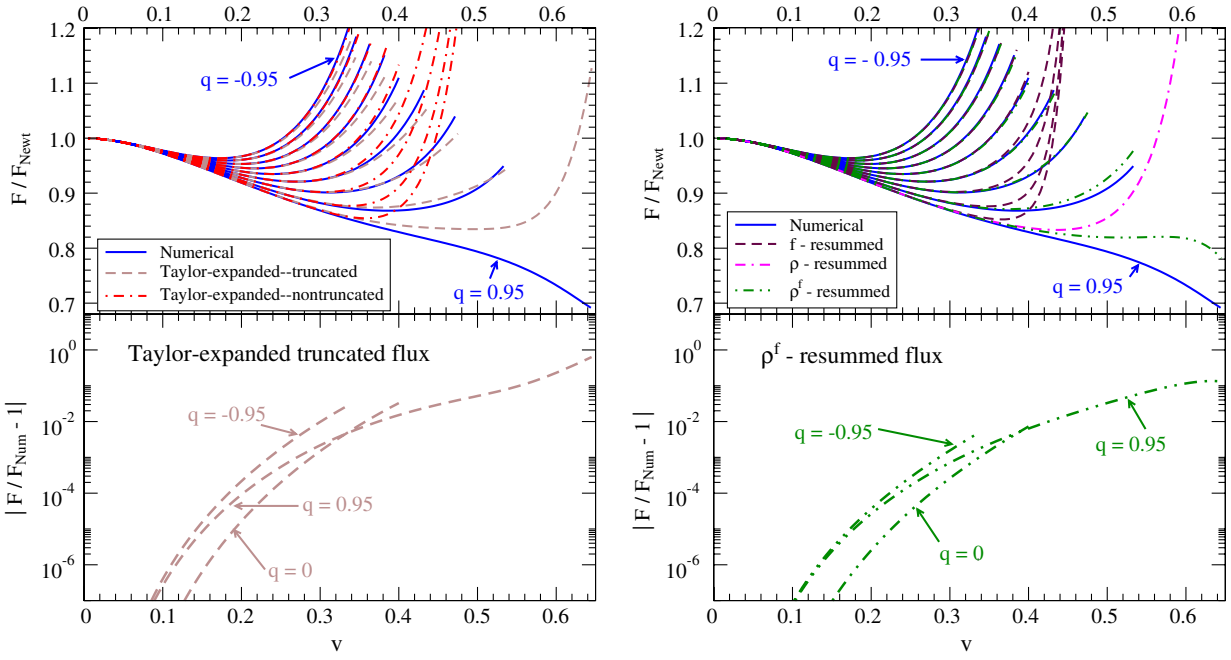

FIG. 9 (color online). Upper panels: Comparison between the numerical and analytical Newtonian-normalized energy flux for a test particle orbiting a Kerr black hole in the equatorial plane. There are nine curves for each waveform's model and numerical data. They correspond to different spins of the Kerr black hole. From top to bottom, the spins are $q = -0.95$, -0.75, -0.5, -0.25, 0, 0.25, 0.5, 0.75, and 0.95. The Taylor-expanded-truncated flux includes test-particle spin terms through 4PN order [13] and nonspinning terms through 5.5PN order [12]. The Taylor-expanded-nontruncated flux includes higher-order PN terms originated by the new PN terms in the $h_{\ell m}$'s computed by Tagoshi and Fujita [14] (see Table I). The ρ-resummed flux is plotted for one spin value $q = 0.95$ in the upper right panel, to show the large improvement when using ρ^f-resummed instead of ρ-resummed flux. Lower panels: fractional difference between the numerical and analytical energy fluxes for the representative spin cases: $q = -0.95$, 0, 0.95.

well with the numerical flux for all spin values except for $q = 0.95$. The lower left panel shows that the fractional differences between the numerical and the Taylor-expanded-truncated fluxes are below 1% until $v = 0.3$ and are below 10% for $q = 0.95$ until $v = 0.55$ and below 10% for all other spin values until the LSO.

In the right panel of Fig. 9, we consider three analytical flux models which use the $f_{\ell m}$, $\rho_{\ell m}$ (for $q = 0.95$ only), and $\rho^f_{\ell m}$, respectively. The fractional difference between the numerical flux and f, ρ, or ρ^f-resummed fluxes is $<0.3\%$ for all spin values when $v < 0.3$. Larger differences appear only when $v > 0.3$ for large and aligned spins, and the f-resummed flux performs especially bad when $v > 0.4$. In the case of $q = 0.95$, we show the significant improvements achieved from the f-resummed to the ρ-resummed and eventually to the ρ^f-resummed flux. The fractional difference with numerical flux at the LSO is reduced from $\sim 3.5 \times 10^4$ to ~ 3 to 13%. The main reason for the bad performance of the f-resummed flux is caused by the new spin term [14] in the (3,3) mode, i.e. $(-q^2 + 9\pi q^2/2 + q89/5)v^7$ in $\hat{Z}_{33\omega_0}$ (real part only), as is in the case of the Taylor-expanded-nontruncated flux. As a matter of fact, we notice that if we did not include this new term computed in Ref. [14] and applied the f resummation, or the ρ resummation only to the nonspinning terms [19,34], we would find a flux not very different from the ρ-resummed flux in the right panel of Fig. 9. In the ρ or ρ^f resummation, this new term is suppressed by an order of magnitude, which leads to the improvements in their performance in modeling the numerical flux. Specifically, this term becomes $(q6187/330 - q^3)v^7$ in f_{33}, $(q5297/2970 + q^3/3)v^7$ in ρ_{33}, and $(-q1073/1188 + q^3 2/3)v^7$ in ρ^f_{33}.

Finally, for large aligned spin $q = 0.95$ at the LSO, the ρ^f-resummed flux is closer to the numerical flux than the Taylor-expanded-truncated flux. Furthermore, we want to emphasize that the ρ^f resummation improves the Taylor-expanded flux substantially over a large range of v and spin values. The differences between numerical and ρ^f-resummed fluxes are smaller than those between the numerical and Taylor-expanded-truncated fluxes, by a factor of 3–5 at low velocities. Considering the large number of orbits an extreme mass-ratio binary spends in this range of velocities or frequencies, such an improvement is indeed significant in correcting the orbital dynamics (see Ref. [35] for a quantitative analysis in the nonspinning case).

IV. FACTORIZED MULTIPOLAR WAVEFORMS FOR GENERIC MASS-RATIO SPINNING, NONPRECESSING BLACK HOLES

In this section, we extend the calculation of Sec. II to generic mass-ratio spinning, nonprecessing black-hole binaries.

In Ref. [22,23], the nonspinning Taylor-expanded multipolar waveforms were computed through 3PN order. In Ref. [25], spinning Taylor-expanded multipolar waveforms were computed through 1.5PN order. Using the definitions

$$M \equiv m_1 + m_2 \tag{37a}$$

$$\delta m \equiv m_1 - m_2, \tag{37b}$$

$$\chi_S \equiv \frac{1}{2}\left(\frac{S_1}{m_1^2} + \frac{S_2}{m_2^2}\right), \tag{37c}$$

$$\chi_A \equiv \frac{1}{2}\left(\frac{S_1}{m_1^2} - \frac{S_2}{m_2^2}\right), \tag{37d}$$

and restricting ourselves to circular, equatorial orbits, we obtain the following modes decomposed with respect to -2 spin-weighted spherical harmonics

$$h_{22} = -8\sqrt{\frac{\pi}{5}}\frac{\nu M}{R}e^{-2i\phi}v^2\left\{1 - \left(\frac{107}{42} - \frac{55}{42}\nu\right)v^2 + \left[2\pi + 12i\log\left(\frac{v}{v_0}\right) - \frac{4}{3}(1-\nu)\chi_S - \frac{4}{3}\frac{\delta m}{M}\chi_A\right]v^3\right\}, \tag{38a}$$

$$h_{21} = -\frac{8i}{3}\sqrt{\frac{\pi}{5}}\frac{\nu\delta m}{R}e^{-i\phi}v^3\left[1 - \left(\frac{3}{2}\chi_S + \frac{3}{2}\frac{M}{\delta m}\chi_A\right)v\right], \tag{38b}$$

$$h_{33} = 3i\sqrt{\frac{6\pi}{7}}\frac{\nu\delta m}{R}e^{-3i\phi}v^3\left\{1 - (4-2\nu)v^2 + \left[3\pi - \frac{21i}{5} + 6i\log\frac{3}{2} + 18i\log\left(\frac{v}{v_0}\right) - \left(2 - \frac{5}{2}\nu\right)\chi_S - \left(2 - \frac{19}{2}\nu\right)\frac{M}{\delta m}\chi_A\right]v^3\right\}, \tag{38c}$$

$$h_{32} = -\frac{8}{3}\sqrt{\frac{\pi}{7}}\frac{\nu M}{R}e^{-2i\phi}v^4(1 - 3\nu + 4\nu\chi_S v), \tag{38d}$$

$$h_{31} = -\frac{i}{3}\sqrt{\frac{2\pi}{35}}\frac{\nu\delta m}{R}e^{-i\phi}v^3\left\{1 - \left(\frac{8}{3} + \frac{2}{3}\nu\right)v^2 + \left[\pi - \frac{7i}{5} - 2i\log 2 + 6i\log\left(\frac{v}{v_0}\right) - \left(2 - \frac{13}{2}\nu\right)\chi_S - \left(2 - \frac{11}{2}\nu\right)\frac{M}{\delta m}\chi_A\right]v^3\right\}, \tag{38e}$$

$$h_{44} = \frac{64}{9}\sqrt{\frac{\pi}{7}}\frac{\nu M}{R}e^{-4i\phi}v^4\left\{1 - 3\nu + \left[\left(-\frac{8}{3} + \frac{164}{15}\nu - \frac{56}{5}\nu^2\right)\chi_S + \left(-\frac{8}{3} + \frac{52}{5}\nu\right)\frac{\delta m}{M}\chi_A\right]v^3\right\}, \tag{38f}$$

$$h_{43} = \frac{9i}{5}\sqrt{\frac{2\pi}{7}}\frac{\nu\delta m}{R}e^{-3i\phi}v^5\left[1 - 2\nu + \left(\frac{5}{2}\nu\chi_S - \frac{5}{2}\nu\frac{M}{\delta m}\chi_A\right)v\right], \tag{38g}$$

$$h_{42} = -\frac{8}{63}\sqrt{\pi}\frac{\nu M}{R}e^{-2i\phi}v^4\left\{1 - 3\nu + \left[\left(-\frac{8}{3} + \frac{236}{15}\nu - \frac{104}{5}\nu^2\right)\chi_S + \left(-\frac{8}{3} + \frac{28}{5}\nu\right)\frac{\delta m}{M}\chi_A\right]v^3\right\}, \tag{38h}$$

$$h_{41} = -\frac{i}{105}\sqrt{2\pi}\frac{\nu\delta m}{R}e^{-i\phi}v^5\left[1 - 2\nu + \left(\frac{5}{2}\nu\chi_S - \frac{5}{2}\nu\frac{M}{\delta m}\chi_A\right)v\right]. \tag{38i}$$

The 1.5PN, 0.5PN, and 1PN order spin terms in the modes h_{22}, h_{21}, h_{33}, respectively, were obtained in Ref. [25]. The 1.5PN-order (0.5PN-order) spin terms in the even (odd) parity modes are computed in Appendix F. The higher-order nonspinning PN terms can be found in Refs. [6,22,23].

To compute the factorized multipolar waveforms for generic mass ratios, we use Eq. (2). For the source terms $\hat{S}_{\rm eff}^{(\epsilon_p)}$, we employ the energy and angular momentum for circular, equatorial orbits computed from the effective-one-body Hamiltonian of Ref. [36] (at the PN order at which we derive the factorized modes, the Taylor-expanded Hamiltonian of Ref. [36] coincides with the Hamiltonian of Ref. [37]). More explicitly, when expanding the effective-one-body energy and angular momentum for circular, equatorial orbits through 1.5PN order, we find

$$\frac{E(v)}{\mu} = 1 - \frac{\nu}{2}v^2\left\{1 - \frac{(9+\nu)}{12}v^2 + \frac{8}{3}\left[\left(1 - \frac{1}{4}\nu\right)\chi_S + \frac{\delta m}{M}\chi_A\right]v^3\right\}, \tag{39}$$

and

$$\frac{L(v)}{\mu} = \nu v^{-1}\left\{1 + \left[\frac{9+\nu}{6} - \nu\left(1 - \frac{1}{4}\nu\right)\chi_S - \nu\frac{\delta m}{M}\chi_A\right]v^2 - \frac{7}{3}\left[\left(1 - \frac{1}{4}\nu\right)\chi_S + \frac{\delta m}{M}\chi_A\right]v^3\right\}. \tag{40}$$

Eqs. (39) and (40) are sufficient for computing the quantity $f_{\ell m}$ in Eq. (2). In fact, similarly to the test-particle case analyzed in Sec. II, the factor $T_{\ell m}$ in the generic mass-ratio case is not modified by spin effects. The factor $\delta_{\ell m}$ is not modified by spin effects either since there are no imaginary

spin terms in Eqs. (38a)–(38i). The nonspinning $\delta_{\ell m}$ expressions for generic mass ratios are given in Eqs. (20)–(29) of Ref. [6]. Thus, inserting Eqs. (39) and (40) in Eq. (2), and using Eqs. (38a)–(38i), we derive the even-parity $f_{\ell m}$ and $\rho_{\ell m}$ and odd-parity $f^L_{\ell m}$ and $\rho^L_{\ell m}$ up to the highest PN accuracy known today. We obtain

$$f_{22} = 1 + \frac{1}{42}(55\nu - 86)v^2 - \frac{4}{3}\left[(1-\nu)\chi_S + \frac{\delta m}{M}\chi_A\right]v^3, \tag{41a}$$

$$f^L_{21} = 1 - \frac{3}{2}\left(\chi_S + \frac{M}{\delta m}\chi_A\right)v, \tag{41b}$$

$$f_{33} = 1 + \left(2\nu - \frac{7}{2}\right)v^2 - \left[\left(2 - \frac{5}{2}\nu\right)\chi_S + \left(2 - \frac{19}{2}\nu\right)\frac{M}{\delta m}\chi_A\right]v^3, \tag{41c}$$

$$f^L_{32} = 1 - \frac{4\nu}{3\nu - 1}\chi_S v, \tag{41d}$$

$$f_{31} = 1 + \left(-\frac{2}{3}\nu - \frac{13}{6}\right)v^2 - \left[\left(2 - \frac{13}{2}\nu\right)\chi_S + \left(2 - \frac{11}{2}\nu\right)\frac{M}{\delta m}\chi_A\right]v^3, \tag{41e}$$

$$f_{44} = 1 - \frac{2625\nu^2 - 5870\nu + 1614}{330(1-3\nu)}v^2 - \frac{4}{15}\left[\frac{42\nu^2 - 41\nu + 10}{1-3\nu}\chi_S + \frac{10 - 39\nu}{1-3\nu}\delta m\chi_A\right]v^3, \tag{41f}$$

$$f^L_{43} = 1 - \frac{5\nu}{2(2\nu-1)}\left(\chi_S - \frac{M}{\delta m}\chi_A\right)v, \tag{41g}$$

$$f_{42} = 1 - \frac{285\nu^2 - 3530\nu + 1146}{330(1-3\nu)}v^2 - \frac{4}{15}\left[\frac{78\nu^2 - 59\nu + 10}{1-3\nu}\chi_S + \frac{10 - 21\nu}{1-3\nu}\delta m\chi_A\right]v^3, \tag{41h}$$

$$f^L_{41} = 1 - \frac{5\nu}{2(2\nu-1)}\left(\chi_S - \frac{M}{\delta m}\chi_A\right)v, \tag{41i}$$

and

$$\rho_{22} = 1 + \frac{1}{84}(55\nu - 86)v^2 - \frac{2}{3}\left[(1-\nu)\chi_S + \frac{\delta m}{M}\chi_A\right]v^3, \tag{42a}$$

$$\rho^L_{21} = 1 - \frac{3}{4}\left(\chi_S + \frac{\delta m}{M}\chi_A\right)v, \tag{42b}$$

$$\rho_{33} = 1 + \left(\frac{2}{3}\nu - \frac{7}{6}\right)v^2 - \left[\left(\frac{2}{3} - \frac{5}{6}\nu\right)\chi_S + \left(\frac{2}{3} - \frac{19}{6}\nu\right)\frac{\delta m}{M}\chi_A\right]v^3, \tag{42c}$$

$$\rho^L_{32} = 1 - \frac{4\nu}{3(3\nu-1)}\chi_S v, \tag{42d}$$

$$\rho_{31} = 1 + \left(-\frac{2}{9}\nu - \frac{13}{18}\right)v^2 - \left[\left(\frac{2}{3} - \frac{13}{6}\nu\right)\chi_S + \left(\frac{2}{3} - \frac{11}{6}\nu\right)\frac{\delta m}{M}\chi_A\right]v^3, \tag{42e}$$

$$\rho_{44} = 1 - \frac{2625\nu^2 - 5870\nu + 1614}{1320(1-3\nu)}v^2 - \left[\frac{42\nu^2 - 41\nu + 10}{15(1-3\nu)}\chi_S + \frac{10 - 39\nu}{15(1-3\nu)}\delta m\chi_A\right]v^3, \tag{42f}$$

$$\rho^L_{43} = 1 - \frac{5\nu}{8(2\nu-1)}\left(\chi_S - \frac{\delta m}{M}\chi_A\right)v, \tag{42g}$$

$$\rho_{42} = 1 - \frac{285\nu^2 - 3530\nu + 1146}{1320(1-3\nu)}v^2 - \left[\frac{78\nu^2 - 59\nu + 10}{15(1-3\nu)}\chi_S + \frac{10 - 21\nu}{15(1-3\nu)}\delta m\chi_A\right]v^3, \tag{42h}$$

$$\rho^L_{41} = 1 - \frac{5\nu}{8(2\nu-1)}\left(\chi_S - \frac{\delta m}{M}\chi_A\right)v. \tag{42i}$$

We may use $E(r)$ instead of $|\boldsymbol{L}|$ as the source term in the odd-parity modes. However, there is no difference between f^L_{lm} and f^H_{lm}, and correspondingly between ρ^L_{lm} and ρ^H_{lm}, through PN orders where spin effects of binaries with generic mass ratio are known.

In the nonspinning case, using 1PN, 2PN, and 3PN corrections, it was shown [6] that the dependence of $\rho_{\ell m}$ on the mass-ratio ν is mild. As a consequence, it was considered meaningful to use test-particle results at PN

orders where generic mass-ratio results are unknown. Since for each mode only the leading-order generic mass-ratio spin terms are known, it is not possible to carry out an exhaustive study and understand how the spin terms in $\rho_{\ell m}$ depend on ν. As obtained in Appendix F, at leading order, the 0.5PN spin terms in the odd-parity modes are proportional to ν. Thus, they are zeros in the test-particle limit but finite in the comparable-mass case. Moreover, we find that the dependence on ν of the 1.5PN spin terms in the even-parity modes is not that simple. Depending on the values of χ_S and χ_A, the relative difference between $h^{(0),1.5\mathrm{PN}}_{\ell m}(\nu = 0.25)$ and $h^{(0),1.5\mathrm{PN}}_{\ell m}(\nu = 0)$ varies from zero to order of unity. Therefore, also the dependence of $h^{(0),1.5\mathrm{PN}}_{\ell m}$ on ν is not mild.

Nevertheless, it is still reasonable to include the test-particle limit spin terms in $f_{\ell m}$ and $\rho_{\ell m}$ such that at least part of the higher-order spin effects are included and to check the results against available numerical (exact) data. Specifically, we combine the test-particle and generic mass-ratio results by replacing all the test-particle terms in $f_{\ell m}$ and $\rho_{\ell m}$, whose generic mass-ratio counterparts are known with their generic expressions.

Thus, in the generic mass-ratio, spinning case, we propose to add to the $f_{\ell m}$'s and $\rho_{\ell m}$'s derived in this section the test-particle limit terms derived in Sec. II. In applying this procedure, we need to make a choice for the dimensionless spin variable q appearing in the test-particle limit $f_{\ell m}$'s and $\rho_{\ell m}$'s. For a black-hole binary with component masses m_1 and m_2 and spins χ_1 and χ_2, we consider here two possibilities motivated by the choice of the deformed-Kerr spin in the effective-one-body formalism. References [19,36] used for the deformed-Kerr spin

$$q_0 = \frac{|\boldsymbol{S}_0|}{M^2} = \frac{1}{M^2}\left|\left(1+\frac{m_2}{m_1}\right)\boldsymbol{S}_1 + \left(1+\frac{m_1}{m_2}\right)\boldsymbol{S}_2\right|, \\ = \sqrt{1-4\nu}\chi_A + \chi_S, \tag{43}$$

while Ref. [37] used the following deformed-Kerr spin

$$q_S = \frac{|\boldsymbol{S}|}{M^2} = \frac{1}{M^2}|\boldsymbol{S}_1 + \boldsymbol{S}_2| = \sqrt{1-4\nu}\chi_A + (1-2\nu)\chi_S. \tag{44}$$

Moreover, in the generic mass-ratio, spinning case, we also propose to use as effective sources in Eq. (2) the Hamiltonian and angular momentum for quasicircular orbits computed using the effective-one-body Hamiltonians [36,37].

In Fig. 10, we compare the amplitudes of the numerical, the Taylor-expanded and the ρ-resummed modes for the five most dominant modes and for the two configurations of equal-mass, equal-spin black-hole binaries of the Caltech-Cornell-CITA collaboration of Ref. [19,38]. We employ the effective sources built using the Hamiltonian and angular momentum for quasicircular orbits of

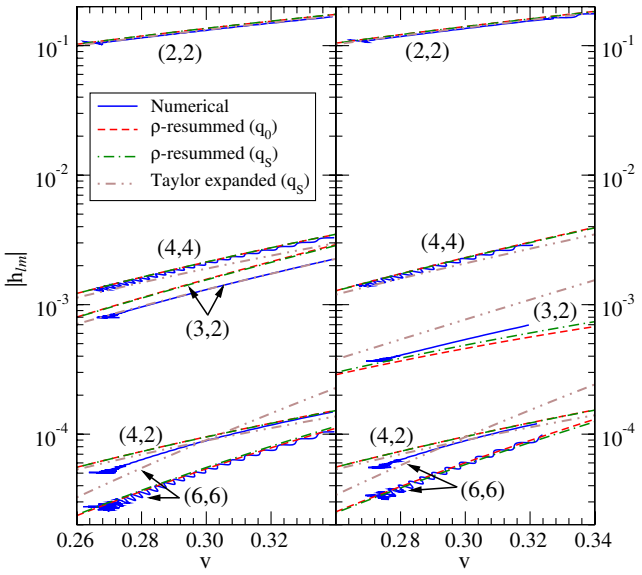

FIG. 10 (color online). Comparisons between the numerical, Taylor-expanded, and ρ-resummed amplitudes of the dominant modes for an equal-mass equal-spin black-hole binary as functions of the orbital velocity v. In the left panel, the component spins are $\chi_1 = \chi_2 = 0.43655$; in the right panel, the component spins are $\chi_1 = \chi_2 = -0.43757$. The numerical amplitudes were produced by the Caltech/Cornell/CITA collaboration.

Ref. [19,36]. The dimensionless spins in the two configurations are $\chi_1 = \chi_2 = 0.43655$ and $\chi_1 = \chi_2 = -0.43757$, respectively. The numerical amplitudes are derived from the numerical simulations published in Ref. [19]. Oscillations in the numerical amplitudes are due to numerical artifacts in the simulations. For the (2,2) mode, the Taylor-expanded amplitudes agree quite well with the numerical amplitude, at least up to the frequency considered. Thus, the improvement due to the ρ resummation is marginal. For higher-order modes, there are large differences between numerical and Taylor-expanded amplitudes, and we find a substantial improvement when we adopt the ρ resummation, except for the (3,3) mode in the spin aligned case ($\chi_1 = \chi_2 = 0.43655$), whose numerical and Taylor-expanded amplitudes overlap, likely by coincidence. For the (2,2), (4,4), and (6,6) modes, the relative difference between numerical and ρ-resummed amplitudes is within 5% [39]. For the (3,2) and (4,2) modes, the relative difference is between 10%–20%. We find that the results in Fig. 10 depend weakly on the choice of q. In fact, using $q = q_0$ defined in Eq. (43) and $q = q_S = q_0/2$ (when $\nu = 0.25$) defined in Eq. (44), the relative amplitude difference is $<2\%$ for the (2,2), (4,4), (4,2), and (6,6) modes and $\sim 5\%$ for the (3,2) mode. Therefore, the uncertainty in the ρ-resummed amplitude due to the choice of q is less than half their systematic difference from the numerical results.

Since we expect a stronger amplitude dependence on q in the case of larger spin magnitudes, we study the

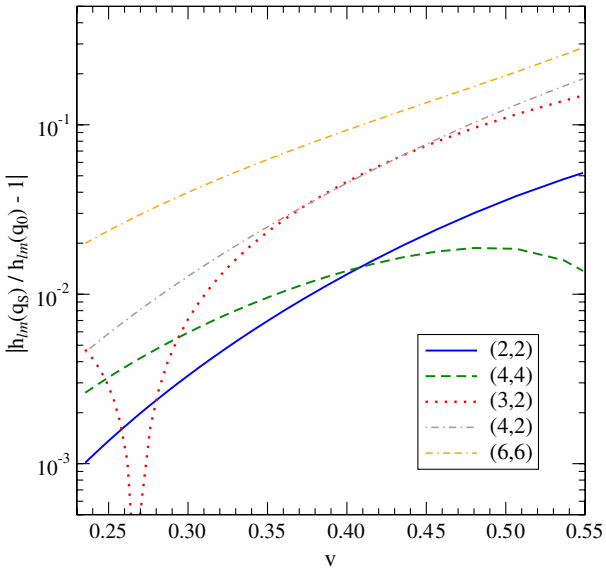

FIG. 11 (color online). Relative difference between ρ-resummed amplitudes of the dominant modes for an equal-mass, equal-spin black-hole binary when the test-particle spin is set to $q = q_0$ and $q = q_S$. The component spins of the binary are $\chi_1 = \chi_2 = 0.95$. The relative amplitude difference is plotted as a function of the orbital velocity v.

ρ-resummed amplitude dependence on the choice of q in Fig. 11, where we show the difference between the amplitudes $|h_{\ell m}(q = q_0)|$ and $|h_{\ell m}(q = q_S)|$ for an equal-mass, equal-spin black-hole binary with component spins $\chi_1 = \chi_2 = 0.95$. The relative amplitude differences are $<5\%$ for the dominating (2,2) and (4,4) modes and $<10\%$ for the weaker (3,2) and (4,2) modes at $v < 0.45$. For the (6,6) mode, since the test-particle spin terms in ρ_{66} are known only through 2PN order, i.e. only one more term is known beyond the generic mass-ratio results, the amplitude dependence on q is entirely determined by this term and is somewhat stronger—reaching 30% at the LSO.

Finally, we check the effect of the test-particle spin terms by comparing $|h_{\ell m}(q = q_0)|$ and $|h_{\ell m}(q = 0)|$ (i.e., removing the test-particle spin terms from the generic mass-ratio amplitudes in the latter) for this binary configuration. The difference, compared to Fig. 11, becomes larger by a factor of a few and reaches 10–25% for the (2,2), (4,4), (3,2), and (4,2) modes in the range of frequencies investigated in this paper. These terms may provide non-negligible corrections to the waveform and flux modeling.

V. CONCLUSIONS

In our study, we employed the spin PN multipolar waveforms derived and decomposed with respect to the -2 spin-weighted spheroidal harmonics in Ref. [13] and transformed them in -2 spin-weighted spherical harmonics. We also took advantage of the new, recently computed [14], higher-order nonspinning and spin PN contributions in several subdominant modes. We also augmented our knowledge of the higher-order spin terms for generic mass-ratios, computing the generic expressions for the half and one-and-half post-Newtonian contributions to the odd-parity (current) and even-parity (odd) multipoles, respectively, (see Appendix F).

Using the above results, we extended the resummation method of factorized multipolar waveforms introduced in Ref. [6] to spinning, nonprecessing black-hole binaries. This factorized multipolar decomposition consists in a multiplicative decomposition of the $h_{\ell m}$ waveform into the product of several factors corresponding to various physical effects and the replacement of the factor $f_{\ell m}$ by its ℓth root $\rho_{\ell m} = (f_{\ell m})^{1/\ell}$.

In the case of a nonspinning test particle orbiting a Kerr black hole in the equatorial plane, we found that the ρ resummation is quite effective in reproducing the numerical multipolar amplitudes and energy flux up to $q \geq 0.75$ and $v \geq 0.4$. However, for larger values of q, we observed that the analytical $\rho_{\ell m}(v)$'s either have a slope larger than the numerical one or they tend to grow as function of v instead of decreasing. This behavior can be cured by factoring out the lower-order PN terms in the $\rho_{\ell m}$, notably the 0.5PN, 1PN, and 1.5PN order terms. Being the lower-order PN terms negative (for $q > 0$), this procedure corresponds to factoring out the zeros of $\rho_{\ell m}$, which turns out to capture the numerical (exact) zeros.

When applying the ρ^f resummation, we found that the fractional amplitude difference between the numerical and analytical (2,2) mode at the LSO is 16% (33%), 0.18% (0.32%), and 0.20% (0.85%) for $q = 0.95$, 0, -0.95, respectively. We indicated in parenthesis the numbers when Taylor-expanded amplitudes are employed. Thus, we found that for the (2,2) mode the improvement of the resummation is marginal. This might be due to the fact that the (2,2) mode is known at rather high PN order (5.5 PN for nonspinning terms and 4PN for spin terms). For the (2,1), (3,3), and (4,4) modes, for which less spin PN terms are known (see Table I), the improvement due to the ρ^f resummation is even more striking. In fact, for those modes, we obtained a fractional amplitude differences 2.4% (4.2), 0.2% (0.58%), and 0.0036% (0.15%); 7.5% (2), 0.027% (0.55%), and 0.13% (0.2%); 16% (7.5), 1.7% (28%), and 0.6% (5.8%), for $q = 0.95$, 0, -0.95, respectively. For $\ell \geq 5$, the ρ^f-resummed amplitudes are certainly better than the Taylor-expanded amplitudes, but they differ from the numerical results quite substantially at high frequency. This is due to the fact that for those modes the spin effects are known only up to 2.5PN order or lower. In summary, we found that the multipolar amplitudes computed with the ρ^f resummation are systematically closer to the numerical (exact) results than Taylor-expanded ones over a large range of v and spin values. The agreement can

be further improved by including suitable adjustable parameters and calibrating them to the numerical results, as done in the nonspinning case in Ref. [35].

Moreover, the numerical energy flux can also be successfully modeled by the ρ^f resummation—for example, we found that the fractional difference between the numerical and ρ^f-resummed flux is 13% (63%), 0.70% (3.3%), and 0.48% (2.9%) for $q = 0.95$, 0, -0.95, respectively, where the numbers in parenthesis refer to the Taylor-expanded-truncated PN flux. For large aligned spins, the ρ^f-resummed flux is much closer to the numerical flux at the LSO than the Taylor-expanded-truncated flux. Furthermore, we emphasize again that the ρ^f resummation improves the Taylor-expanded flux substantially over a large range of v and spin values and especially at low frequency where the majority of the signal-to-noise ratio of a binary accumulates.

We have also extended the factorized resummation to generic mass-ratio, nonprecessing, spinning black-hole binaries and proposed, as in Ref. [6], to augment the generic mass-ratio $\rho_{\ell m}$ with higher-order test-particle spin contributions. Unlike in the nonspinning case [6], in the spinning case only the leading-order generic mass-ratio spin terms are known. Using this limited information, we found that the dependence on ν of the spin terms is not necessarily mild. It depends on the mass ratio and the spin values. Nevertheless, we explored the possibility of adding the spin contributions from the test-particle limit case to the generic mass-ratio amplitudes.

When adding the test-particle limit contributions, we proposed to identify q with the Kerr-deformed spin in the effective-one-body description. Using the two choices currently available in the literature, that is $q = |\mathbf{S}_0|/M^2$ [19,36] or $q = |\mathbf{S}|/M^2$ [37], we found that the resummed amplitudes of the (2,2), (4,4), (4,2), and (6,6) modes agree with numerical simulation results [19] to within 2%, for equal-mass, equal-spin binaries with spins $|\chi_1| = |\chi_2| \simeq 0.44$. The (3,2) mode amplitude agrees with numerical results at 5% level. The relative difference between the two choices of resummed amplitudes is less than half their difference from numerical results. When the spins are near extremal, e.g., $\chi_1 = \chi_2 = 0.95$, we found a mild but non-negligible q dependence of the resummed amplitudes. Finally, when setting $q = 0$, that is removing the test-particle spin terms from the generic mass-ratio amplitudes, we obtain that the results vary by 10–20% for the (2,2), (4,4), (3,2), and (4,2) modes in the range of frequencies investigated in this paper.

The study carried out in this paper should be considered as a first step in the modeling of extreme-mass-ratio inspirals and comparable-mass black-hole binaries in presence of spins. We expect that in the extreme-mass-ratio inspiral case, the amplitude and flux agreement can be further improved by including in our $\rho^f_{\ell m}$ a few adjustable parameters and calibrate them to the numerical data, as already done in Ref. [35] for nonspinning extreme-mass-ratio inspirals. In the comparable-mass case, more detailed comparisons with accurate numerical-relativity simulations will allow us to nail down the choice of the spin parameter q and allow us to carry out direct comparisons between the numerical and analytical $\rho_{\ell m}$, thus helping in modeling the latter.

ACKNOWLEDGMENTS

We thank Larry Kidder and Andreas Ross for useful discussions and Bala Iyer for useful comments. A. B. and Y. P. acknowledge support from NSF Grants Nos. PHY-0603762 and PHY-0903631. A. B. acknowledges support also from NASA grant NNX09AI81G. H. T. acknowledges support from JSPS Grand-in-Aid for Scientific Research No. 20540271.

APPENDIX A: TAYLOR-EXPANDED MULTIPOLAR WAVEFORMS $\hat{Z}_{\ell m \omega_0}$

In order to compute the multipolar waveforms for a test particle around a Kerr black hole, we transform the Teukolsky equation into the frequency domain and expand it into the -2 spin-weighted spheroidal harmonics. The resulting equation is an ordinary differential equation about the radial coordinate. This radial Teukolsky equation can be solved formally by using the Green function. Since the Green function is represented by homogeneous solutions of the radial Teukolsky equation, the central issue of this problem is to obtain the homogeneous solutions. There are two methods for obtaining them.

In the first method, we transform the radial Teukolsky equation into the Sasaki-Nakamura equation. In the Schwarzschild case, the homogeneous Sasaki-Nakamura equation becomes the homogeneous Regge-Wheeler equation. We expand the homogeneous Sasaki-Nakamura or Regge-Wheeler equation in terms of $\epsilon \equiv GM\omega$, where ω is the angular frequency of the wave. In the case of circular orbit, ω becomes $\omega_0 = m\Omega$ (we revive the gravity constant G here). We look for the solution in power series in ϵ. This is thus a kind of post-Minkowskian expansion. One difference between the ordinary post-Minkowskian approximation and this approximation is that we must impose correct boundary conditions at the horizon. Closed analytic representation of the solution at each order is necessary in order to obtain the asymptotic amplitudes which constitute the Green function. The lowest-order solutions are represented by spherical Bessel functions. The higher-order solutions can, in principle, be derived iteratively. However, it becomes more difficult to perform this iteration and to derive the solution in closed analytic form at higher orders. The highest order computation so far was done in the Schwarzschild case by Tanaka *et al.* [12] in which the closed analytic formulas for a

homogeneous solution are obtained up to $\mathcal{O}(\epsilon)$ for arbitrary ℓ and up to $\mathcal{O}(\epsilon^3)$ for $\ell = 2$ and 3 and up to $\mathcal{O}(\epsilon^2)$ for $\ell = 4$. The formulas are explicitly given in a review paper [30]. Those computations are sufficient for obtaining the energy flux through 5.5PN order. Since the formulas for the $\hat{Z}_{\ell m\omega_0}$'s are not given in the literature, we write them below. For each mode, we write the terms up to $\mathcal{O}(v^{11-2(\ell-2)})$ relative to the lowest-order term.

Furthermore, in the Kerr case, so far the highest order computation was done by Tagoshi *et al.* [13] in which the closed analytic formulas for a homogeneous solution are obtained at $\mathcal{O}(\epsilon)$ for arbitrary ℓ modes and at $\mathcal{O}(\epsilon^2)$ for $\ell = 2$ and 3 modes. These computations are sufficient for obtaining the energy flux through 4PN order.

Two of the authors have recently obtained the $\mathcal{O}(\epsilon^2)$ closed analytic formulas for $\ell = 4$ mode [14]. This order is necessary to derive the multipolar waveforms through 3PN order beyond $C_{4m}^{(N,0)}$, i.e. 4PN order beyond $C_{22}^{(N,0)}$ (see Table I). More details of the computation and complete results are given elsewhere [14]. Here, we show only the explicit formulas for $\hat{Z}_{\ell m\omega_0}$ defined in Eq. (17). We write the spin-dependent 4PN-order $\hat{Z}_{\ell m\omega_0}$ in which each mode contains terms up to $\mathcal{O}(v^{8-(\ell-2)-\epsilon_p})$ relative to the lowest-order term. (ϵ_p is the parity of each mode).

The second method to obtain the homogeneous Teukolsky function is based on the Mano-Suzuki-Takasugi formalism [31]. In this formalism, the homogeneous solutions of the Teukolsky equation are represented with the series of hypergeometric functions and confluent hypergeometric functions. The expansion coefficients of the two series solutions are the same, and they are closely related to the series expansion in power of ϵ. Thus, if we compute this series up to higher order, we automatically obtain the higher-order PN expansion formulas. Such computation was applied to the evaluation of the PN expansion of the black-hole absorption effect in the Kerr case [40]. This method was also applied to the energy flux through 5.5PN order in the Schwarzschild case, confirming the results obtained with the above iteration method [12]. We apply this method to the Kerr case and obtain the 4PN-order multipolar waveforms, which agree with the results obtained with the above iteration method. This method has also been recently applied to the computation of the 5.5PN-order multipolar waveforms in the Schwarzschild case by Fujita and Iyer [15]. The nonspinning terms of expressions below agree with their results up to $\mathcal{O}(v^{11-2(\ell-2)})$.

We have

$$
\begin{aligned}
\hat{Z}_{22\omega_0} = 1 &- \frac{107v^2}{42} + \left[2\pi - \frac{4q}{3} + 12i\log\left(\frac{v}{v_0}\right)\right]v^3 + \left(-\frac{2173}{1512} + q^2\right)v^4 \\
&+ \left[-\frac{107\pi}{21} - \frac{460q}{189} - \frac{214}{7}i\log\left(\frac{v}{v_0}\right)\right]v^5 + \left[\frac{27027409}{646800} - \frac{856\,\mathrm{eulerlog}_2(v^2)}{105} + \frac{2\pi^2}{3} + \frac{428}{105}i\pi\right. \\
&\left. - \frac{8\pi q}{3} - \frac{4}{3}iq + \frac{32q^2}{567} - 8i(2q - 3\pi)\log\left(\frac{v}{v_0}\right) - 72\log^2\left(\frac{v}{v_0}\right)\right]v^6 - \left[\frac{2173\pi}{756} - \frac{24509q}{3402} - 2\pi q^2\right. \\
&\left. + \frac{2173}{126}i\log\left(\frac{v}{v_0}\right) - 12iq^2\log\left(\frac{v}{v_0}\right)\right]v^7 + \left[-\frac{846557506853}{12713500800} + \frac{45796\,\mathrm{eulerlog}_2(v^2)}{2205} - \frac{107\pi^2}{63}\right. \\
&\left. + \frac{2671117q^2}{666792} - \frac{22898}{2205}i\pi + \left(\frac{214}{63}i - \frac{920\pi}{189}\right)q - \frac{4}{63}i(460q + 963\pi)\log\left(\frac{v}{v_0}\right) + \frac{1284}{7}\log^2\left(\frac{v}{v_0}\right)\right]v^8 \\
&+ \left[-\frac{1712}{105}\pi\,\mathrm{eulerlog}_2(v^2) - \frac{64i\zeta(3)}{3} - \frac{4\pi^3}{3} + \frac{856i\pi^2}{63} + \frac{27027409\pi}{323400} - \frac{259i}{81}\right. \\
&\left. - \left(\frac{3424}{35}i\,\mathrm{eulerlog}_2(v^2) - 8i\pi^2 + \frac{1712\pi}{35} - \frac{27027409i}{53900}\right)\log\left(\frac{v}{v_0}\right) - 144\pi\log^2\left(\frac{v}{v_0}\right) - 288i\log^3\left(\frac{v}{v_0}\right)\right]v^9 \\
&+ \left[\frac{232511}{39690}(2\,\mathrm{eulerlog}_2(v^2) - i\pi) - \frac{2173\pi^2}{2268} - \frac{866305477369}{9153720576} - \frac{2173}{63}i\pi\log\left(\frac{v}{v_0}\right)\right. \\
&\left. + \frac{2173}{21}\log^2\left(\frac{v}{v_0}\right)\right]v^{10} + \left[\frac{91592\pi\,\mathrm{eulerlog}_2(v^2)}{2205} + \frac{3424i\zeta(3)}{63} + \frac{214\pi^3}{63} - \frac{45796i\pi^2}{1323}\right. \\
&\left. - \frac{846557506853\pi}{6356750400} + \frac{3959i}{486} + \left(\frac{183184}{735}i\,\mathrm{eulerlog}_2(v^2) - \frac{428i\pi^2}{21} + \frac{91592\pi}{735} - \frac{846557506853i}{1059458400}\right)\log\left(\frac{v}{v_0}\right)\right. \\
&\left. + \frac{2568}{7}\pi\log^2\left(\frac{v}{v_0}\right) + \frac{5136}{7}i\log^3\left(\frac{v}{v_0}\right)\right]v^{11}, \qquad \text{(A1)}
\end{aligned}
$$

$$
\begin{aligned}
\hat{Z}_{21\omega_0} = 1 &- \frac{3q}{2}v - \frac{17}{28}v^2 + \left[\pi - \frac{61q}{126} - \frac{i}{2}(1 + 4\log 2) + 6i\log\left(\frac{v}{v_0}\right)\right]v^3 \\
&+ \left[-\frac{43}{126} - \frac{3q\pi}{2} + 3q^2 + \frac{3}{4}iq(1 + 4\log 2) - 9iq\log\left(\frac{v}{v_0}\right)\right]v^4 \\
&+ \left[-\frac{17\pi}{28} - \frac{68q}{27} - \frac{3q^3}{4} + \frac{17}{56}i(1 + 4\log 2) - \frac{51}{14}i\log\left(\frac{v}{v_0}\right)\right]v^5 \\
&+ \left[\frac{15223771}{1455300} - \frac{61\pi q}{126} + \frac{28565q^2}{4536} + \frac{\pi^2}{6} - \frac{214\,\mathrm{eulerlog}_1(v^2)}{105}\right. \\
&+ \frac{109}{210}i\pi + \left(-\frac{65}{252}i + \frac{61}{63}i\log 2\right)q - (1 + 2\log 2 + 2i\pi)\log 2 \\
&\left.+ 3\left(1 + 2i\pi - \frac{61}{63}iq + 4\log 2\right)\log\left(\frac{v}{v_0}\right) - 18\log^2\left(\frac{v}{v_0}\right)\right]v^6 \\
&+ \left[\frac{107}{35}q\,\mathrm{eulerlog}_1(v^2) - \frac{2689q^3}{756} + 3\pi q^2 - \frac{3iq^2}{4} - 6iq^2\log 2\right. \\
&- \frac{\pi^2 q}{4} - \frac{109i\pi q}{140} - \frac{374592223q}{17463600} + 3i\pi q\log 2 + 3q\log^2 2 + \frac{3}{2}q\log 2 \\
&- \frac{43\pi}{126} + \frac{43i}{252} + \frac{43}{63}i\log 2 + \left(18iq^2 - 9i\pi q - \frac{9q}{2} - 18q\log 2 - \frac{43i}{21}\right)\log\left(\frac{v}{v_0}\right) \\
&\left.+ 27q\log^2\left(\frac{v}{v_0}\right)\right]v^7 + \left[\frac{187310657}{42378336} + \frac{1819\,\mathrm{eulerlog}_1(v^2)}{1470} - \frac{17\pi^2}{168} - \frac{1853i\pi}{5880}\right. \\
&+ \frac{17\log^2 2}{14} + \frac{17}{14}i\pi\log 2 + \frac{17\log 2}{28} + \left(-\frac{51}{28} - \frac{51i\pi}{14} - \frac{51\log 2}{7}\right)\log\left(\frac{v}{v_0}\right) \\
&\left.+ \frac{153}{14}\log^2\left(\frac{v}{v_0}\right)\right]v^8 + \left[\frac{107}{105}(2i\pi + 1 + 4\log 2)i\,\mathrm{eulerlog}_1(v^2) - \frac{8i\zeta(3)}{3}\right. \\
&- \frac{\pi^3}{6} + \frac{407i\pi^2}{252} + \frac{15965281\pi}{1455300} - \frac{24580669i}{4365900} + \frac{4}{3}i\log^3 2 - 2\pi\log^2 2 + i\log^2 2 \\
&- \frac{1}{3}i\pi^2\log 2 + \frac{109}{105}\pi\log 2 - \frac{15223771}{727650}i\log 2 + \left(-\frac{428}{35}i\,\mathrm{eulerlog}_1(v^2) + i\pi^2\right. \\
&\left.- \frac{109\pi}{35} + \frac{15223771i}{242550} - 12i\log^2 2 + 12\pi\log 2 - 6i\log 2\right)\log\left(\frac{v}{v_0}\right) + (9i - 18\pi \\
&\left.+ 9i\log(16))\log^2\left(\frac{v}{v_0}\right) - 36i\log^3\left(\frac{v}{v_0}\right)\right]v^9 + \left[\frac{54222281699}{4767562800} + \frac{4601\,\mathrm{eulerlog}_1(v^2)}{6615}\right. \\
&- \frac{43\pi^2}{756} - \frac{4687i\pi}{26460} + \frac{43\log^2 2}{63} + \frac{43}{63}i\pi\log 2 + \frac{43\log 2}{126} - \frac{43}{42}(2i\pi + 1 + 4\log 2)\log\left(\frac{v}{v_0}\right) \\
&\left.+ \frac{43}{7}\log^2\left(\frac{v}{v_0}\right)\right]v^{10} + \left[-\frac{1819}{2940}(2i\pi + 1 + 4\log 2)i\,\mathrm{eulerlog}_1(v^2)\right. \\
&+ \frac{34i\zeta(3)}{21} + \frac{17\pi^3}{168} - \frac{6919i\pi^2}{7056} + \frac{871003801\pi}{211891680} - \frac{500228329i}{254270016} - \frac{17}{21}i\log^3 2 + \frac{17}{14}\pi\log^2 2 \\
&- \frac{17}{28}i\log^2 2 + \frac{17}{84}i\pi^2\log 2 - \frac{1853\pi\log 2}{2940} - \frac{187310657i\log 2}{21189168} \\
&+ \left(\frac{1819}{245}i\,\mathrm{eulerlog}_1(v^2) - \frac{17i\pi^2}{28} + \frac{1853\pi}{980} + \frac{187310657i}{7063056} + \frac{51}{7}i\log^2 2\right. \\
&\left.- \frac{51}{7}\pi\log 2 + \frac{51}{14}i\log 2\right)\log\left(\frac{v}{v_0}\right) - \frac{153}{28}i(2i\pi + 1 + 4\log 2)\log^2\left(\frac{v}{v_0}\right) \\
&\left.+ \frac{153}{7}i\log^3\left(\frac{v}{v_0}\right)\right]v^{11}, \qquad \text{(A2)}
\end{aligned}
$$

$$\begin{aligned}\hat{Z}_{33\omega_0} = 1 &- 4v^2 + \left[3\pi - 2q - \frac{21}{5}i - 6i\log\left(\frac{2}{3}\right) + 18i\log\left(\frac{v}{v_0}\right)\right]v^3 + \left(\frac{123}{110} + \frac{3q^2}{2}\right)v^4 \\ &+ \left[\frac{29q}{60} - 12\pi + \frac{84}{5}i + 24i\log\left(\frac{2}{3}\right) - 72i\log\left(\frac{v}{v_0}\right)\right]v^5 \\ &+ \left[\frac{19388147}{280280} - \frac{67q^2}{32} - \frac{78\,\mathrm{eulerlog}_3(v^2)}{7} - 6\pi q + \frac{3\pi^2}{2} - \frac{246}{35}i\pi + \frac{87}{20}iq\right. \\ &+ 12iq\log\left(\frac{2}{3}\right) - 18\log^2\left(\frac{2}{3}\right) - \frac{126}{5}\log\left(\frac{2}{3}\right) - 18i\pi\log\left(\frac{2}{3}\right) \\ &\left.+ \frac{18}{5}\left(21 - 10iq + 15i\pi + 30\log\left(\frac{2}{3}\right) - 45\log\left(\frac{v}{v_0}\right)\right)\log\left(\frac{v}{v_0}\right)\right]v^6 \\ &+ \left[-q^3 + \frac{9\pi q^2}{2} - \frac{63iq^2}{10} + 9iq^2\log\left(\frac{3}{2}\right) + \frac{89q}{5} + \frac{369\pi}{110} - \frac{2583i}{550} + \frac{369}{55}i\log\left(\frac{3}{2}\right)\right. \\ &\left.+ \left(27iq^2 + \frac{1107i}{55}\right)\log\left(\frac{v}{v_0}\right)\right]v^7 + \left[\frac{312\,\mathrm{eulerlog}_3(v^2)}{7} - 6\pi^2 + \frac{984i\pi}{35} - \frac{72614419}{350350} + 72\log^2\left(\frac{3}{2}\right)\right. \\ &- 72i\pi\log\left(\frac{3}{2}\right) - \frac{504}{5}\log\left(\frac{3}{2}\right) + \left(-\frac{1512}{5} - 216i\pi + 432\log\left(\frac{3}{2}\right)\right)\log\left(\frac{v}{v_0}\right) + 648\log^2\left(\frac{v}{v_0}\right)\Big]v^8 \\ &+ \left[-\frac{234}{7}\pi\,\mathrm{eulerlog}_3(v^2) + \frac{234}{5}i\,\mathrm{eulerlog}_3(v^2) - \frac{468}{7}i\log\left(\frac{3}{2}\right)\mathrm{eulerlog}_3(v^2) - 72i\zeta(3)\right. \\ &- \frac{9\pi^3}{2} + \frac{1509i\pi^2}{70} + \frac{64722993\pi}{280280} - \frac{92343253i}{300300} - 36i\log^3\left(\frac{3}{2}\right) - 54\pi\log^2\left(\frac{3}{2}\right) + \frac{378}{5}i\log^2\left(\frac{3}{2}\right) \\ &+ \left(9i\pi^2 + \frac{1476}{35}\pi + \frac{58164441}{140140}i\right)\log\left(\frac{3}{2}\right) + \left(27i\pi^2 - \frac{1404}{7}i\,\mathrm{eulerlog}_3(v^2) + \frac{4428\pi}{35}\right. \\ &+ \frac{174493323i}{140140} - 324i\log^2\left(\frac{3}{2}\right) - \left(324\pi - \frac{2268}{5}i\right)\log\left(\frac{3}{2}\right)\Big)\log\left(\frac{v}{v_0}\right) \\ &\left.+ \left(\frac{3402i}{5} - 486\pi - 972i\log\left(\frac{3}{2}\right)\right)\log^2\left(\frac{v}{v_0}\right) - 972i\log^3\left(\frac{v}{v_0}\right)\right]v^9, \end{aligned} \tag{A3}$$

$$\begin{aligned}\hat{Z}_{32\omega_0} = 1 &- \frac{4q}{3}v - \frac{193}{90}v^2 + \left[\frac{7q}{9} + 2\pi - 3i + 12i\log\left(\frac{v}{v_0}\right)\right]v^3 + \left[-\frac{1451}{3960} - \frac{8\pi q}{3} + \frac{100q^2}{27} + 4iq - 16iq\log\left(\frac{v}{v_0}\right)\right]v^4 \\ &+ \left[-\frac{4q^3}{3} - \frac{560q}{891} - \frac{193\pi}{45} + \frac{193i}{30} - \frac{386}{15}i\log\left(\frac{v}{v_0}\right)\right]v^5 + \left[\frac{2160500827}{75675600} - \frac{104\,\mathrm{eulerlog}_2(v^2)}{21} + \frac{1283q^2}{405}\right. \\ &+ \frac{14\pi q}{9} - \frac{19iq}{5} + \frac{2\pi^2}{3} - \frac{74i\pi}{21} + \left(\frac{28iq}{3} + 24i\pi + 36\right)\log\left(\frac{v}{v_0}\right) - 72\log^2\left(\frac{v}{v_0}\right)\Big]v^6 \\ &- \frac{1451}{1980}\left[\pi - \frac{3i}{2} + 6i\log\left(\frac{v}{v_0}\right)\right]v^7 + \left[-\frac{19111297859}{495331200} + \frac{10036}{945}\,\mathrm{eulerlog}_2(v^2)\right. \\ &- \frac{193\pi^2}{135} + \frac{7141i\pi}{945} + \left(-\frac{386}{5} - \frac{772i\pi}{15}\right)\log\left(\frac{v}{v_0}\right) + \frac{772}{5}\log^2\left(\frac{v}{v_0}\right)\Big]v^8 \\ &+ \left[-\frac{208}{21}\pi\,\mathrm{eulerlog}_2(v^2) + \frac{104}{7}i\,\mathrm{eulerlog}_2(v^2) - \frac{64i\zeta(3)}{3} - \frac{4\pi^3}{3} + \frac{394i\pi^2}{63}\right. \\ &+ \frac{2441581627\pi}{37837800} - \frac{20967548963i}{227026800} + \left(\frac{2160500827i}{6306300} - \frac{416}{7}i\,\mathrm{eulerlog}_2(v^2) + 8i\pi^2 + \frac{296\pi}{7}\right)\log\left(\frac{v}{v_0}\right) \\ &\left.+ (-144\pi + 216i)\log^2\left(\frac{v}{v_0}\right) - 288i\log^3\left(\frac{v}{v_0}\right)\right]v^9, \end{aligned} \tag{A4}$$

$$\hat{Z}_{31\omega_0} = 1 - \frac{8}{3}v^2 + \left[\pi - \frac{50q}{9} - \frac{7}{5}i - 2i\log 2 + 6i\log\left(\frac{v}{v_0}\right)\right]v^3 + \left(\frac{607}{198} + \frac{17q^2}{6}\right)v^4 + \left(\frac{73q}{12} - \frac{8\pi}{3} + \frac{56}{15}i + \frac{16}{3}i\log 2 - 16i\log\left(\frac{v}{v_0}\right)\right)v^5 + \left[\frac{10753397}{1513512} + \frac{18173q^2}{2592} - \frac{26\,\mathrm{eulerlog}_1(v^2)}{21} - \frac{50\pi q}{9} + \frac{\pi^2}{6} + \left(\frac{1373}{180} + \frac{100}{9}\log 2\right)iq - \frac{82}{105}i\pi - 2i\pi\log 2 - \frac{14}{5}\log 2 - 2\log^2 2 + \left(\frac{42}{5} - \frac{100}{3}iq + 6i\pi + 12\log 2\right)\log\left(\frac{v}{v_0}\right) - 18\log^2\left(\frac{v}{v_0}\right)\right]v^6 + \left[-\frac{187q^3}{27} + \frac{17\pi q^2}{6} - \frac{119iq^2}{30} - \frac{17}{3}iq^2\log 2 - \frac{6541q}{891} + \frac{607\pi}{198} - \frac{4249i}{990} - \frac{607}{99}i\log 2 + \left(17iq^2 + \frac{607i}{33}\right)\log\left(\frac{v}{v_0}\right)\right]v^7 + \left[-\frac{12785953}{1091475} + \frac{208}{63}\,\mathrm{eulerlog}_1(v^2) - \frac{4\pi^2}{9} + \frac{656i\pi}{315} + \frac{16\log^2 2}{3} + \frac{16}{3}i\pi\log 2 + \frac{112\log 2}{15} + \left(-\frac{112}{5} - 16i\pi - 32\log 2\right)\log\left(\frac{v}{v_0}\right) + 48\log^2\left(\frac{v}{v_0}\right)\right]v^8 + \left[\frac{26}{21}\left(-\pi + \frac{7}{5}i + 2i\log 2\right)\mathrm{eulerlog}_1(v^2) - \frac{8i\zeta(3)}{3} - \frac{\pi^3}{6} + \frac{503i\pi^2}{630} + \frac{60325537\pi}{7567560} - \frac{85747069i}{8108100} + \frac{4}{3}i\log^3 2 - 2\pi\log^2 2 + \frac{14}{5}i\log^2 2 - \frac{1}{3}i\pi^2\log 2 - \frac{164}{105}\pi\log 2 - \frac{10753397}{756756}i\log 2 + \left(-\frac{52}{7}i\,\mathrm{eulerlog}_1(v^2) + i\pi^2 + \frac{164\pi}{35} + \frac{10753397i}{252252} - 12i\log^2 2 + 12\pi\log 2 - \frac{84}{5}i\log 2\right)\log\left(\frac{v}{v_0}\right) + \left(\frac{126i}{5} - 18\pi + 36i\log 2\right)\log^2\left(\frac{v}{v_0}\right) - 36i\log^3\left(\frac{v}{v_0}\right)\right]v^9, \tag{A5}$$

$$\hat{Z}_{44\omega_0} = 1 - \frac{593}{110}v^2 + \left(4\pi - \frac{8q}{3} - \frac{42}{5}i + 8i\log 2 + 24i\log\left(\frac{v}{v_0}\right)\right)v^3 + \left(\frac{1068671}{200200} + 2q^2\right)v^4 + \left[\frac{6774q}{1375} - \frac{1186\pi}{55} + \frac{12453i}{275} - \frac{2372}{55}i\log 2 - \frac{7116}{55}i\log\left(\frac{v}{v_0}\right)\right]v^5 + \left[\frac{42783901441}{499458960} - \frac{50272\,\mathrm{eulerlog}_4(v^2)}{3465} - \frac{624721q^2}{123750} - \frac{32\pi q}{3} + \frac{1216iq}{75} - \frac{64}{3}iq\log 2 + \frac{8\pi^2}{3} - \frac{91288i\pi}{3465} - 32\log^2 2 + 32i\pi\log 2 + \frac{336\log 2}{5} + \left(-64iq + 96i\pi + \frac{1008}{5} - 192\log 2\right)\log\left(\frac{v}{v_0}\right) - 288\log^2\left(\frac{v}{v_0}\right)\right]v^6 + \left[\frac{1068671\pi}{50050} - \frac{3206013i}{71500} + \frac{1068671}{25025}i\log 2 + \frac{3206013}{25025}i\log\left(\frac{v}{v_0}\right)\right]v^7, \tag{A6}$$

$$\hat{Z}_{43\omega_0} = 1 - \frac{5q}{4}v - \frac{39}{11}v^2 + \left[\frac{1438q}{825} + 3\pi - \frac{32i}{5} + 6i\log 3 - 6i\log 2 + 18i\log\left(\frac{v}{v_0}\right)\right]v^3 + \left[\frac{7206}{5005} + \frac{37q^2}{8} - \frac{15\pi q}{4} + 8iq - \frac{15}{2}iq\log 3 + \frac{15}{2}iq\log 2 - \frac{45}{2}iq\log\left(\frac{v}{v_0}\right)\right]v^4 + \left[-\frac{15q^3}{8} + \frac{29941q}{200200} - \frac{117\pi}{11} + \frac{1248i}{55} - \frac{234}{11}i\log 3 + \frac{234}{11}i\log 2 - \frac{702}{11}i\log\left(\frac{v}{v_0}\right)\right]v^5 + \left[\frac{1272567389}{27747720} - \frac{3142}{385}\,\mathrm{eulerlog}_3(v^2) + \frac{3\pi^2}{2} - \frac{5821i\pi}{385} - 18\log^2\left(\frac{3}{2}\right) + 18i\pi\log\left(\frac{3}{2}\right) + \frac{192}{5}\log\left(\frac{3}{2}\right) + \left(\frac{576}{5} + 54i\pi - 108\log\left(\frac{3}{2}\right)\right)\log\left(\frac{v}{v_0}\right) - 162\log^2\left(\frac{v}{v_0}\right)\right]v^6 + \left[\frac{21618\pi}{5005} - \frac{230592i}{25025} + \frac{43236}{5005}i\log\left(\frac{3}{2}\right) + \frac{129708}{5005}i\log\left(\frac{v}{v_0}\right)\right]v^7, \tag{A7}$$

$$\hat{Z}_{42\omega_0} = 1 - \frac{437}{110}v^2 + \left[2\pi - \frac{17q}{3} - \frac{21}{5}i + 12i\log\left(\frac{v}{v_0}\right)\right]v^3 + \left(\frac{1038039}{200200} + \frac{20}{7}q^2\right)v^4 + \left[\frac{36353q}{2750} - \frac{437\pi}{55} + \frac{9177i}{550} - \frac{2622}{55}i\log\left(\frac{v}{v_0}\right)\right]v^5 + \left[\frac{44982355673}{2497294800} - \frac{12568\ \mathrm{eulerlog}_2(v^2)}{3465} + \frac{1265648q^2}{275625} - \frac{34\pi q}{3} + \frac{1727iq}{75} + \frac{2\pi^2}{3} - \frac{22822i\pi}{3465} + \left(-68iq + 24i\pi + \frac{252}{5}\right)\log\left(\frac{v}{v_0}\right) - 72\log^2\left(\frac{v}{v_0}\right)\right]v^6 + \left[\frac{1038039\pi}{100100} - \frac{3114117i}{143000} + \frac{3114117}{50050}i\log\left(\frac{v}{v_0}\right)\right]v^7, \tag{A8}$$

$$\hat{Z}_{41\omega_0} = 1 - \frac{5q}{4}v - \frac{101}{33}v^2 + \left[\frac{7q}{825} + \pi - \frac{32i}{15} - 2i\log 2 + 6i\log\left(\frac{v}{v_0}\right)\right]v^3 + \left[\frac{42982}{15015} + \frac{331q^2}{56} - \frac{5\pi q}{4} + \frac{8iq}{3} + \frac{5}{2}iq\log 2 - \frac{15}{2}iq\log\left(\frac{v}{v_0}\right)\right]v^4 + \left[-\frac{275q^3}{168} + \frac{5199317q}{1801800} - \frac{101\pi}{33} + \frac{3232i}{495} + \frac{202}{33}i\log 2 - \frac{202}{11}i\log\left(\frac{v}{v_0}\right)\right]v^5 + \left[\frac{1250147453}{249729480} - \frac{3142}{3465}\mathrm{eulerlog}_1(v^2) + \frac{\pi^2}{6} - \frac{5821i\pi}{3465} - 2\log^2 2 - 2i\pi\log 2 - \frac{64\log 2}{15} + \left(\frac{64}{5} + 6i\pi + 12\log 2\right)\log\left(\frac{v}{v_0}\right) - 18\log^2\left(\frac{v}{v_0}\right)\right]v^6 + \left[\frac{42982\pi}{15015} - \frac{1375424i}{225225} - \frac{85964}{15015}i\log 2 + \frac{85964}{5005}i\log\left(\frac{v}{v_0}\right)\right]v^7, \tag{A9}$$

$$\hat{Z}_{55\omega_0} = 1 - \frac{263}{39}v^2 + \left[-\frac{10q}{3} + 5\pi - \frac{181i}{14} + 10i\log\left(\frac{5}{2}\right) + 30i\log\left(\frac{v}{v_0}\right)\right]v^3 + \left(\frac{5q^2}{2} + \frac{9185}{819}\right)v^4 + \left[\frac{26944q}{2457} - \frac{1315\pi}{39} + \frac{47603i}{546} - \frac{2630}{39}i\log\left(\frac{5}{2}\right) - \frac{2630}{13}i\log\left(\frac{v}{v_0}\right)\right]v^5, \tag{A10}$$

$$\hat{Z}_{54\omega_0} = 1 - \frac{6q}{5}v - \frac{4451}{910}v^2 + \left[\frac{7513q}{2925} + 4\pi - \frac{52i}{5} + 8i\log 2 + 24i\log\left(\frac{v}{v_0}\right)\right]v^3 + \left[\frac{10715}{2184} + \frac{707q^2}{125} - \frac{24\pi q}{5} + \frac{312iq}{25} - \frac{48}{5}iq\log 2 - \frac{144}{5}iq\log\left(\frac{v}{v_0}\right)\right]v^4 + \left[-\frac{8902\pi}{455} + \frac{8902i}{175} - \frac{17804}{455}i\log 2 - \frac{53412}{455}i\log\left(\frac{v}{v_0}\right)\right]v^5, \tag{A11}$$

$$\hat{Z}_{53\omega_0} = 1 - \frac{69}{13}v^2 + \left[-\frac{442q}{75} + 3\pi - \frac{543i}{70} + 6i\log\left(\frac{3}{2}\right) + 18i\log\left(\frac{v}{v_0}\right)\right]v^3 + \left[\frac{91q^2}{30} + \frac{12463}{1365}\right]v^4 + \left[\frac{47296q}{2275} - \frac{207\pi}{13} + \frac{37467i}{910} - \frac{414}{13}i\log\left(\frac{3}{2}\right) - \frac{1242}{13}i\log\left(\frac{v}{v_0}\right)\right]v^5, \tag{A12}$$

$$\hat{Z}_{52\omega_0} = 1 - \frac{6q}{5}v - \frac{3911}{910}v^2 + \left[\frac{2317q}{2925} + 2\pi - \frac{26i}{5} + 12i\log\left(\frac{v}{v_0}\right)\right]v^3 + \left[\frac{63439}{10920} + \frac{833q^2}{125} - \frac{12\pi q}{5} + \frac{156iq}{25} - \frac{72}{5}iq\log\left(\frac{v}{v_0}\right)\right]v^4 + \left[-\frac{3911\pi}{455} + \frac{3911i}{175} - \frac{23466}{455}i\log\left(\frac{v}{v_0}\right)\right]v^5, \tag{A13}$$

$$\hat{Z}_{51\omega_0} = 1 - \frac{179}{39}v^2 + \left[-\frac{538q}{75} + \pi - \frac{181i}{70} - 2i\log 2 + 6i\log\left(\frac{v}{v_0}\right)\right]v^3 + \left[\frac{33q^2}{10} + \frac{5023}{585}\right]v^4 + \left[\frac{208192q}{8775} - \frac{179\pi}{39} + \frac{32399i}{2730} + \frac{358}{39}i\log 2 - \frac{358}{13}i\log\left(\frac{v}{v_0}\right)\right]v^5, \tag{A14}$$

$$\hat{Z}_{66\omega_0} = 1 - \frac{113}{14}v^2 + \left[-4q + 6\pi - \frac{249i}{14} + 12i\log 3 + 36i\log\left(\frac{v}{v_0}\right)\right]v^3 + \left(\frac{1372317}{73304} + 3q^2\right)v^4, \tag{A15}$$

$$\hat{Z}_{65\omega_0} = 1 - \frac{7q}{6}v - \frac{149}{24}v^2 + \left[\frac{2927q}{882} + 5\pi - \frac{104i}{7} + 10i\log\left(\frac{5}{2}\right) + 30i\log\left(\frac{v}{v_0}\right)\right]v^3, \tag{A16}$$

$$\hat{Z}_{64\omega_0} = 1 - \frac{93}{14}v^2 + \left[-\frac{56q}{9} + 4\pi - \frac{83i}{7} + 8i\log 2 + 24i\log\left(\frac{v}{v_0}\right)\right]v^3 + \left[\frac{109q^2}{33} + \frac{3261767}{219912}\right]v^4, \tag{A17}$$

$$\hat{Z}_{63\omega_0} = 1 - \frac{7q}{6}v - \frac{133}{24}v^2 + \left[\frac{461q}{294} + 3\pi - \frac{312i}{35} + 6i\log\left(\frac{3}{2}\right) + 18i\log\left(\frac{v}{v_0}\right)\right]v^3, \tag{A18}$$

$$\hat{Z}_{62\omega_0} = 1 - \frac{81}{14}v^2 + \left[-\frac{68q}{9} + 2\pi - \frac{83i}{14} + 12i\log\left(\frac{v}{v_0}\right)\right]v^3 + \left[\frac{115q^2}{33} + \frac{14482483}{1099560}\right]v^4, \tag{A19}$$

$$\hat{Z}_{61\omega_0} = 1 - \frac{7q}{6}v - \frac{125}{24}v^2 + \left[\frac{611q}{882} + \pi - \frac{104i}{35} - 2i\log 2 + 6i\log\left(\frac{v}{v_0}\right)\right]v^3, \tag{A20}$$

$$\hat{Z}_{77\omega_0} = 1 - \frac{319}{34}v^2 + \left[-\frac{14q}{3} + 7\pi - \frac{4129i}{180} + 14i\log\left(\frac{7}{2}\right) + 42i\log\left(\frac{v}{v_0}\right)\right]v^3, \tag{A21}$$

$$\hat{Z}_{76\omega_0} = 1 - \frac{8q}{7}v - \frac{1787}{238}v^2, \tag{A22}$$

$$\hat{Z}_{75\omega_0} = 1 - \frac{271}{34}v^2 + \left[-\frac{974q}{147} + 5\pi - \frac{4129i}{252} + 10i\log\left(\frac{5}{2}\right) + 30i\log\left(\frac{v}{v_0}\right)\right]v^3, \tag{A23}$$

$$\hat{Z}_{74\omega_0} = 1 - \frac{8q}{7}v - \frac{14543}{2142}v^2, \tag{A24}$$

$$\hat{Z}_{73\omega_0} = 1 - \frac{239}{34}v^2 + \left[-\frac{1166q}{147} + 3\pi - \frac{4129i}{420} + 6i\log\left(\frac{3}{2}\right) + 18i\log\left(\frac{v}{v_0}\right)\right]v^3, \tag{A25}$$

$$\hat{Z}_{72\omega_0} = 1 - \frac{8q}{7}v - \frac{13619}{2142}v^2, \tag{A26}$$

$$\hat{Z}_{71\omega_0} = 1 - \frac{223}{34}v^2 + \left[-\frac{1262q}{147} + \pi - \frac{4129i}{1260} - 2i\log 2 + 6i\log\left(\frac{v}{v_0}\right)\right]v^3, \tag{A27}$$

$$\hat{Z}_{88\omega_0} = 1 - \frac{3653}{342}v^2, \qquad \hat{Z}_{86\omega_0} = 1 - \frac{353}{38}v^2, \qquad \hat{Z}_{84\omega_0} = 1 - \frac{2837}{342}v^2, \qquad \hat{Z}_{82\omega_0} = 1 - \frac{2633}{342}v^2. \tag{A28}$$

$$\hat{Z}_{87\omega_0} = 1 - \frac{9q}{8}v, \qquad \hat{Z}_{85\omega_0} = 1 - \frac{9q}{8}v, \qquad \hat{Z}_{83\omega_0} = 1 - \frac{9q}{8}v, \qquad \hat{Z}_{81\omega_0} = 1 - \frac{9q}{8}v. \tag{A29}$$

APPENDIX B: EXPRESSIONS OF THE $C_{\ell m}$'S MODES FOR $4 < \ell < 8$

$$\hat{C}_{55} = \hat{Z}_{55\omega_0} - \frac{400q}{2457}v^5, \tag{B1a}$$

$$\hat{C}_{54} = \hat{Z}_{54\omega_0} + \frac{6q}{5}v - \frac{19213q}{2925}v^3 + \left[-\frac{332q^2}{125} + \frac{24\pi q}{5} - \frac{252iq}{25} + \frac{48}{5}iq\log 2 + \frac{144}{5}iq\log\left(\frac{v}{v_0}\right)\right]v^4, \tag{B1b}$$

$$\hat{C}_{53} = \hat{Z}_{53\omega_0} + \frac{64q}{25}v^3 - \frac{8q^2}{15}v^4 - \frac{20976q}{2275}v^5, \tag{B1c}$$

$$\hat{C}_{52} = \hat{Z}_{52\omega_0} + \frac{6q}{5}v - \frac{14017q}{2925}v^3 + \left[-\frac{458q^2}{125} + \frac{12\pi q}{5} - \frac{126iq}{25} + \frac{72}{5}iq\log\left(\frac{v}{v_0}\right)\right]v^4, \tag{B1d}$$

$$\hat{C}_{51} = \hat{Z}_{51\omega_0} + \frac{96q}{25}v^3 - \frac{4q^2}{5}v^4 - \frac{103312q}{8775}v^5, \tag{B1e}$$

$$\hat{C}_{66} = \hat{Z}_{66\omega_0}, \qquad \hat{C}_{65} = \hat{Z}_{65\omega_0} + \frac{7q}{6}v - \frac{7043q}{882}v^3, \tag{B1f}$$

$$\hat{C}_{64} = \hat{Z}_{64\omega_0} + \frac{20q}{9}v^3 - \frac{10q^2}{33}v^4, \qquad \hat{C}_{63} = \hat{Z}_{63\omega_0} + \frac{7q}{6}v - \frac{611q}{98}v^3, \tag{B1g}$$

$$\hat{C}_{62} = \hat{Z}_{62\omega_0} + \frac{32q}{9}v^3 - \frac{16q^2}{33}v^4, \qquad \hat{C}_{61} = \hat{Z}_{61\omega_0} + \frac{7q}{6}v - \frac{4727q}{882}v^3, \tag{B1h}$$

$$\hat{C}_{77} = \hat{Z}_{77\omega_0}, \qquad \hat{C}_{76} = \hat{Z}_{76\omega_0} + \frac{8q}{7}v, \qquad \hat{C}_{75} = \hat{Z}_{75\omega_0} + \frac{96q}{49}v^3, \qquad \hat{C}_{74} = \hat{Z}_{74\omega_0} + \frac{8q}{7}v, \tag{B1i}$$

$$\hat{C}_{73} = \hat{Z}_{73\omega_0} + \frac{160q}{49}v^3, \qquad \hat{C}_{72} = \hat{Z}_{72\omega_0} + \frac{8q}{7}v, \qquad \hat{C}_{71} = \hat{Z}_{71\omega_0} + \frac{192q}{49}v^3, \tag{B1j}$$

$$\hat{C}_{87} = \hat{Z}_{87\omega_0} + \frac{9q}{8}v, \qquad \hat{C}_{85} = \hat{Z}_{85\omega_0} + \frac{9q}{8}v, \qquad \hat{C}_{83} = \hat{Z}_{83\omega_0} + \frac{9q}{8}v, \qquad \hat{C}_{81} = \hat{Z}_{81\omega_0} + \frac{9q}{8}v. \tag{B1k}$$

APPENDIX C: EXPRESSIONS OF THE $f_{\ell m}$'S MODES FOR $\ell > 4$

1. The odd-parity $f^L_{\ell m}$'s and even-parity $f_{\ell m}$'s

$$f_{55} = 1 - \frac{487}{78}v^2 - \frac{10q}{3}v^3 + \left(\frac{5q^2}{2} + \frac{50569}{6552}\right)v^4 + \frac{1225q}{117}v^5, \tag{C1a}$$

$$f^L_{54} = 1 - \frac{2908}{455}v^2 - \frac{2q}{3}v^3 + \left(2q^2 + \frac{2168}{195}\right)v^4, \tag{C1b}$$

$$f_{53} = 1 - \frac{125}{26}v^2 - \frac{10q}{3}v^3 + \left(\frac{5q^2}{2} + \frac{69359}{10920}\right)v^4 + \frac{2191q}{195}v^5, \tag{C1c}$$

$$f^L_{52} = 1 - \frac{2638}{455}v^2 - \frac{2q}{3}v^3 + \left(2q^2 + \frac{15194}{1365}\right)v^4, \tag{C1d}$$

$$f_{51} = 1 - \frac{319}{78}v^2 - \frac{10q}{3}v^3 + \left(\frac{5q^2}{2} + \frac{28859}{4680}\right)v^4 + \frac{6797q}{585}v^5, \tag{C1e}$$

$$f_{66} = 1 - \frac{53}{7}v^2 - 4qv^3 + \left(3q^2 + \frac{133415}{9163}\right)v^4, \qquad f^L_{65} = 1 - \frac{185}{24}v^2 - \frac{4q}{3}v^3, \tag{C1f}$$

$$f_{64} = 1 - \frac{43}{7}v^2 - 4qv^3 + \left(3q^2 + \frac{312982}{27489}\right)v^4, \qquad f^L_{63} = 1 - \frac{169}{24}v^2 - \frac{4q}{3}v^3, \tag{C1g}$$

$$f_{62} = 1 - \frac{37}{7}v^2 - 4qv^3 + \left(3q^2 + \frac{1395521}{137445}\right)v^4, \qquad f^L_{61} = 1 - \frac{161}{24}v^2 - \frac{4q}{3}v^3, \tag{C1h}$$

$$f_{77} = 1 - \frac{151}{17}v^2 - \frac{14q}{3}v^3, \qquad f^L_{76} = 1 - \frac{1072}{119}v^2, \tag{C1i}$$

$$f_{75} = 1 - \frac{127}{17}v^2 - \frac{14q}{3}v^3, \qquad f^L_{74} = 1 - \frac{8878}{1071}v^2, \tag{C1j}$$

$$f_{73} = 1 - \frac{111}{17}v^2 - \frac{14q}{3}v^3, \qquad f^L_{72} = 1 - \frac{8416}{1071}v^2, \qquad f_{71} = 1 - \frac{103}{17}v^2 - \frac{14q}{3}v^3, \tag{C1k}$$

$$f_{88} = 1 - \frac{1741}{171}v^2, \qquad f^L_{87} = 1 - \frac{3913}{380}v^2, \qquad f_{86} = 1 - \frac{167}{19}v^2, \qquad f^L_{85} = 1 - \frac{725}{76}v^2, \tag{C1l}$$

$$f_{84} = 1 - \frac{1333}{171}v^2, \qquad f^L_{83} = 1 - \frac{3433}{380}v^2, \qquad f_{82} = 1 - \frac{1231}{171}v^2, \qquad f^L_{81} = 1 - \frac{3337}{380}v^2. \tag{C1m}$$

2. The odd-parity $f^H_{\ell m}$'s

$$\begin{aligned} f^H_{21} = 1 &- \frac{3q}{2}v - \frac{3}{28}v^2 - \frac{5q}{4}v^3 + \left(3q^2 - \frac{97}{126}\right)v^4 - \frac{3q}{112}(28q^2 + 45)v^5 + \left(\frac{75q^2}{14} - \frac{214\,\mathrm{eulerlog}_1(v^2)}{105} + \frac{70479293}{11642400}\right)v^6 \\ &+ \left(-\frac{535q^3}{168} + \frac{107}{35}q\,\mathrm{eulerlog}_1(v^2) - \frac{12363787q}{1058400}\right)v^7 + \left(\frac{107\,\mathrm{eulerlog}_1(v^2)}{490} + \frac{5770262917}{1412611200}\right)v^8 \\ &+ \left(\frac{10379\,\mathrm{eulerlog}_1(v^2)}{6615} - \frac{23353414831}{13869273600}\right)v^{10}, \end{aligned} \tag{C2a}$$

$$\begin{aligned} f^H_{32} = 1 &- \frac{74}{45}v^2 - \frac{8q}{3}v^3 + \left(2q^2 - \frac{86}{55}\right)v^4 - \frac{106q}{45}v^5 + \left(\frac{16q^2}{45} - \frac{104\,\mathrm{eulerlog}_2(v^2)}{21} + \frac{96051082}{4729725}\right)v^6 \\ &+ \left(\frac{7696\,\mathrm{eulerlog}_2(v^2)}{945} - \frac{708338174}{42567525}\right)v^8, \end{aligned} \tag{C2b}$$

$$f^H_{43} = 1 - \frac{67}{22}v^2 - \frac{10q}{3}v^3 + \left(\frac{5q^2}{2} - \frac{1667}{3640}\right)v^4 + \frac{7481q}{4620}v^5 + \left(\frac{11083164791}{277477200} - \frac{3142\,\mathrm{eulerlog}_3(v^2)}{385}\right)v^6, \tag{C2c}$$

$$f^H_{41} = 1 - \frac{169}{66}v^2 - \frac{10q}{3}v^3 + \left(\frac{5q^2}{2} + \frac{145021}{120120}\right)v^4 + \left(\frac{89027q}{13860} - \frac{10q^3}{3}\right)v^5 + \left(\frac{10765133231}{2497294800} - \frac{3142\,\mathrm{eulerlog}_1(v^2)}{3465}\right)v^6, \tag{C2d}$$

$$f^H_{54} = 1 - \frac{1998}{455}v^2 - 4qv^3 + \left(3q^2 + \frac{3188}{1365}\right)v^4, \qquad f^H_{52} = 1 - \frac{1728}{455}v^2 - 4qv^3 + (3q^2 + \frac{4826}{1365})v^4, \tag{C2e}$$

$$f^H_{65} = 1 - \frac{137}{24}v^2 - \frac{14q}{3}v^3, \qquad f^H_{63} = 1 - \frac{121}{24}v^2 - \frac{14q}{3}v^3, \qquad f^H_{61} = 1 - \frac{113v^2}{24} - \frac{14q}{3}v^3, \tag{C2f}$$

$$f^H_{76} = 1 - \frac{834}{119}v^2, \qquad f^H_{74} = 1 - \frac{6736}{1071}v^2, \qquad f^H_{72} = 1 - \frac{6274}{1071}v^2. \tag{C2g}$$

APPENDIX D: EXPRESSIONS OF THE $\rho_{\ell m}$'S MODES FOR $\ell > 4$

1. The odd-parity $\rho^L_{\ell m}$'s and even-parity $\rho_{\ell m}$'s

$$\rho_{55} = 1 - \frac{487}{390}v^2 - \frac{2q}{3}v^3 + \left(\frac{q^2}{2} - \frac{3353747}{2129400}\right)v^4 - \frac{241q}{195}v^5, \tag{D1a}$$

$$\rho^L_{54} = 1 - \frac{2908}{2275}v^2 - \frac{2q}{15}v^3 + \left(\frac{2q^2}{5} - \frac{16213384}{15526875}\right)v^4, \tag{D1b}$$

$$\rho_{53} = 1 - \frac{25}{26}v^2 - \frac{2q}{3}v^3 + \left(\frac{q^2}{2} - \frac{410833}{709800}\right)v^4 - \frac{103q}{325}v^5, \tag{D1c}$$

$$\rho^L_{52} = 1 - \frac{2638}{2275}v^2 - \frac{2q}{15}v^3 + \left(\frac{2q^2}{5} - \frac{7187914}{15526875}\right)v^4, \tag{D1d}$$

$$\rho_{51} = 1 - \frac{319}{390}v^2 - \frac{2q}{3}v^3 + \left(\frac{q^2}{2} - \frac{31877}{304200}\right)v^4 + \frac{139q}{975}v^5, \tag{D1e}$$

$$\rho_{66} = 1 - \frac{53}{42}v^2 - \frac{2q}{3}v^3 + \left(\frac{q^2}{2} - \frac{1025435}{659736}\right)v^4,$$
$$\rho^L_{65} = 1 - \frac{185}{144}v^2 - \frac{2q}{9}v^3, \tag{D1f}$$

$$\rho_{64} = 1 - \frac{43}{42}v^2 - \frac{2q}{3}v^3 + \left(\frac{q^2}{2} - \frac{476887}{659736}\right)v^4,$$
$$\rho^L_{63} = 1 - \frac{169}{144}v^2 - \frac{2q}{9}v^3, \tag{D1g}$$

$$\rho_{62} = 1 - \frac{37}{42}v^2 - \frac{2q}{3}v^3 + \left(\frac{q^2}{2} - \frac{817991}{3298680}\right)v^4,$$
$$\rho^L_{61} = 1 - \frac{161}{144}v^2 - \frac{2q}{9}v^3, \tag{D1h}$$

$$\rho_{77} = 1 - \frac{151}{119}v^2 - \frac{2q}{3}v^3, \qquad \rho^L_{76} = 1 - \frac{1072}{833}v^2, \tag{D1i}$$

$$\rho_{75} = 1 - \frac{127}{119}v^2 - \frac{2q}{3}v^3, \qquad \rho^L_{74} = 1 - \frac{8878}{7497}v^2, \tag{D1j}$$

$$\rho_{73} = 1 - \frac{111}{119}v^2 - \frac{2q}{3}v^3, \qquad \rho^L_{72} = 1 - \frac{8416}{7497}v^2,$$
$$\rho_{71} = 1 - \frac{103}{119}v^2 - \frac{2q}{3}v^3, \tag{D1k}$$

$$\rho_{88} = 1 - \frac{1741}{1368}v^2, \qquad \rho^L_{87} = 1 - \frac{3913}{3040}v^2,$$
$$\rho_{86} = 1 - \frac{167}{152}v^2, \qquad \rho^L_{85} = 1 - \frac{725}{608}v^2, \tag{D1l}$$

$$\rho_{84} = 1 - \frac{1333}{1368}v^2, \qquad \rho^L_{83} = 1 - \frac{3433}{3040}v^2,$$
$$\rho_{82} = 1 - \frac{1231}{1368}v^2, \qquad \rho^L_{81} = 1 - \frac{3337}{3040}v^2. \tag{D1m}$$

2. The odd-parity $\rho^H_{\ell m}$'s

$$\rho^H_{21} = 1 - \frac{3q}{4}v - \frac{3}{224}(21q^2 + 4)v^2 - \frac{1}{896}(q(189q^2 + 596))v^3 + \left(-\frac{405q^4}{2048} + \frac{1767q^2}{1792} - \frac{21809}{56448}\right)v^4$$
$$- \left(\frac{1701q^5}{8192} - \frac{1191q^3}{7168} + \frac{69851q}{75264}\right)v^5 + \left(\frac{7839703541}{2607897600} - \frac{15309q^6}{65536} + \frac{4113q^4}{16384} + \frac{342289q^2}{200704} - \frac{107\,\mathrm{eulerlog}_1(v^2)}{105}\right)v^6$$
$$+ \left(-\frac{72171q^7}{262144} + \frac{19683q^5}{65536} + \frac{3131q^3}{344064} + \frac{107}{140}q\,\mathrm{eulerlog}_1(v^2) - \frac{40609146713q}{10431590400}\right)v^7$$
$$+ \left(\frac{107\,\mathrm{eulerlog}_1(v^2)}{1960} + \frac{48499995300301}{22782593433600}\right)v^8 + \left(\frac{2333563\,\mathrm{eulerlog}_1(v^2)}{5927040} + \frac{3762995064239}{8679083212800}\right)v^{10}, \tag{D2a}$$

$$\rho^H_{32} = 1 - \frac{74}{135}v^2 - \frac{8q}{9}v^3 + \left(\frac{2q^2}{3} - \frac{164726}{200475}\right)v^4 - \frac{2138q}{1215}v^5 + \left(\frac{8q^2}{135} - \frac{104\,\mathrm{eulerlog}_2(v^2)}{63} + \frac{61271294666}{10343908575}\right)v^6$$
$$+ \left(\frac{7696\,\mathrm{eulerlog}_2(v^2)}{8505} + \frac{1593740014406}{3072140846775}\right)v^8, \tag{D2b}$$

$$\rho^H_{43} = 1 - \frac{67}{88}v^2 - \frac{5q}{6}v^3 + \left(\frac{5q^2}{8} - \frac{6934313}{7047040}\right)v^4 - \frac{13847q}{9240}v^5 + \left(\frac{1597804689571}{195343948800} - \frac{1571\,\mathrm{eulerlog}_3(v^2)}{770}\right)v^6, \quad \text{(D2c)}$$

$$\rho^H_{41} = 1 - \frac{169}{264}v^2 - \frac{5q}{6}v^3 + \left(\frac{5q^2}{8} - \frac{2204777}{7047040}\right)v^4 + \left(\frac{151q}{27720} - \frac{5q^3}{6}\right)v^5 + \left(\frac{1299523316251}{1758095539200} - \frac{1571\,\mathrm{eulerlog}_1(v^2)}{6930}\right)v^6, \quad \text{(D2d)}$$

$$\rho^H_{54} = 1 - \frac{1998}{2275}v^2 - \frac{4q}{5}v^3 + \left(\frac{3q^2}{5} - \frac{16699324}{15526875}\right)v^4, \quad \text{(D2e)}$$

$$\rho^H_{52} = 1 - \frac{1728}{2275}v^2 - \frac{4q}{5}v^3 + \left(\frac{3q^2}{5} - \frac{6936754}{15526875}\right)v^4, \quad \text{(D2f)}$$

$$\begin{aligned}\rho^H_{65} &= 1 - \frac{137}{144}v^2 - \frac{7q}{9}v^3,\\ \rho^H_{63} &= 1 - \frac{121}{144}v^2 - \frac{7q}{9}v^3,\\ \rho^H_{61} &= 1 - \frac{113}{144}v^2 - \frac{7q}{9}v^3,\end{aligned} \quad \text{(D2g)}$$

$$\rho^H_{76} = 1 - \frac{834}{833}v^2, \qquad \rho^H_{74} = 1 - \frac{6736}{7497}v^2, \qquad \rho^H_{72} = 1 - \frac{6274}{7497}v^2. \quad \text{(D2h)}$$

APPENDIX E: EXPRESSIONS OF THE $\delta_{\ell m}$'S MODES FOR $4 < \ell \leq 7$

$$\delta_{55} = \frac{31}{42}v^3, \qquad \delta_{53} = \frac{31}{70}v^3, \qquad \delta_{51} = \frac{31}{210}v^3, \quad \text{(E1a)}$$

$$\delta_{54} = \frac{12q}{5}v^4 + \frac{8}{15}v^3, \qquad \delta_{52} = \frac{6q}{5}v^4 + \frac{4}{15}v^3, \quad \text{(E1b)}$$

$$\delta_{66} = \frac{43}{70}v^3, \qquad \delta_{64} = \frac{43}{105}v^3, \qquad \delta_{62} = \frac{43}{210}v^3, \quad \text{(E1c)}$$

$$\delta_{65} = \frac{10}{21}v^3, \qquad \delta_{63} = \frac{2}{7}v^3, \qquad \delta_{61} = \frac{2}{21}v^3, \quad \text{(E1d)}$$

$$\delta_{77} = \frac{19}{36}v^3, \qquad \delta_{75} = \frac{95}{252}v^3, \quad \text{(E1e)}$$

$$\delta_{73} = \frac{19}{84}v^3, \qquad \delta_{71} = \frac{19}{252}v^3. \quad \text{(E1f)}$$

APPENDIX F: MULTIPOLE MOMENTS FOR GENERIC ℓ AND m

In Refs. [6,22], the authors have computed the even- and odd-parity 1PN multipoles for generic ℓ and m. Those calculations were crucial in understanding the ℓ scaling of the $f_{\ell m}$'s, suggesting the introduction of the $\rho_{\ell m}$'s functions.

In this Appendix, we calculate the 0.5PN spin terms in the odd-parity multipoles $\hat{h}^{(1)}_{\ell m}$ and the 1.5PN spin terms in the even-parity multipoles $\hat{h}^{(0)}_{\ell m}$. Just for completeness, we also reproduce the 1PN nonspinning terms in the odd-parity multipoles $\hat{h}^{(1)}_{\ell m}$, already computed in Ref. [6].

Henceforth, we make use of the standard multi-index notation for tensors of arbitrary rank, which are displayed as

$$T_L \equiv T_{i_1 i_2 \ldots i_\ell}, \quad \text{(F1)}$$

where each index i_1 to i_ℓ runs from 1 to 3. We also employ the notation $T_{\langle L\rangle} = \mathrm{STF}_L[T_L]$ to denote the symmetric trace-free projection over the indices i_1 to i_ℓ. For example, we have

$$T_{\langle ij\rangle} = \frac{1}{2}(T_{ij} + T_{ji}) - \frac{1}{3}\delta_{ij}\delta^{pq}T_{pq}. \quad \text{(F2)}$$

Repeated multi-indices imply summation over all corresponding indices, e.g.

$$T_L S^L \equiv T_{i_1 i_2 \ldots i_\ell} S^{i_1 i_2 \ldots i_\ell}. \quad \text{(F3)}$$

Reference [22] computed the expression of the full waveform as an expansion in -2 spin-weighted spherical harmonics through the coefficients $U_{\ell m}$ and $V_{\ell m}$ as follows

$$h_{lm} = \frac{1}{\sqrt{2}R}(U_{\ell m} - iV_{\ell m}), \quad \text{(F4)}$$

where

$$U_{\ell m} = \frac{16\pi}{(2\ell+1)!!}\sqrt{\frac{(\ell+1)(\ell+2)}{2\ell(\ell-1)}}U_L \mathcal{Y}^{\ell m *}_L, \quad \text{(F5a)}$$

$$V_{\ell m} = -\frac{32\pi\ell}{(2\ell+1)!!}\sqrt{\frac{(\ell+2)}{2\ell(\ell+1)(\ell-1)}}V_L \mathcal{Y}^{\ell m *}_L. \quad \text{(F5b)}$$

The radiative moments U_L and V_L are the lth time derivatives of the multipole moments I_L and J_L, respectively, as we neglect tail contributions for our purposes here. In terms of the vector $\hat{\boldsymbol{r}}$ defined above Eqs. (F11), the quantity $\mathcal{Y}^{\ell m}_L$ is defined as follows

$$Y^{\ell m} = \mathcal{Y}^{\ell m}_L \hat{r}_L. \tag{F6}$$

1. Odd-parity 0.5PN spin multipoles

The odd-parity contributions to the waveforms are provided by the expansion coefficients $V_{\ell m}$, which in turn are determined by the current-multipole moments J_L. In the circular orbital case, the nonspinning 1PN current-multipole moment J_L is given by [6]

$$J^{\rm NS}_L = (\nu M r^{\ell+1}\Omega)[K_1 \hat{L}^{\langle i_\ell}_N n^{L-1\rangle} + v^2 K_2 \hat{L}^{\langle i_\ell}_N n^{L-3} \lambda^{i_{\ell-2} i_{\ell-1}\rangle}], \tag{F7}$$

where Ω is the orbital frequency, $v = (M\Omega)^{1/3}$ and

$$\boldsymbol{n} = \frac{\boldsymbol{r}}{r}, \qquad \hat{\boldsymbol{L}}_N = \frac{\boldsymbol{r}\times\dot{\boldsymbol{r}}}{|\boldsymbol{r}\times\dot{\boldsymbol{r}}|}, \qquad \boldsymbol{\lambda} = \hat{\boldsymbol{L}}_N \times \boldsymbol{n}, \tag{F8}$$

and where

$$K_1 = c_{\ell+1} + v^2\Big\{-\frac{\nu}{2\ell} + \frac{2\ell+3}{2\ell} b_{\ell+1} + 2\nu\frac{\ell+1}{\ell} b_{\ell-1} + \frac{1}{2}\Big[\frac{\ell+1}{\ell} - \frac{(\ell-1)(\ell+4)}{(\ell+2)(2\ell+3)}\Big] c_{\ell+3}\Big\}, \tag{F9a}$$

$$K_2 = \frac{(\ell-1)(\ell-2)(\ell+4)}{2(\ell+2)(2\ell+3)} c_{\ell+3}, \tag{F9b}$$

$$b_\ell = X_2^\ell + (-)^\ell X_1^\ell, \tag{F9c}$$

$$c_\ell = X_2^{\ell-1} + (-)^\ell X_1^{\ell-1}, \tag{F9d}$$

where c_ℓ coincides with Eq. (5), and $X_{1,2} = m_{1,2}/M$. For circular orbits, we have

$$\boldsymbol{n} = (\cos\phi_{\rm orb}, \sin\phi_{\rm orb}, 0), \tag{F10a}$$

$$\boldsymbol{\lambda} = (-\sin\phi_{\rm orb}, \cos\phi_{\rm orb}, 0), \tag{F10b}$$

$$\hat{\boldsymbol{L}}_N = (0, 0, 1). \tag{F10c}$$

In terms of the vector $\hat{\boldsymbol{r}} = (\sin\theta\cos\phi, \sin\theta\sin\phi, \cos\theta)$, the following expressions will prove very helpful below:

$$\boldsymbol{n} = [\hat{\boldsymbol{r}}]_{\theta=\pi/2,\phi=\phi_{\rm orb}}, \tag{F11a}$$

$$\boldsymbol{\lambda} = [\partial_\phi \hat{\boldsymbol{r}}]_{\theta=\pi/2,\phi=\phi_{\rm orb}}, \tag{F11b}$$

$$\hat{\boldsymbol{L}}_N = -[\partial_\theta \hat{\boldsymbol{r}}]_{\theta=\pi/2,\phi=\phi_{\rm orb}}. \tag{F11c}$$

The 0.5PN-order contribution to J_L that is linear in the spins is given by Ref. [41]

$$J^{\rm S}_L = \frac{(\ell+1)}{2}{\rm STF}_L\Big\{\sum_A S^{i_\ell}_A y^{L-1}_A\Big\}. \tag{F12}$$

To rewrite Eq. (F12) in the center-of-mass frame, we use $\boldsymbol{y}_1 = X_2\boldsymbol{r}$ and $y_2 = -X_1\boldsymbol{r}$, which leads to the following

$$J^{\rm S}_L = \frac{(\ell+1)}{2}[(X_2^{\ell-1}S_1^{<i_\ell} + (-)^{\ell-1}X_1^{\ell-1}S_2^{\langle i_\ell})x^{L-1\rangle}] \equiv \nu M^2 r^{\ell-1}\frac{(\ell+1)}{2}\hat{\Sigma}^{\langle i_\ell}_{(\ell)} n^{L-1\rangle}, \tag{F13}$$

where

$$\hat{\boldsymbol{\Sigma}}_{(\ell)} = X_1 X_2^{\ell-2}\boldsymbol{\chi}_1 + (-)^{\ell-1}X_2 X_1^{\ell-2}\boldsymbol{\chi}_2, \tag{F14}$$

and we define $\boldsymbol{\chi}_1 = \boldsymbol{S}_1/m_1^2$ and $\boldsymbol{\chi}_2 = \boldsymbol{S}_2/m_2^2$. For nonprecessing binaries, we have $\hat{\boldsymbol{\Sigma}}_{(\ell)} = \hat{\Sigma}_{(\ell)}\hat{\boldsymbol{L}}_N$, and hence we can write down the total 1PN-order current-multipole moment as

$$J_L = (\nu M r^{\ell+1}\Omega){\rm STF}_L\Big\{\hat{L}^{i_\ell}_N\Big[K_1 n^{L-1} + v^2 K_2 n^{L-3}\lambda^{i_{\ell-2}i_{\ell-1}} + v\frac{(\ell+1)}{2}\hat{\Sigma}_{(\ell)} n^{L-1}\Big]\Big\}. \tag{F15}$$

Next, in order to compute the radiative coefficient $V_{\ell m}$, we first need $J_{\ell m} = J_L \mathcal{Y}^{\ell m}_L$. It is therefore useful to rewrite all vectors appearing in J_L in terms of $\hat{\boldsymbol{r}}$ as follows:

$$J_L = (\nu M r^{\ell+1}\Omega){\rm STF}_L\Big\{\partial_\theta n^{i_\ell}\Big[K_1 n^{L-1} + v^2 K_2 n^{L-3}\partial_\phi n^{i_{\ell-2}}\partial_\phi n^{i_{\ell-1}} + v\frac{(\ell+1)}{2}\hat{\Sigma}_{(\ell)} n^{L-1}\Big]\Big\}_{\rm orb}, \tag{F16}$$

where the "orb" subscript is shorthand for evaluating the bracket at $\theta = \pi/2$, $\phi = \phi_{\rm orb}$. The purpose of this rewriting is to allow us to eventually make use of Eq. (F6), together with the following identities

$$\partial_\theta n^{\langle L\rangle} = \ell(\partial_\theta n^{\langle i_\ell} n^{L-1\rangle} \tag{F17a}$$

$$\partial^2_\phi n^{\langle L-1\rangle} = (\ell-1)\{(\ell-2)n^{\langle L-3}\partial_\phi n^{i_{\ell-2}}\partial_\phi n^{i_{\ell-1}\rangle} - [n^{\langle i_{\ell-1}} - (\boldsymbol{n}\cdot\hat{\boldsymbol{L}}_N)\hat{L}^{\langle i_{\ell-1}}_N]n^{L-2\rangle}\}. \tag{F17b}$$

By substituting Eqs. (F17) into Eq. (F16), the current-multipole moments become

$$J_L = (\nu M r^{\ell+1}\Omega)\mathrm{STF}_L\left\{\frac{K_1}{\ell}\partial_\theta n^L + v^2\frac{K_2}{\ell(\ell-2)}\partial_\theta n^L + v^2\frac{K_2}{\ell(\ell-1)(\ell-2)}\partial_\theta\partial_\phi^2 n^L + v^2\frac{(\ell+1)}{2\ell}\hat{\Sigma}_{(\ell)}\partial_\theta n^L\right\}_{\mathrm{orb}}. \tag{F18}$$

Contracting Eq. (F18) with $Y_L^{\ell m*}$ then yields

$$J_{\ell m} = \frac{c_{\ell+1}}{\ell}(\nu M r^{\ell+1}\Omega)[\partial_\theta Y^*_{\ell m}(\theta,\phi_{\mathrm{orb}})]_{\theta=\pi/2} \times\left\{1 + v\frac{(\ell+1)}{2c_{\ell+1}}\hat{\Sigma}_{(\ell)} - v^2\left[\frac{\nu}{2\ell} - \frac{2\ell+3}{2\ell}\frac{b_{\ell+1}}{c_{\ell+1}} - 2\nu\frac{\ell+1}{\ell}\frac{b_{\ell-1}}{c_{\ell+1}} + \frac{1}{2}\left(\frac{m^2(\ell+4)}{(\ell+2)(2\ell+3)} - \frac{\ell+1}{\ell}\right)\frac{c_{\ell+3}}{c_{\ell+1}}\right]\right\}. \tag{F19}$$

From the parity properties of associated Legendre polynomials, $J_{\ell m}$ is nonvanishing only if $\ell + m$ is odd. The next step consists of converting $r^{\ell+1}$ into an expansion in v by means of Kepler's third law,

$$r^{\ell+1} = (Mv^{-2})^{\ell+1}\left[1 - v^2(\ell+1)\left(1 - \frac{\nu}{3}\right)\right], \tag{F20}$$

and substituting it into Eq. (F19) yields

$$J_{\ell m} = \frac{c_{\ell+1}}{\ell}(Mv^{-2})^{\ell+1}\nu v^3[\partial_\theta Y^*_{\ell m}(\theta,\phi_{\mathrm{orb}})]_{\theta=\pi/2} \times\left(1 + v\frac{(\ell+1)}{2c_{\ell+1}}\hat{\Sigma}_{(\ell)} - v^2\left\{(\ell+1)\left(1-\frac{\nu}{3}\right) + \frac{\nu}{2\ell} - \frac{2\ell+3}{2\ell}\frac{b_{\ell+1}}{c_{\ell+1}} - 2\nu\frac{\ell+1}{\ell}\frac{b_{\ell-1}}{c_{\ell+1}} + \frac{1}{2}\left[\frac{m^2(\ell+4)}{(\ell+2)(2\ell+3)} - \frac{\ell+1}{\ell}\right]\frac{c_{\ell+3}}{c_{\ell+1}}\right\}\right). \tag{F21}$$

Taking ℓ time derivatives and multiplying by the appropriate normalization factor finally gives

$$V_{\ell m} = -\frac{32\pi\ell}{(2\ell+1)!!}\sqrt{\frac{(\ell+2)}{2\ell(\ell+1)(\ell-1)}}\nu M(-im)^\ell v^{(\ell+1)}\frac{c_{\ell+1}}{\ell}[\partial_\theta Y^*_{\ell m}(\theta,\phi_{\mathrm{orb}})]_{\theta=\pi/2}\left\{1 + v\frac{(\ell+1)}{2c_{\ell+1}}\hat{\Sigma}_{(\ell)} - v^2\left[(\ell+1)\left(1-\frac{\nu}{3}\right) + \frac{\nu}{2\ell} - \frac{2\ell+3}{2\ell}\frac{b_{\ell+1}}{c_{\ell+1}} - 2\nu\frac{\ell+1}{\ell}\frac{b_{\ell-1}}{c_{\ell+1}} + \frac{1}{2}\left(\frac{m^2(\ell+4)}{(\ell+2)(2\ell+3)} - \frac{\ell+1}{\ell}\right)\frac{c_{\ell+3}}{c_{\ell+1}}\right]\right\}, \tag{F22}$$

The overall factor in front of the bracket in Eq. (F22) coincides with the Newtonian contribution as given by Eq. (3), using Eqs. (F4) and (4b). Hence by definition [see Eq. (2)], we find

$$\hat{h}^{(1)}_{\ell m} = 1 + v\frac{(\ell+1)}{2c_{\ell+1}}\hat{\Sigma}_{(\ell)} - v^2\left[(\ell+1)\left(1-\frac{\nu}{3}\right) + \frac{\nu}{2\ell} - \frac{2\ell+3}{2\ell}\frac{b_{\ell+1}}{c_{\ell+1}} - 2\nu\frac{\ell+1}{\ell}\frac{b_{\ell-1}}{c_{\ell+1}} + \frac{1}{2}\left(\frac{m^2(\ell+4)}{(\ell+2)(2\ell+3)} - \frac{\ell+1}{\ell}\right)\frac{c_{\ell+3}}{c_{\ell+1}}\right]. \tag{F23}$$

Again, the 1PN-order terms in the above equation were computed in Appendix A of Ref. [6].

Quite interestingly, we find that in the nonspinning test-particle limit ($m_2 \ll m_1$, $\chi_1 = |\boldsymbol{\chi}_1| = am_1 \equiv q$, $\chi_2 = 0$), only the odd-parity mode $\ell = 2$ contains the 0.5PN spin term, for all the other odd-parity modes the 0.5PN spin terms vanish. In fact, using Eqs. (F9d) and (F14), we find that if we set $\chi_2 = 0$, the 0.5PN spin terms reduces to

$$\hat{h}^{(1),0.5\mathrm{PN}}_{\ell m} = -\frac{(\ell+1)m_1^2\chi_1}{2[m_1m_2 + (-1)^\ell m_1^\ell m_2^{2-\ell}]}v. \tag{F24}$$

If $\ell = 2$, then $\hat{h}^{(1),0.5\mathrm{PN}}_{21} = -3/2vq$ when $\nu \to 0$, while if $\ell > 2$, we have $\hat{h}^{(1),0.5\mathrm{PN}}_{\ell m} \propto \nu q v$ and the latter goes to zero as $\nu \to 0$. The fact that the odd-parity modes with $\ell > 2$ vanish is consistent with the -2 spin-weighted spherical $C_{\ell m}$'s computed in the main part of this paper. However, it is worth noticing that the odd-parity -2 spin-weighted spheroidal $Z_{\ell m}$'s *do* contain 0.5PN spin terms.

Moreover, for the case of finite symmetric mass-ratio ν, we find that the 0.5PN spin terms in Eq. (F23) coincide with what was derived in PN theory [22]. The ℓ dependence of the 0.5PN spin term in Eq. (F23) varies depending on the binary mass ratio and the spin magnitudes. For example, we find that for maximally spinning and aligned black holes ($\chi_1 = \chi_2 = 1$) if the masses are equal, the 0.5PN spin term in Eq. (F23) scales as ℓ but if the masses are unequal, it generally does not scale as ℓ.

Finally, we derive the corresponding generic 0.5PN spin contributions to $f^{(1)}_{\ell m}$ and $\rho^{(1)}_{\ell m}$. Since we know that there is no quadratic spin contribution at 1PN order in $f^{(1)}_{\ell m}$, we need to introduce a 1PN quadratic spin term in $\rho^{(1)}_{\ell m}$. Thus, the spin portions read

$$f^{(1),0.5\mathrm{PN}}_{\ell m} = \hat{h}^{(1),0.5\mathrm{PN}}_{\ell m}, \qquad \rho^{(1),0.5\mathrm{PN}}_{\ell m} = \tfrac{1}{\ell}\hat{h}^{(1),0.5\mathrm{PN}}_{\ell m}, \qquad \rho^{(1),1\mathrm{PN}}_{\ell m} = -\frac{\ell-1}{2\ell^2}(\hat{h}^{(1),0.5\mathrm{PN}}_{\ell m})^2. \tag{F25}$$

2. Even-parity 1.5PN spin multipoles

The 1.5PN spin contributions to the even-parity waveform come from two distinct sources. The first is the 1.5PN

spin mass multipole moment $I_L^{\rm S}$, given by (in the center-of-mass frame, for nonprecessing, circular orbits)

$$I_L^{\rm S} = M^2\nu^2\frac{2\ell}{\ell+1}r^\ell\tilde{\Sigma}_{(l)}{\rm STF}_L\left[\ell\Omega n^L + \frac{\ell-1}{r^2\Omega}n^{L-2}v^{i_{\ell-1}}v^{i_\ell}\right], \tag{F26}$$

where

$$\tilde{\Sigma}_{(\ell)} = X_2^{\ell-2}\chi_1 + (-)^\ell X_1^{\ell-2}\chi_2. \tag{F27}$$

Making use of the following identity which is valid for circular orbits

$${\rm STF}_L\left[\frac{(\ell-1)}{r^2}n^{L-2}v^{i_{\ell-1}}v^{i_\ell}\right] = {\rm STF}_L\left[\frac{1}{\ell}\frac{d^2}{dt^2}n^L + \Omega^2 n^L\right], \tag{F28}$$

we can rewrite $I_L^{\rm S}$ as follows

$$I_L^{\rm S} = M^2\nu^2\frac{2\ell}{\ell+1}r^\ell\tilde{\Sigma}_{(l)}{\rm STF}_L\left[(\ell+1)\Omega n^L + \frac{1}{\ell\Omega}\frac{d^2}{dt^2}n^L\right]. \tag{F29}$$

The second contribution comes from the Newtonian mass multipole moments, in two different ways. First, since the coordinate transformation that takes us from a generic frame to the center-of-mass frame involves the spins at 1.5PN order, the Newtonian mass multipole moments acquire a spin contribution when reexpressed in the center-of-mass frame. Second, when we use Kepler's law at 1.5PN order to rewrite the orbital separation r as an expansion in $v = (M\Omega)^{1/3}$, spin terms are generated which contribute to the 1.5PN spinning waveform. In a general frame, the Newtonian mass multipole moments are given by

$$I_L^{\rm N} = {\rm STF}_L[m_1 y_1^L + m_2 y_2^L]. \tag{F30}$$

The coordinate transformation to the center-of-mass frame is given by [42]

$$\boldsymbol{y}_1 = X_2\boldsymbol{r} + \frac{\nu}{M}\boldsymbol{v}\times\boldsymbol{\Delta}, \tag{F31a}$$

$$\boldsymbol{y}_2 = -X_1\boldsymbol{r} + \frac{\nu}{M}\boldsymbol{v}\times\boldsymbol{\Delta}. \tag{F31b}$$

Therefore, in the center-of-mass frame, the Newtonian mass multipole moments read

$$I_L^{\rm N} = M\nu c_\ell r^l n^{\langle L\rangle} + \nu^2\ell c_{\ell-1}r^{l-1}n^{\langle L-1}(\boldsymbol{v}\times\Delta)^{i_\ell\rangle}. \tag{F32}$$

For nonprecessing, circular orbits, Eq. (F32) may be rewritten as

$$I_L^{\rm N} = M\nu c_\ell r^l n^{\langle L\rangle}\left[1 + \nu\frac{\ell c_{\ell-1}}{c_\ell}(X_2\chi_2 - X_1\chi_1)v^3\right]. \tag{F33}$$

Adding together both contributions (F29) and (F33), contracting with $\mathcal{Y}^*_{\ell m}$ and finally taking ℓ time derivatives as well as multiplying by the appropriate overall factor, we arrive at the following expression for the even-parity radiative moment

$$U_{\ell m} = \frac{16\pi}{(2\ell+1)!!}\sqrt{\frac{(\ell+1)(\ell+2)}{2\ell(\ell-1)}}M\nu c_\ell(-im\Omega)^\ell r^\ell \times Y^*_{\ell m}(\pi/2,\phi_{\rm orb})\left[1 + \nu\frac{\ell c_{\ell-1}}{c_\ell}(X_2\chi_2 - X_1\chi_1)v^3 + \frac{\nu}{c_\ell}\left(\frac{2\ell}{\ell+1}\right)\left(\ell+1-\frac{m^2}{\ell}\right)\tilde{\Sigma}_{(\ell)}v^3\right]. \tag{F34}$$

The overall factor in front of the bracket in Eq. (F34) coincides with the Newtonian contribution as given by Eq. (3), using Eqs. (F4) and (4a). Next, we use Kepler's third law to replace the orbital separation r by the following expansion in v. Again, we do not write the 1PN order nonspinning contributions explicitly here to keep formulas short.

$$r = Mv^{-2}\left\{1 + \left[\frac{2}{3}(X_1^2\chi_1 + X_2^2\chi_2) + \nu(\chi_1+\chi_2)\right]v^3\right\}^{-1}. \tag{F35}$$

Substituting (F35) into (F34), we can finally isolate the 1.5PN spin contribution to the even-parity waveform as

$$\hat{h}^{(0),1.5{\rm PN}}_{\ell m} = \left\{-\ell\left[\frac{2}{3}(X_1^2\chi_1 + X_2^2\chi_2) + \nu(\chi_1+\chi_2)\right] + \nu\frac{\ell c_{\ell-1}}{c_\ell}(X_2\chi_2 - X_1\chi_1) + \frac{\nu}{c_\ell}\left(\frac{2\ell}{\ell+1}\right)\left(\ell+1-\frac{m^2}{\ell}\right)\tilde{\Sigma}_{(\ell)}\right\}v^3. \tag{F36}$$

In the nonspinning test-particle limit, Eq. (F36) simply reduces to

$$\hat{h}^{(0),1.5{\rm PN}}_{\ell m} \to -\frac{2\ell}{3}qv^3; \tag{F37}$$

thus, it scales as ℓ. Finally, we derive the corresponding generic 1.5PN spin contribution to $f^{(0)}_{\ell m}$ and $\rho^{(0)}_{\ell m}$ and they read

$$f^{(0),1.5{\rm PN}}_{\ell m} = \hat{h}^{(0),1.5{\rm PN}}_{\ell m}, \qquad \rho^{(0),1.5{\rm PN}}_{\ell m} = \frac{1}{\ell}f^{(0),1.5{\rm PN}}_{\ell m}. \tag{F38}$$

Therefore, the generic $f^{(0)}_{\ell m}$ and $\rho^{(0)}_{\ell m}$ expressions through 1.5PN are given by the above equation combined with the 1PN nonspinning result given in Eq. (A15) of Ref. [6] (note that there is no 1.5PN nonspinning contribution to $f^{(0)}_{\ell m}$ or $\rho^{(0)}_{\ell m}$).

[1] S. J. Waldman (LIGO Scientific Collaboration), Classical Quantum Gravity **23**, S653 (2006).
[2] F. Acernese *et al.* (Virgo Collaboration), Classical Quantum Gravity **25**, 114045 (2008).
[3] B. F. Schutz, Classical Quantum Gravity **26**, 094020 (2009).
[4] M. Sasaki and H. Tagoshi, Living Rev. Relativity **6**, 6 (2003).
[5] L. Blanchet, Living Rev. Relativity **9**, 4 (2006).
[6] T. Damour, B. R. Iyer, and A. Nagar, Phys. Rev. D **79**, 064004 (2009).
[7] The factorized waveform for the (2,2) mode appeared first in Ref. [8].
[8] T. Damour and A. Nagar, Phys. Rev. D **76**, 064028 (2007).
[9] N. Yunes and E. Berti, Phys. Rev. D **77**, 124006 (2008).
[10] T. Damour and A. Nagar, Phys. Rev. D **79**, 081503 (2009).
[11] A. Buonanno, Y. Pan, H. P. Pfeiffer, M. A. Scheel, L. T. Buchman, and L. E. Kidder, Phys. Rev. D **79**, 124028 (2009).
[12] T. Tanaka, H. Tagoshi, and M. Sasaki, Prog. Theor. Phys. **96**, 1087 (1996).
[13] H. Tagoshi, M. Shibata, T. Tanaka, and M. Sasaki, Phys. Rev. D **54**, 1439 (1996).
[14] H. Tagoshi and R. Fujita (unpublished).
[15] R. Fujita and B. R. Iyer, Phys. Rev. D **82**, 044051 (2010).
[16] R. Fujita and H. Tagoshi, Prog. Theor. Phys. **112**, 415 (2004).
[17] R. Fujita and H. Tagoshi, Prog. Theor. Phys. **113**, 1165 (2005).
[18] R. Fujita, W. Hikida, and H. Tagoshi, Prog. Theor. Phys. **121**, 843 (2009).
[19] Y. Pan, A. Buonanno, L. Buchman, T. Chu, L. Kidder, H. Pfeiffer, and M. Scheel, Phys. Rev. D **81**, 084041 (2010).
[20] E. Poisson, Phys. Rev. D **47**, 1497 (1993).
[21] H. Tagoshi and M. Sasaki, Prog. Theor. Phys. **92**, 745 (1994).
[22] L. E. Kidder, Phys. Rev. D **77**, 044016 (2008).
[23] L. Blanchet, G. Faye, B. R. Iyer, and S. Sinha, Classical Quantum Gravity **25**, 165003 (2008).
[24] We note that in perturbation-theory calculations this constant cancels out in the combination $h_+ - ih_\times$ [21].
[25] K. G. Arun, A. Buonanno, G. Faye, and E. Ochsner, Phys. Rev. D **79**, 104023 (2009).
[26] J. M. Bardeen, W. H. Press, and S. A. Teukolsky, Astrophys. J. **178**, 347 (1972).
[27] Note that in Ref. [6] the authors chose $r_0 = 2M$.
[28] I. B. Khriplovich and A. A. Pomeransky, Phys. Lett. A **252**, 17 (1999).
[29] H. Asada and T. Futamase, Phys. Rev. D **56**, R6062 (1997).
[30] Y. Mino, M. Sasaki, M. Shibata, H. Tagoshi, and T. Tanaka, Prog. Theor. Phys. Suppl. **128**, 1 (1997).
[31] S. Mano, H. Suzuki, and E. Takasugi, Prog. Theor. Phys. **95**, 1079 (1996).
[32] H. Tagoshi and T. Nakamura, Phys. Rev. D **49**, 4016 (1994).
[33] E. K. Porter and B. S. Sathyaprakash, Phys. Rev. D **71**, 024017 (2005).
[34] The new higher-order PN terms computed in Ref. [14] were not available at the time Ref. [19] appeared.
[35] N. Yunes, A. Buonanno, S. A. Hughes, M. C. Miller, and Y. Pan, Phys. Rev. Lett. **104**, 091102 (2010).
[36] T. Damour, P. Jaranowski, and G. Schäfer, Phys. Rev. D **78**, 024009 (2008).
[37] E. Barausse and A. Buonanno, Phys. Rev. D **81**, 084024 (2010).
[38] T. Chu, H. P. Pfeiffer, and M. A. Scheel, Phys. Rev. D **80**, 124051 (2009).
[39] Note that Ref. [19] found a relative difference on the order 1% in the (2,2) mode comparison. However, Ref. [19] compared effective-one-body waveforms generated using the full *nonadiabatic* effective-one-body evolution. In Fig. 10, the analytical amplitudes are generated using the *adiabatic* quasicircular effective-one-body evolutions.
[40] H. Tagoshi, S. Mano, and E. Takasugi, Prog. Theor. Phys. **98**, 829 (1997).
[41] L. Blanchet, A. Buonanno, and G. Faye, Phys. Rev. D **74**, 104034 (2006).
[42] Strictly speaking this transformation contains nonspinning 1PN contributions. We shall not write those explicitly here to keep formulas as light as possible, as we are only concerned with spinning terms relative to the leading-order Newtonian contribution.